MASTERARBEIT

Tectonic Evolution of the Budějovice Basin (Czech Republic), with special focus on the Hluboká-Fault

Clemens Porpaczy, Bakk. rer. nat.

angestrebter akademischer Grad

Master of Science (M.Sc.)

Wien, 2011

Studienkennzahl lt. Studienblatt):	A 066 815
Studienrichtung lt. Studienblatt:	Masterstudium Erdwissenschaften
Betreuer:	Dr. Kurt Decker

Contents

Abstract

The Budějovice Basin on the Bohemian Massif in the Southern part of the Czech Republic is a fault-bounded sedimentary basin delimited by NW-SE and NNE-SSW striking fault systems. The NW-striking Hluboká-Fault zone confines the basin to the NE, partly appearing as a morphological scarp in the landscape. Assessment of the kinematic history and timing of fault activity along this border fault as well as reconstruction of the tectonic evolution of the Budějovice Basin was the main objective of this master thesis.

Structural geological research concentrated on outcrops situated close to the Hluboká-Fault Zone. Field data include both ductile (foliation, folds and stretching lineation) and brittle structures (fault planes, deformation bands, tension gashes). Data were collected from outcrops located in crystalline basement rocks, Permian, Cretaceous and Miocene sediments of the Budějovice Basin in order to obtain information about the relative timing of the different fault movement events. Additional structural data were obtained from five interpreted 2D seismic profiles across the Hluboká-Fault and the parallel Zbudov-Fault.

Structural data are supplemented by computer aided 3D-modeling of the crystalline basement and the sedimentary basin fill to understand the tectonic evolution of the Budějovice Basin. Drilling reports from the Czech Geological Survey in Prague (Geofond), a high resolution DEM and geological maps of the region were used for modeling the geometry of the basin, as well as the distribution of Upper Cretaceous and Miocene sediments. The 3D Basin Model is based on subcrop information obtained from 679 wells.

Data indicate that the first movement of the NW-SE striking Hluboká-Fault System occurred at low to very low metamorphic conditions in late-Variscan times (deformation D_2). The fault strikes parallel to preexisting structural anisotropies in the crystalline basement (ductile foliation and folds, D_1). The ductile structures are overprinted by brittle faults. These include brittle normal faults and mineralized extension gashes indicative for SW-directed extension (D_3) and sub-vertical, dextral strike-slip faults striking parallel to the Hluboká-Fault (D_4). Structures of D_3 occur in Variscan phyllite, Permian sediments

and Cretaceous shale suggesting a post-Cretaceous Deformation age. Faults of D_4 occurring in strata of the Zliv Fm. give evidence that dextral strike-slip faulting post-dates the Miocene.

Interpretations of the 3D basin model show that the crystalline basement plunges towards the eastern border of the basin with a dip of approximately 5°. On the north-eastern and eastern border of the basin the Hluboká and Rudolfov Fault offset the crystalline Basement for up to about 340 m. Borehole and seismic data show that the Hluboká Fault fault steeply dips towards SW with up to 85°.

Information obtained from interpreted seismic sections and the 3D-basin model show Upper Cretaceous sediments as the main sedimentary infill of the Budéjovice Basin, increasing in thickness from W to E. Interpreted seismic sections crossing the Hluboká Fault depict large, synformal fold geometries of constant thickness for Upper Cretaceous reflectors rising towards the northeastern basin margin. Seismic further displays an angular unconformity between Upper Cretaceous and overlying Miocene sediments. Neither Cretaceous nor Miocene growth strata have been observed in the seismic. The analyzed geological data therefore indicates that the main subsidence of the Budéjovice Basin occurred due to post-Cretaceous tilting.

Zusammenfassung

Das Budweiser Becken im Süden der tschechischen Republik ist ein störungsgebundenes Sedimentbecken, das die Kristallineinheiten der Böhmischen Masse überlagert. Das Becken wird allseits von NW-SE- sowie NNE-SSW-streichenden Störungszonen begrenzt. Die NW-streichende Hluboká (Frauenberg) Störung begrenzt das Becken gegen NE und tritt in der Landschaft teilweise als markante Geländestufe in Erscheinung. Die Bewertung der Kinematik und die relative zeitliche Zuordnung der Störungsaktivität der Hluboká Störung sowie die Rekonstruktion der tektonischen Entwicklung des Budweiser Beckens bilden den Schwerpunkt dieser Masterarbeit.

Für die kinematische Bwertung wurden strukturgeologische Daten in Aufschlüssen entlang der Hluboká Störung-Zone aufgenommen. Die ausgewerteten Geländedaten umfassen sowohl duktile (Foliationen, Falten, Streckungslineare) als auch spröde Strukturen (Störungsflächen, Deformationsbänder, Zerrspalten). Das Alter der verschiedenen Deformationsereignisse wurde anhand von Strukturen aus Aufschlüssen in verschieden alten Formationen ermittelt. Daten liegen aus Aufschlüssen des kristallinen Untergrunds, der permischen, kretazischen und miozänen Sedimente des Budweiser Beckens vor. Weiters wurden fünf seismische Profile über die Hluboká Störung und die parallel dazu verlaufende Zbudov Störung ausgewertet.

Eine weitere Grundlage für die Rekonstruktion der tektonische Entwicklung des Budweiser Beckens bildet die computergestützte 3D-Modellierung des kristallinen Untergrunds und der Sedimentfüllung des Beckens. Die Modellierung stützt sich auf Daten von 679 Bohrungen (Bohrungsberichte des Tschechischen Geologischen Dienstes – Geofond Prag), ein hochauflösendes DHM sowie die geologische Karten 1:25 000 der Region. Anhand der genannten Datengrundlage wurde die Beckenform sowie die Mächtigkeit der oberkretazischen und der miozänen Sedimente modelliert.

Die Ergebnisse der Strukturgeologischen Felddaten und der Dünnschliffanalysen zeigen, dass das Hluboká Störungsystems unter niedrigen bis sehr niedrigen metamorphen Bedingungen in spätvariszischer Zeit angelegt wurde (Deformation D_2). Die Störung streicht parallel zur variszischen Schieferung und duktilen Falten (D_1).

Die spätvariszischen Strukturen werden von spröden Störungen überprägt. Diese setzen sich aus spröden Abschiebungen und mineralisierten Zerrspalten (D_3) sowie subvertikalen, dextralen Blattverschiebungen (D_4), die parallel zur Hluboká Störung streichen, zusammen. Abschiebungen und Zerrspalten (D_3) zeigen SW-NE-gerichtete Dehnung an. Das Vorhandensein dieser Strukturen (D_3) in variszischem Phyllit, permischen Sedimenten und kretazischen Tonen weist auf post-kretazisches Deformationsalter hin. Das Auftreten dextraler Störungen in miozänen Sedimenten der Zliv Fm. läßt auf ein post-miozänes Deformationsalter von D_4 schließen.

Das 3D Beckenmodell zeigt, dass der kristalline Untergrund des Budweiser Beckens mit etwa ca. 5° nach Osten einfällt. Am nordöstlichen Beckenrand ist der Beckenuntergrund an der Hluboká Störung um ca. 340 m vertikal versetzt. Bohrungsdaten und Seismik dokumentieren, dass die Störung steil mit bis zu 85° nach SW einfällt. Den südöstlichen Beckenrand bildet die Rudolfov (Rudolfstadt) Störung, die mit etwa 50° zum Becken hin einfällt.

Seismikdaten und die Interpretation des 3D Beckenmodells zeigen, dass kretazische Sedimente den größten Anteil der Beckenfüllung bilden. Die Mächtigkeit dieser Serien nimmt von W nach E zu. Seismikprofile über die Hluboká Störung bilden eine großmaßstäbliche Synform der kretazischen Reflektoren am NE Beckenrand ab. Die Synform bildet mit den überlagernden, horizontal geschichteten miozänen Sedimenten eine markante Winkeldiskordanz. Die in der Seismik abgebildeten Reflexionsmuster bieten keinen Hinweis auf syntektonische Sedimente (Growth Strata) in der kretazischen und miozänen Beckenfüllung. Die ausgewerteten geologischen Daten weisen daher darauf hin, dass die Absenkung des Budweiser Beckens im Wesentlichen auf post-kretazisches Kippen zurückzuführen ist.

Acknowledgements

First of all I would like to express my gratitude to my supervisor Dr. Kurt Decker for supporting me with his knowledge during the first field trips to my research area and for constant help and patience in the process of writing this master thesis.

My appreciation especially goes to my project co-worker Dana Homolova for helping me with the interpretation of Czech literature and drilling reports and other problems related to the language barrier between Czech and German.

I also would like to thank Werner Chwatal from the Technical University of Vienna for processing of seismic data and help with interpretation of seismic profiles.

Numerous people throughout the Department for Geodynamics and Sedimentology helped me with words and deeds during the completion of this master thesis:
Magda Bottig and Ulli Exner helped me with various problems concerning the computer program GOCAD®.
My room colleagues Stephanie Neuhuber, Esther Hintersberger, Anton Tanzberger, Asma Nasir, Andreas Beidinger, Andras Zamolyi and Eun Young Lee who always had an open ear for questions that arose due to problems that needed to be solved.
Above all my university mates Johannes Steinbrener, Jasmin Kaiser, Philipp Stadler, Dominik Rehm, Bernhard Bretis and Alex Rath for their companionship and help during the time that we spend together at university and on field trips to many wonderful locations.

Finally I want to stress the importance of my father and my whole family for the time of my studies at the university. Through all those years they supported me in any imaginable way, giving me the opportunity to fully concentrate on my studies.

1. Introduction

The work at hand was done under the supervision of Dr. Kurt Decker at the Department of Geodynamics and Sedimentology at the University of Vienna as part of the Austrian Interfacing Project – AIP in collaboration with Czech geoscientists. This project aims at the classification of the near-regional faults (< 25 km) of the Temelin Nuclear Power Plant in the Czech Republic by using various approaches. These include: Geophysical measurements like Ground Penetrating Radar (GPR) and 2D seismic fault mapping, palaeoseismological trenching, age dating and correlation of quaternary terraces of the Vltava river in the Budějovice basin and intensive structural field work.

The main question hereby was, if faults in an area which is generally associated with low to moderate seismicity, were likely to cause major earthquakes in younger, quaternary times, which would proof that these faults have to be regarded as “active” (**Mallard, 1991**).

In this context the Budějovice Basin 15 km SSE of the Power Plant raised the main attention for our investigations. Especially the northeastern margin of the basin, highlighted by the linear topograghic scarps of the Zbudov Fault and the Hluboká Fault - which is the most prominent fault scarp in the area - were of major interest.

In this framework my master thesis focussed on the poorly known kinematic history and timing of fault activity along the Hluboká and Zbudov Fault in pre-quarternary times including the tectonic and sedimentary evolution of the Budějovice Basin.

Geological research was not only carried out through fieldwork in outcrops in the vicinity of the Hluboká Fault Zone, but also through the interpretation of five seismic profiles, which were recorded in summer and fall 2009, crossing the Hluboká Fault and the parallel Zbudov Fault.

Beside structural field work and seismic fault mapping another approach included the acquisition of subcrop information based on drilling reports obtained from the Czech Geological Survey (Geofond) in Prague. Nearly 1000 drilling reports from wells situated in the lowlands and at the eastern margin of the Budějovice Basin were collected in order to create a computer aided 3D model of the basins bedrock. Additionally, the sedimentary basin fill was modeled according to the borehole informations obtained from the drilling reports, in order to see if sedimentary layers are disrupted or offset by slip along the Hluboká and Zbudov Fault.

Taking the above mentioned background into account, the scientific questions and goals of this master are:

1) Resolving the kinematic history and timing of fault activity along the Hluboka Fault Zone.

2) Characterizing the spatial geometry of the Hluboká and Zbudov Fault through seismic fault mapping at the eastern and northeastern margin of the Budějovice Basin.

3) Combining information obtained from drilling reports and seismic 2D sections in order to create a computer aided 3D model, helping to resolve the tectonic and sedimentary evolution of the Budejovice Basin

2. Geological and geographical overview

The town of České Budějovice (Budweis), situated in the southern part of the Czech Republic, is the capital city of the South Bohemian Region. České Budějovice is situated in the southeastern part of the Budějovice Basin depression. The area of the Budejovice Basin is estimated to be roughly 900 km² in size. The oval-shaped basin is aligned on a NW-SE trending axis and extends from České Budějovice in the southeast to Vodňany in the northwest. Along with the larger Třeboň Basin around the city of Třeboň east of České Budějovice, the Budějovice Basin is part of the so-called South Bohemian Basins, covering an area of ca. 2300 km². They are divided by the Lišov Horst (Rudolfov Ridge) trending in N-S direction between the basin depressions (**Fig. 1**). The crystalline Basement and the margins of South Bohemian Basins are composed of mica schists, biotitic, sillimanite-biotitic to biotite-cordieritic paragneisses and leucocrate migmatites of the Moldanubian Unit as well as igneous rocks of the South Bohemian Pluton.

The metamorphites originated from the complex multiphase fold-thrust deformation of the Cadomian and the Variscan tectono-metamorphic cycle (**McCann, 2008; Váchal et al., 2010**).

The Budějovice Basin can be classified as a rather small and shallow sedimentary basin, with a length in NW-SE direction of approximately 48 km and a width in SW-NE direction of 19 km. The depocenter of the basin with a depth of about 400 m beneath the surface is located in the southeastern part of the basin. The basin is deeper than the Třeboň Basin with about 320 m thick sedimentary fill. Both basins have experienced a similar geological history, which is not only reflected in the sedimentary record, but also in the tectonic framework they were developed in (**Slánská; 1976**).

Probably developed as pull-apart basins on metamorphic basement of the Moldanubian terrane and South Bohemian Pluton (**McCann, 2008**), the South Bohemian Basins evolved at the intersection of the NW-striking Jáchymov (Joachimsthal) Fault zone and the NNE-striking Blanice-Kaplice-Rodl-Fault zone.

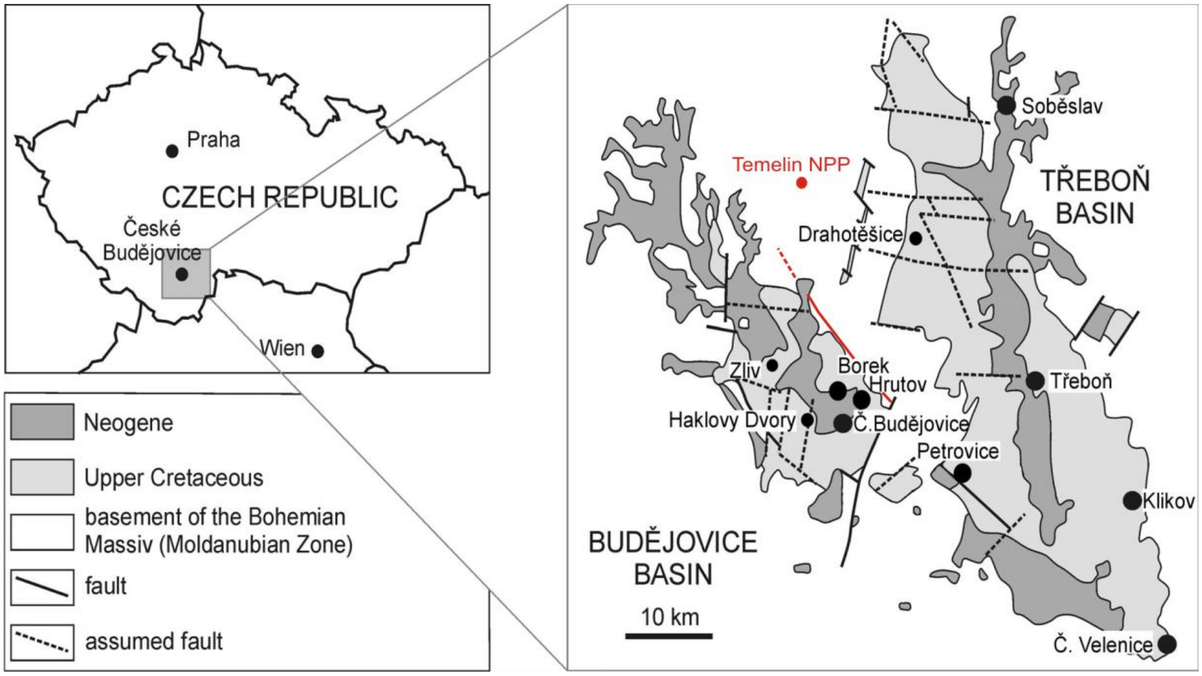

Fig. 1: Location of the South Bohemian Basins. Hluboká Fault at the northeastern margin of the Budejovice Basin indicated in red. Assumed faults (dotted lines) striking in ESE-WNW direction are interpreted as conjugated wrench faults to the Blanice-Kaplice-Rodl Fault Zone (see also **Fig. 4**), separating the basins in NNE-SSW direction. In contrast to the northern part of the Budějovice Basin which is delimited by marked morphological borders, the southern part is clearly controlled by a tectonic setting where border faults like the Hluboká Fault depict sharp contacts between the basin lowland and the surrounding crystalline basement. (**modified after Vachova & Kvaček, 2009**).

2.1. Previous geological investigations

Geological research in the area of the South Bohemian Basins mostly concentrated on the sedimentary deposits covering the crystalline basement. Detailed studies concerning the Late Palaeozoic,- Cretaceous and Tertiary sediments in southern Bohemia were carried out by **Falke, 1972,1975; Slánská, 1976; Holub and Tásler, 1978; Malkovský, 1987; Huber, 2003; Vachova, 2009**. The sedimentary deposits of the Upper Cretaceous Klikov-Formation in the South Bohemian Basins were of special interest to sedimentologists and palaeontologist due to their rich mircroflora. Whereas the sedimentological record and the greater tectonic setting of the Bohemian Massif in the southern part was well investigated (**Fritz & Neuhuber, 1993; Wallbrecher et al. 1993; Brandmayr et al., 1995, 1997; Büttner & Kruhl, 1997; Finger et al. 2007; Büttner, 2007**),the kinematic relationship of processes in central Bohemia around the South Bohemian Basins received less attention in scientific literature (**Šimůnek et al., 1995**).

2.2. Geologic evolution of the Bohemian Massif

Marking the easternmost part of the European Variscan belt, the Bohemian Massif with its rhombic shape can be subdivided into four units, which include from SE to NW: the Moravian, the Moldanubian, the Teplá-Barrandian and the Saxothuringian (**Fig.2**). All of which represent continental microplates being composed of Precambrian basement and Early Paleozoic sedimentary sequences which were consolidated due to the Variscan orogeny (**Hejl et al., 2003**).

Present reconstructions of the European Variscan belt assume a fan-like symmetry, characterized by two branches with opposite vergences (**Pitra et al., 1999**).

Whereas the northern branch including the Saxothuringian and Rhenohercynian depicts an overall northwestward vergence, the Moldanubian in the south is presented by generally southeastward vergence. Mostly unmetamorphosed, the Teplá-Barrandian terrane represents a discontinuous “median zone” separating those two orogenic branches in the Bohemian Massif (**Pitra et al., 1999**)

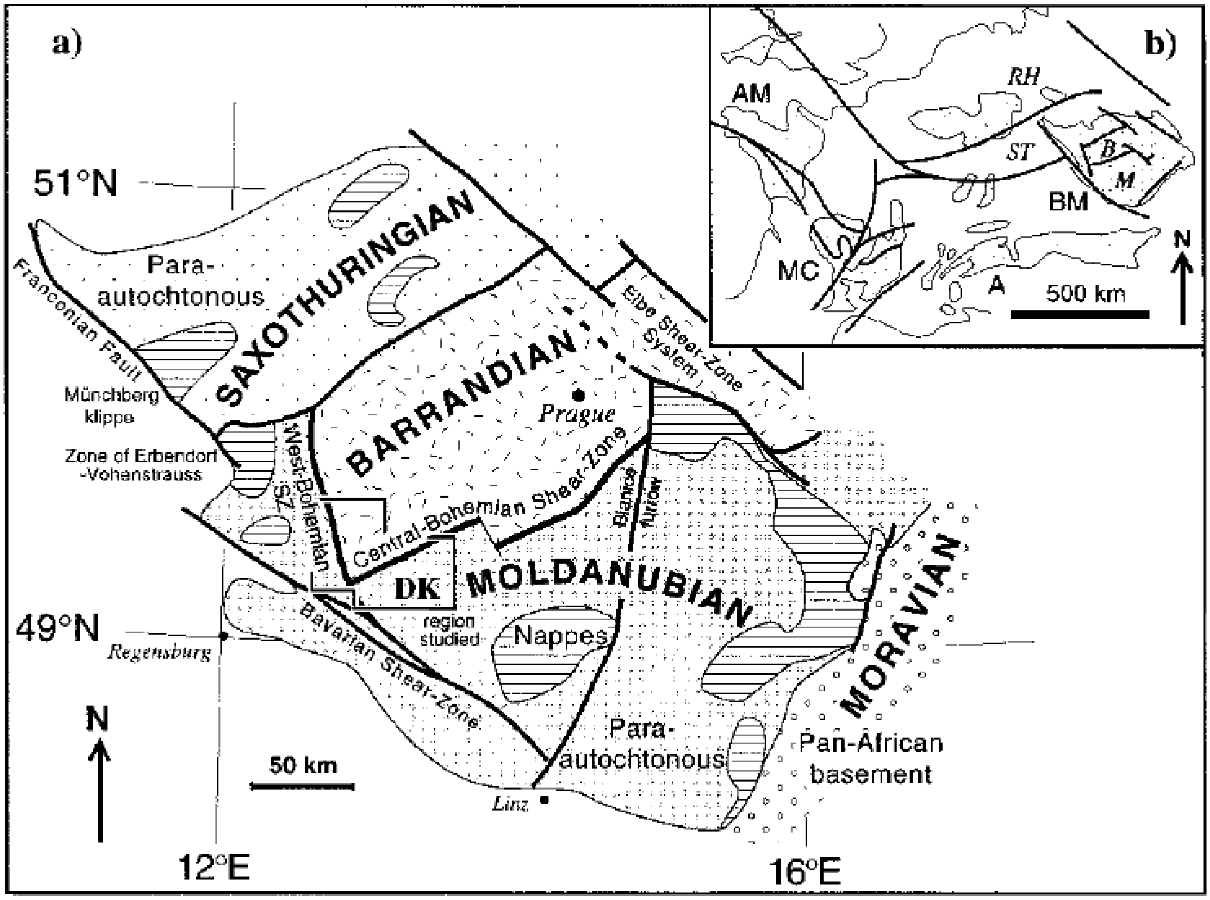

Fig. 2: a) Tectonic sketch of the Bohemian Massif. **b)** European Variscan massif: BM, Bohemian Massif; AM, Armorican Massif; MC, Massif Central; A, Alps; M, Moldanubian Zone; B, Teplá-Barrandian; ST, Saxothuringian Zone; RH, Rhenohercynian Zone (**Pitra et al., 1999**)

High-temperature and medium-to high-pressure metamorphism during Devonian and Late Carboniferous times, associated to a continent-collisional setting by the subduction of the Paleo-Tethys underneath Laurasia, was followed by nappe stacking, crustal thickening and subsequent crustal collapse (**Fritz & Neubauer, 1993; Büttner, 2007**).
As a consequence of uplift and exhumation of the Moldanubian crust due to the Variscan northwest/southeast compression (**Zulauf, 1997**), the upper parts of the Variscan nappe pile were thrust southeastwards over the Moravian foreland. A process induced by the main Variscan Moravo-Moldanubian Phase (345-330 Ma), succeeded by the Bavarian Phase (330-315 Ma), characterized through reheating due to regional metamorphism (**Finger et al., 2007**).

The subsequent collapse of the Variscan crust was accompanied by the intrusion of late-to post-Variscan granitoids including the South Bohemian Pluton, which is dated to about 330-308 Ma (e.g. Weinsberger,- Eisgarner and Mauthausner Granites in lower Austria), (**Büttner, 2007)**.

Magmatic underplating as well as delamination of the lithospheric mantle is seen as the driving force for high-T/low-P metamorphism and the large scale plutonism in the southeastern Moldanubian zone (**Büttner & Kruhl, 1997**).

Following the consolidation of the Bohemian Massif due to the Variscan orogeny in late Paleozoic times, tectonic activity in the lower Mesozoic remained sparse. Middle Triassic to Late Bathonian sediments are absent from the area of the Bohemian Massif, which probably formed a coherent land mass supplying clastics to the adjacent sedimentary basins (**Malkovsky, 1987**).

Recurring tectonic activity associated with the Alpine orogeny reactivated Variscan structures in many cases due to its similar stress regime of generally north directed compression. Evidence for this process is given by brittle overprints of ductile, late-Variscan shear zones in southern Bohemia (e.g. Danube and Pfahl Shear Zone) (**Brandmayr et al., 1995, 1997**).

The present-day NW-and N-directed compressional stress field throughout the European Variscan Massif reflects a combination of Alpine collision and Atlantic ridge-push forces which came into evidence during the early Miocene and intensified further during the late Pliocene–early Quaternary (**Ziegler & Dèzes, 2007**).

2.3. Lithostratigraphic units of the Moldanubian Unit

The Moldanubian zone on Austrian and Czech territory between the Teplá-Barrandian unit in the northwest and the Moravian zone in the southeast is generally subdivided into three major geological units, comprising the Gföhl and Drosendorf metamorphic units, which represent pre-Variscan (Precambrian/Early Palaeozoic) crust, and the Variscan granitoids (**Fig, 3; Finger et al., 2007**)

The structural lower part of the Moldanubian nappe pile is represented by the parautochthonous Drosendorf Unit overlain by the allochthonous Gföhl Unit (Gföhl nappe complex). Furthermore the Drosendorf Unit is subdivided from bottom to top into a Monotonous series and a Variegated series, which is not commonly accepted, as some authors suggest the Monotonous series as a stand-alone unit (Ostrong Unit) underlying the Drosendorf nappe complex (e.g. **Fuchs, 1991; Büttner & Kruhl, 1997; Matura, 2003**).

Probably representing a part of Gondwana mainland, the Precambrian Monotonous series consists of uniform paragneisses with intercalations of quartzites, calcsilicates and amphibolites, separated from the Variegated series by a tectonic contact (**Büttner & Kruhl, 1997**). The younger, Paleozoic Variegated series comprises para-and orthogneisses, ultramafic rocks, micaschists, marbles, quartzites, graphitic rocks and amphibolites (**Hejl et al., 2003; Walter, 2007**).

At the top of the Moldanubian lithostratigraphic column, the allochthonous Gföhl nappe complex covers areas east of the South Bohemian Pluton and around České Budějovice in southern Bohemia. High-grade metamorphic conditions (up to granulite facies) define the Gföhl Unit (Gföhl gneiss and Gföhl granulite), consisting mainly of para-and orthogneisses, amphibolites, metagabbros, granulites and eclogites (**Walter, 2007**).

Following the formation and emplacement of these Moldanubian nappe units from Proterozoic to upper Paleozoic times, the widespread plutonic complexes of the Central and South Bohemian Batholith intruded syn-orogenic during the lower Carboniferous over a period of approximately 30-50 Ma (**Wessely, 2006; Büttner, 2007**).

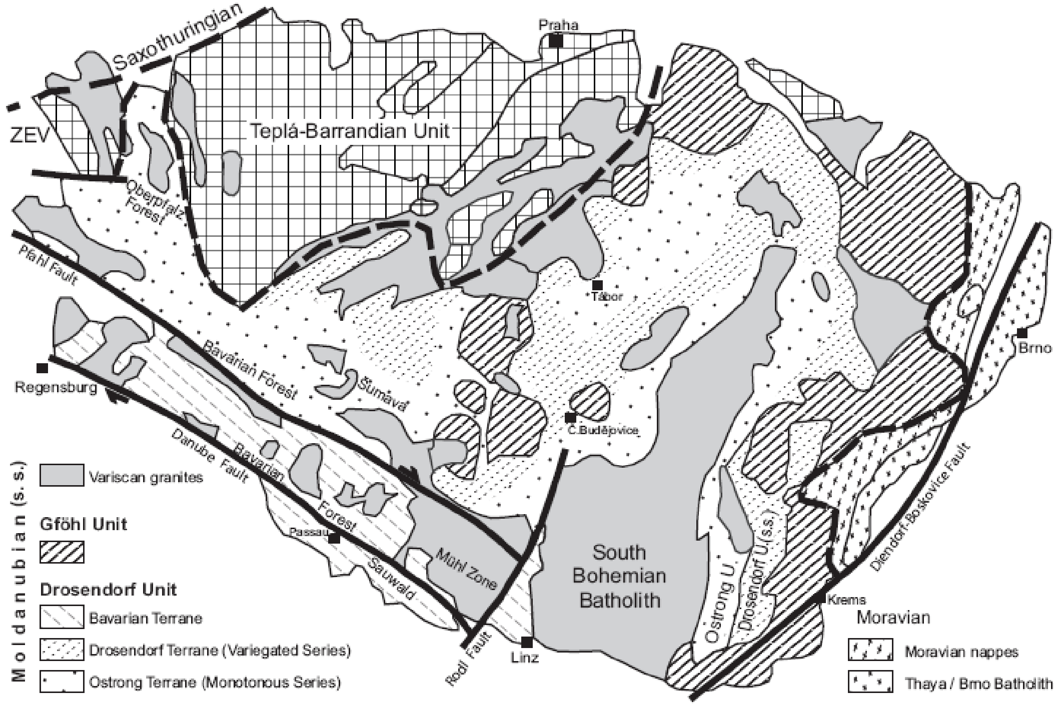

Fig. 3: Map of the lithostratigraphic units in central and southern Bohemia (**Finger et al., 2007**)

2.4. Permocarboniferous sediments in southern Bohemia

Only a few remnants of Permocarboniferous sediments are still present in southern Bohemia, representing the oldest sedimentary successions in this region. Siltstones and shalestones of late Palaeozoic origin represent continental sediments of the NNE-SSW trending intramontane depressions of the Bohemian Massif. In the Southern Bohemian Region these sediments exclusively occur in the 12 km broad Blanice Graben between Český Brod in the north and České Budějovice in the south (**Fig 4.**). The graben can be divided into three parts: a) northern part with outcrops near Český Brod and Kostelec nad Č. Lesy which represent the largest areal distribution of late Paleozoic sediments, b) central part with occurrences in the vicinity of Vlašim and Tábor, and c) southern part with outcrops near České Budějovice (including the Lhotice coal district) (**Chlupáč & Vrána, 1994**).

These Permocarboniferous sediments represent the periodic transport from the denuded part of the massif. Proluvial, deluvial, fluviatile, lacustrine, swamp and rarely eolian sediments were distinguished in the late Palaeozoic basins by **Holub & Tasler (1978)**. During periods of higher humidity in the Permian, pyroclastics and coal seams where deposited and red to reddish-brown sediments (red-bed type sediments) during arid periods. The Deposition of sediments started in the Upper Carboniferous (Gzhelian) and lasted till the Lower Permian (**Falke, 1972, 1975; Malkovský, 1987; Chlupáč & Vrána, 1994**).

To the northeast of České Budějovice, the Permocarboniferous occurs isolated in the asymmetrical Lhotice Basin of 18 km² between Lhotice and Jelmo (**Fig. 5**). With a depocenter of ca. 250 m, the Lhotice Basin is bounded by faults running in NNE-SSW direction of the Blanice Graben system and cross faults. Drillings near Vrato east of České Budějovice give evidence that Permocarboniferous sediments reach below the Cretaceous sediments of the Budejovice Basin. The Lhotice Basin is interpreted as a pull-apart basin, which emerged in the late Paleozoic due to the left lateral movement of the Blanice-Kaplice-Rodl Fault System **(Falke, 1972).**

The grabens and half-grabens associated with the Blanice-Kaplice-Rodl Fault System appear to be post-Variscan structures developed upon a slightly undulating surface of the early Bohemain Massif which had been deeply eroded to the granitic layer, forming much of the graben basement (**Jindrich, 1971**).

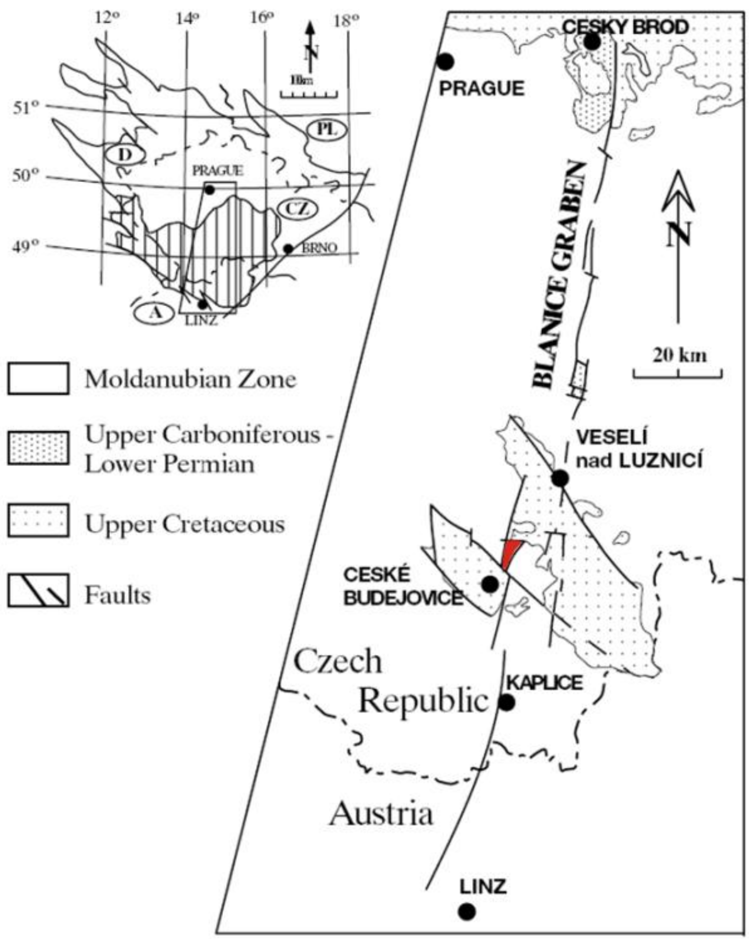

Fig. 4: Outline geological map of the southern Bohemian Massif showing the Blanice-Kaplice-Rodl-Fault zone. Lhotice Basin indicated in red. Vertical lines correspond to the exposed part of the Moldanubian Block (modified after **Kosler, 2001**).

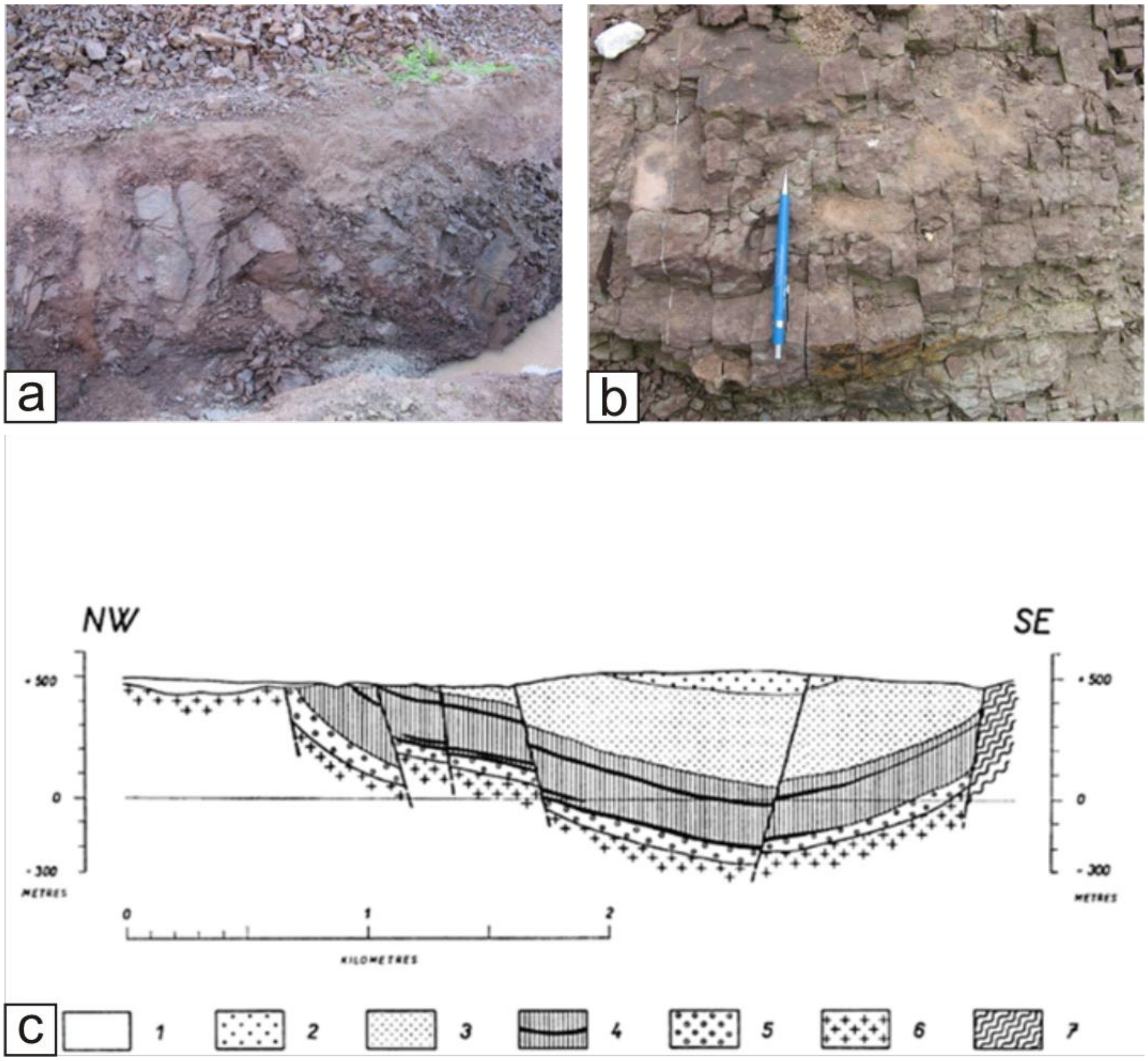

Fig: 5: a) Watersupply trench in Usilne in Permocarboniferous red shale and siltstone. **b)** Outcrop CP_011 southwest of Usilne exposing red siltstone and sandstone. Tension gashes indicate NE-SW directed extension. **c)** Geological cross-section through the southern part of the Permo-Carboniferous of the Blanice graben near České Budějovice between (Lhotice and Jelmo). 1 – Upper Cretaceous and Quaternary, 2 – reddish and variegated mudstones and sandstones (middle Lower Permian), 3 – reddish and variegated sandstones and mudstones with interbeds of micritic limestone (middle Lower Permian), 4 – grey complex, in the upper part faintly variegated, with 1-2 anthracite seams (Lower Permian), 5 – grey arkosic sandstones and conglomerates with silty and clayey intercalations and 1 antracite seam (Upper Gzhelian) 6 – granitic rocks 7 – metamorphics (gneiss and migmatite of the Moldanubicum) (modified after **Falke, 1972**).

2.5. Mesozoic and Cenozoic sedimentation

Following the consolidation of the Bohemian Massif and subsequent Permocarboniferous sedimentation (see chapter 2.4.) the time span from late Permian to early Triassic remained tectonically quiet. From middle Triassic to middle Jurassic the Bohemian Massif was uplifted due to an unknown mechanism (**Malkovsky, 1987**). During the Upper Jurassic, from Callovian to Tithonian, the NW–SE-trending Saxonian strait transected this high, thus linking the North German Basin with the Tethys shelves. However, this seaway was interrupted during the Early Cretaceous in response to wrench deformations, attributed to the build-up of pre- and syn-collisional compression in the foreland of the evolving Karpathian–East-Alpine orogen (**Ziegler & Dèzes, 2007**).

In the latest Jurassic and earliest Cretaceous, climatic conditions caused the lowering of the sea level. Combined with the uplift of the Bohemian Massif, these processes induced the closure of the Saxonian strait. The Permocarboniferous fault system was reactivated and convergent dextral wrench movements induced the deep truncation of Jurassic and Triassic strata. Thereby, up to 1500 m of sediments were eroded prior to the deposition of Middle to Upper Cretaceous Albian and Cenomanian sands (**Ziegler, 1990**). These Pre-Upper Cretaceous fluvial-lacustrine sediments, referred to as České Budějovice Formation consist of conglomerates, sandstones and shalestones. Marking the bottom of the stratigraphic column, the České Budějovice Formation covers the deeply weathered crystalline basin floor, or buries – only locally within the basin – relicts of Upper Paleozoic and Permo-Carboniferous sediments (**Huber, 2003**), (**Fig. 6**).

The main sedimentation started in the Upper Cretaceous with clastic, freshwater sediments of the Klikov-Formation. Due to the SE-directed drainage system in the Upper Cretaceous, the Klikov-Formation covered an area expanding into Austrian territory, were it is also known as "Gmündner Schichten". The sedimentary deposits of the Klikov-Formation represent the periodic transport from the denuded part of the Bohemian Massif. The presence of marine microplankton in the lower part of some cycles indicates shallow-marin influence, while the upper parts of the cycles are interpreted of fluviolacustrine origin (**McCann, 2008**).

Neogene	**Pliocene**	**Dacian**	**Ledenice Formation**
	Miocene	**Sarmatian**	**Domanin Formation**
		Upper Badenian	
		Lower Badenian	**Upper Mydlovary Formation**
		Karpathian	**Lower Mydlovary Formation**
		Ottnangian	**Zliv Formation**
Paleogene	**Oligocene**	**Lower Rupelian**	**Lipnice Formation**
		Lattorfian	
Cretaceous	**Upper Cretaceous**	**Upper Santonian**	**Upper Klikov Formation**
		Middle Santonian	
		Lower Santonian	**Lower Klikov Formation**
		Coniacian	
	Pre-Upper Cretaceous		**České Budějovice Formation**

Fig. 6: Stratigraphy of the Budějovice Basin (modified after **Šimůnek et al., 1995**)

Slánská 1976 described cyclothems reflecting relative stages of Uplift and Subsidence of the Basin in the Sedimentary succession of the Klikov Formation. The ideal cyclothem consists from bottom to top of light grey sandstone beds, red beds and grey beds. Light grey sandstone beds (A), forming the basal member of the cyclothem, are made up of course to medium grained conglomeratic sandstones, poorly sorted and sometimes cemented by siderite and limonite (**Fig. 7**). The middle part of a cyclothem consists of reddish-brown, poorly sorted sediments, principally conglomeratic muddy, fine to medium sandstones or conglomeratic, sandy mudstones and sandy claystones (B). Dark-grey sandstones (C) with variable amounts of carbonized plant debris and greenish grey claystones partly used in the local ceramic industry are forming the top member of each cyclothem (**Fig. 8; Fig. 9**), (**Slanska, 1976**).

Fig. 7: Sandpit near Hrdejovice (Outcrop CP_010) showing the basal member (A) of a cyclothem of the Klikov-Formation consisting of poorly sorted course to medium grained conglomeratic sandstones, partly cemented by siderite and limonite.

Fig. 8: Claypit north of Munice (Outcrop CP_002). The Reddish, greenish and grey claystones are typical for the top member (C) of the Klikov-Formation.

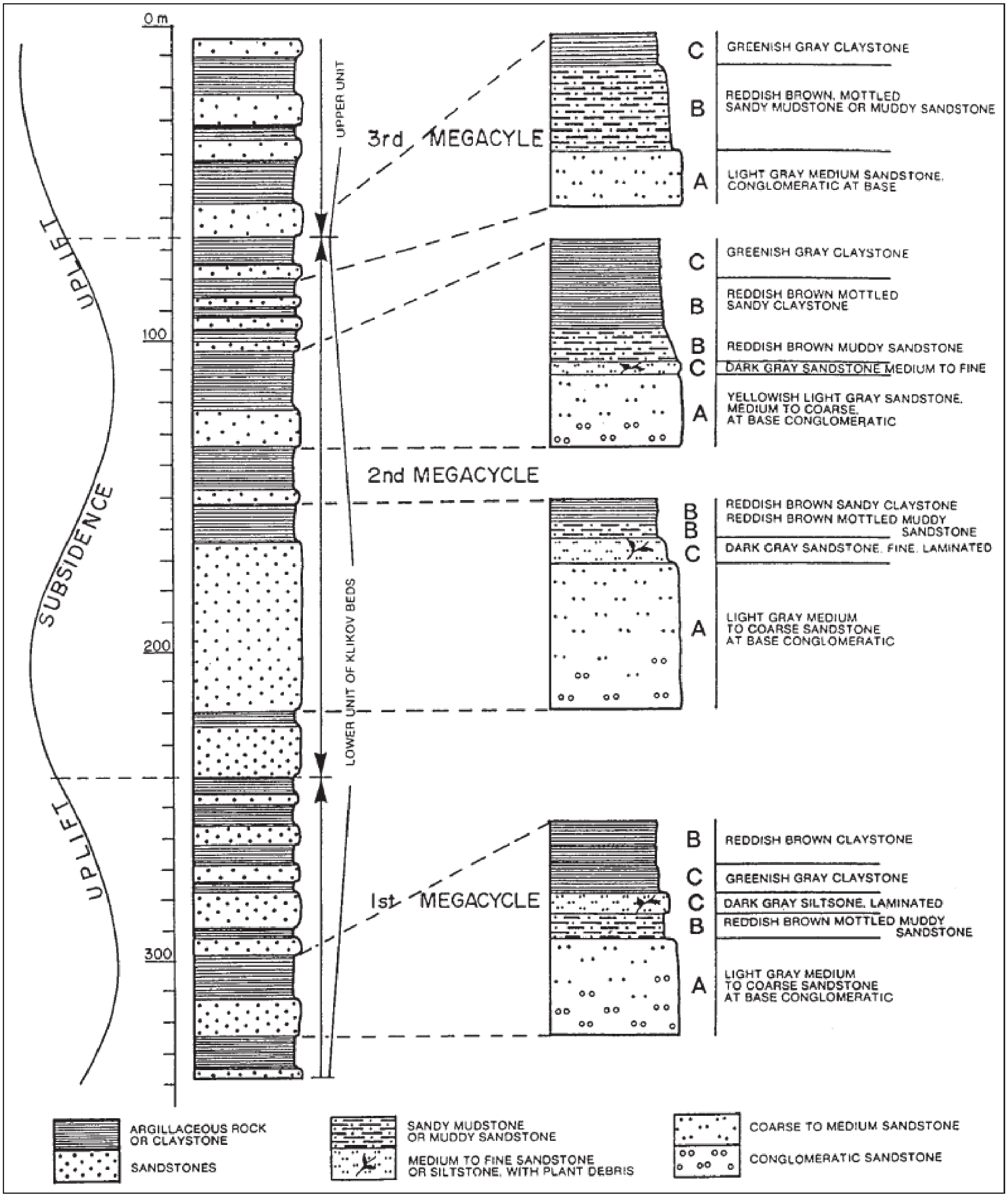

Fig. 9: Schematic profil of a common cyclothems of the Klikov-Formation (**Slanska, 1976**). For appreviations see Text above.

The Neogene filling of the basin is to be considered with respect to the drainage pattern during the middle Miocene, when a predominant part of Bohemia was drained into the Alpine-Karpathian foredeep to the SE. In the Pliocene the streams drained north- and southwards from the upheaving area of central Bohemia. The Paleogene Lipnice Formation, succeeding the Klikov Formation after a hiatus of approximately 30 Ma, is preserved only in relics, composed of fluviatile and lacustrine silicified sandstones. The following Zliv Formation marks the oldest Miocene unit, composed of silicified conglomerates and sandstones (**Fig. 10**). Ranging in thickness up to 80 m, the overlying Mydlovary Formation as the thickest and most extensive complex of Miocene sediments is composed of clays, diatomaceous earth and coal. The Badenian Transgression from the Alpine-Carpathian Foreland had a major influence on the deposition of the Mydlovary Formation. From the Tethys in the southeast, the sea advanced through the river valleys deep into the interior of the Bohemian Massif, resulting in the deposition of diatomites and temporary change to brackish conditions. The fresh-water Moldavite-bearing Domanin Formation, succeeding the Mydlovary Formation and overlying it partly, consists of psammites and psephites. Stratigraphically this complex corresponds probably to the earliest Sarmatian.

Fig. 10: Zliv-Formation near Mydlovary (Outcrop CP_013). Conglomerate with well-rounded Qtz-components (ca. 0,5 -2 cm in diameter) in sandy matrix.

The Pliocene Ledenice Formation, lying unconformably on the Mydlovary Formation as the youngest Miocene unit, is build up by fresh-water, generally lacustrine sediments (**Fig.11**), (**Suk, 1984; Chlupáč & Vrána, 1994**). Senonian to Pliocene sedimentation during the Alpine orogeny has previously been interpreted to be related to the episodic reactivation of Variscan NNE-and NW-striking faults zones mostly by vertical movements (**Váchal et al., 2010**).

Formation	ČESKO-BUDĚJOVICE FORMATION	KLIKOV FORMATION	LIPNICE FORMATION	ZLIV FORMATION	MYDLOVARY FORMATION	LEDENICE FORMATION
Age	Pre-Upper Cretaceous	Upper Cretaceous	Oligocene	Miocene(?Helvetian ?Carpathian)	Miocene (?Tortonian -?Pontian)	Pliocene
Main rock types	Conglomerates, sandstones, shales	Conglomerates, sandstones, mudstones, sandy and/or silty claystones	Gravels, sands, conglomerates (siliceous cement), sandstones, quartzite (quartz-limonite cement)	Conglomerates, sandstones (clayey quartz cement), sandy clays (silicified), volcanic conglomerate	Gravels, sands, sandstones, clays, claystones, diatomite, lignite, marl, tuffs, tuffites	Sands, sandy clays, diatomite
Cyclic sedimentation	Present	Pronounced	Absent	Absent	Absent	Absent
Main components of sand fractions	Quartz, orthoclase, plagioclase, muscovite, biotite, chlorite, calcite, plant fragments	Quartz, orthoclase, microcline, plagioclase, biotite, muscovite, chlorite, plant fragments	Quartz, minor feldspars (altered)	Quartz, pyroclastic material (volcanic glass), plant fragments, tests of diatoms	Quartz, feldspars, biotite, pyroclastic material	Quartz, tests of diatoms
Main components of clay	Mica, smectite, chlorite, kaolinite, limonite, silica	Kaolinite, illite, limonite, hematite, organic matter	Kaolinite, limonite, hematite, silica	Kaolinite, smectite, limonite, silica, organic matter	Kaolinite, smectite, illite, limonite, silica, calcite, organic matter	Kaolinite, illite, limonite
Siderite	-	Major amount	-	Accessory amount	Accessory am.	-
Calcite	Concretions, euhedral grains	-	-	-	Micrite (major amount in the Třeboň Basin)	-
Others	Anatase, biotite	Mineral of the crandallite group	-	-	Quartzine	-
Heavy minerals	Apatite, garnet, zircon, tourmaline, rutile	Zircon, tourmaline, rutile, kyanite, opaques, andalusite, staurolite, monazite, spinel. In places: corundum (VRÁNA,1991)	Zircon, tourmaline, rutile, kyanite, opaques, monazite, andalusite, staurolite, spinel	Zircon, tourmaline, rutile, kyanite, opaques, anatase, andalusite, garnet, clinozoisite, monazite, staurolite, sillimanite, spinel, sphene	Zircon, tourmaline, rutile, zoisite, kyanite, garnet, sillimanite, epidote, amphibole, etc.	-
Crystallinity of kaolinite	Poorly-ordered pseudomonoclinic	Well-orderded triclinic	Well-ordered triclinic to poorly-ordered pseudomonoclinic	Poorly-ordered pseudomonoclinic	Poorly-ordered pseudomonoclinic	Poorly-ordered pseudomonoclinic
Cement	Quartzose, carbonaceous	Ferrugineous (limonite, hematite, siderite), barite	Ferrugineous, quartzose	Ferrugineous, siliceous (opal), quartzose	Quartzose, ferrugineous, calcareous	Quartzose
Bedding type and other characteristic features	Cleavage, slickensided fractures, weak metamorphism	Massive, cross-bedding, graded bedding, horizontal	Horizontal	Undistinctive	Cross-bedding, horizontal	Horizontal
Environment and conditions of deposition	Lacustrine	Fluvial, lacustrine, alluvial fans, flood plains, river-channels, lakes	Lacustrine	Fluvio-lacustrine	Fluvio-lacustrine, river channels, overbank floods, backswamps, lakes	

Fig. 11: Lithostratigraphic units of the Budějovice Basin (**Huber, 2003**). The moldavite-bearing Domanin-Formation of upper Badenian/Sarmatian Age, overlying the Mydlovary Formation and underlying the Ledenice-Formation is not considered by the cited author.

2.6. The kinematic evolution of the southern Bohemian Massif

Previous geological studies concerning structural geology and especially paleostress determinations mostly concentrated on the northern, eastern and western parts of the Bohemian Massif (e.g. **Peterek et al., 1997; Adamovic & Coubal, 1999; Haviř, 2000, 2005; Pešková et al., 2010**).

In the southeastern section of the Bohemian Massif detailed investigations were done along the Moldanubian-Moravian thrust boundary zone (**Fritz & Neubauer, 1993; Fritz, 1996; Fritz et al., 1996** and references cited therein). The previously mentioned large-scale set of conjugate shear zones in southern Bohemia was widely discussed in **Wallbrecher et al., 1993** and **Brandmayr et al., 1995; 1997** (see Chapter 2.5).

In general, geological research with emphasis on structural geology was mostly restricted to the border areas of the Bohemian Massif with little attention paid to the central region with the South Bohemian Basins.

For the discontinuous and polyphase geological history of the Moldanubian sector in southern Bohemia (**Finger et al., 2007**) three deformation phases have been described so far for the tectonometamorphic/geodynamic evolution in scientific literature (e.g. **Büttner & Kruhl 1997; Büttner 2007; Zulauf et al., 1997, Zulauf 2001**).

Nappe stacking of the parautochthonous Drosendorf unit and the allochthonous Gföhl unit and their subsequent north-northeast directed thrusting onto the Ostrong unit under upper amphibolite to granulite facies conditions corresponds to the oldest deformational phase D_1 (**Büttner & Kruhl, 1997; Büttner 2007**). Defined by fabrics of the Drosendorf unit indicative for top-to-north and top-to-northeast kinematics, D_1 was subsequently followed by ductile flow in east-west direction (D_2). N-to NE compression (D_1) was converted into E-W compression (D_2) by clockwise rotation of the stressfield following the oblique collision of the Moldanubian indenter against the Bruno-Vistulian foreland (**Fritz, 1991; Fritz & Neubauer, 1993**). Generally associated with nappe stacking and thrust kinematics, D_1 and D_2 were mostly studied at the Moravo-Moldanubian border zone in the southeastern section of the Bohemian Massif, making it difficult to assess to what degree these deformation events affected the centre of the Modanubian Block.

The third deformation event D_3 clearly postdates Moldanubian nappe stacking and melt emplacement. It is characterized by Late-Variscan NNW-SSE directed compression and lower-greenschist to subgreenschist facies folding and thrusting in the centre of the Bohemian Massif (**Zulauf, 2001**). At the southwestern margin of the Moldanubian Unit, D_3 is manifested through strike-slip shearing and the formation of the dextral NW-striking Danube and Pfahl shear zones during Carboniferous to Permian times with possible brittle reactivation during the Alpine event (**Büttner, 2007**).

2.7. The Late-Variscan fault pattern in southern Bohemia

The major fault pattern in southern Bohemia is dominated by two major fault systems (**Fig. 12**) striking in NW-SE and NNE-SSW to NE-SW direction, respectively. The main structural framework of the Bohemian Massif is particularly dominated by NW-SE trending basement blocks following a broad zone of essentially NW-striking faults paralleling the direction of the Tornquist-Teisseyre Line, which forms the boundary between the stable Fennoscandian East European craton and the fragmented platform of Western Europe (**Malkovsky, 1987; Matte et al., 1990; Ziegler, 1990**).

The eastern part of southern Bohemia is dominated by NNE-SSW to NE-SW striking faults. From east to west those are the Diendorf-, Vitis-, Karlstift and Rodl-Kaplice-Blanice shear zone. In the western part of southern Bohemia, the Danube shear zone and the Pfahl shear zone represent the NW-SE striking fault systems. These faults moved with dextral (NW-SE) and sinistral (NNE-SSW to NE-SW) shear sense in the Paleozoic. This spatial tectonic framework is traditionally interpreted as a conjugated set of wrench faults by N-S directed compression during the Variscan orogeny, probably caused by indentation of an underlying crustal block moving to the north (**Wessely. 2006**).

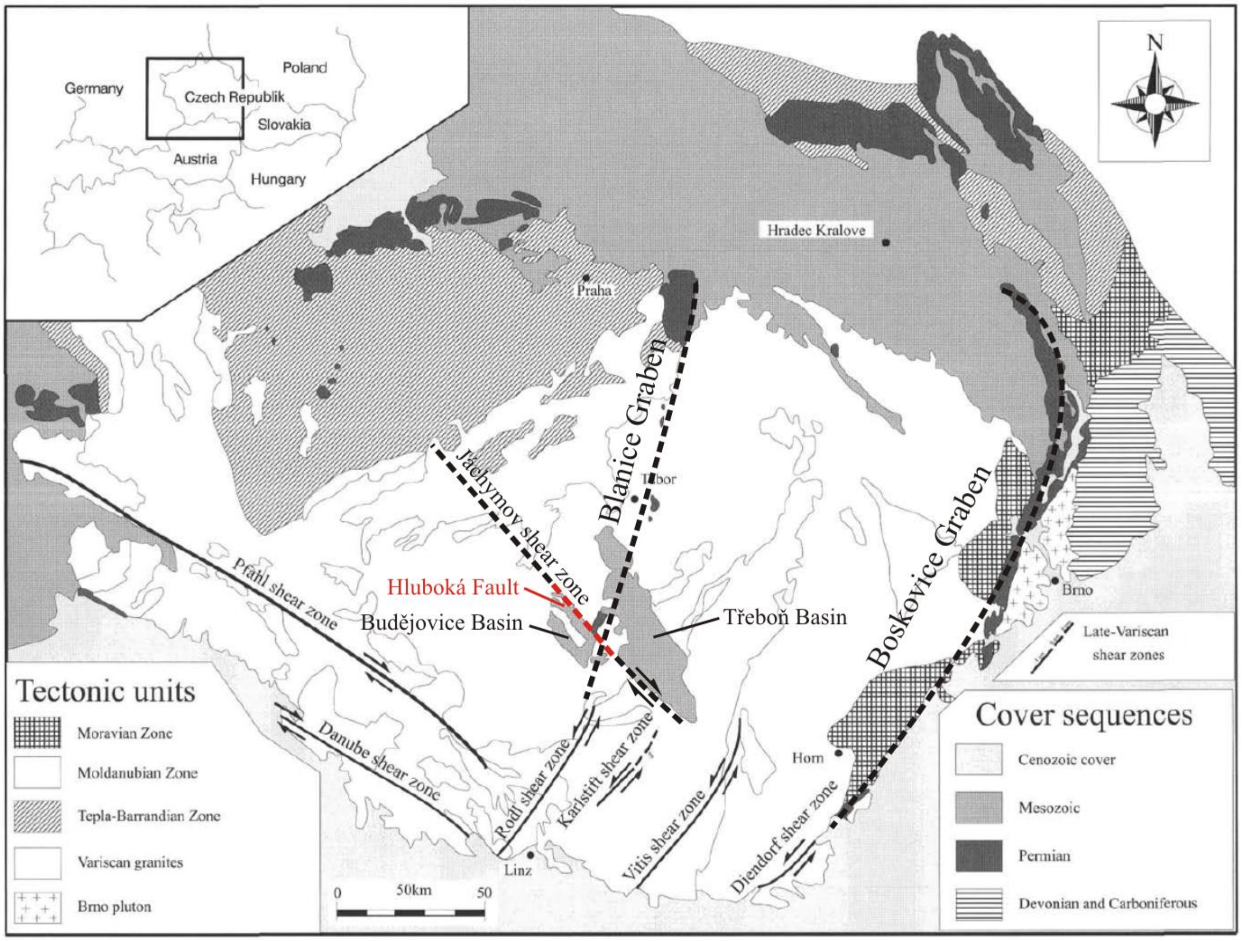

Fig. 12: Lithotectonic units and shear zones of the Southern Bohemian Massif. The continuation of the Rodl shear zone into the Blanice Graben and the Diendorf shear zone into the Boskovice Graben to the north are traced along the Permian deposits. The South Bohemian Basins with their mainly Mesozoic sedimentary fill are shown south of Tabor. Being part of the Jáchymov shear zone, the Hluboká Fault confines the Budějovice Basin to the NE (indicated in red) (**modified after Brandmayr et al., 1997**).

Dating of initial fault activity has been done by several authors (**Brandmayr et al., 1995, 1997; Wallbrecher et al., 1993**). $^{40}Ar/^{39}Ar$ muscovite cooling ages from mylonites of 287 Ma for the NW-SE-striking dextral systems and ca. 288-281 Ma for the NNE-SSW-striking sinistral fault systems indicate Lower-Permian deformation (**Brandmayr et al., 1995**). Dating upon microgranodiorite dykes emplaced along the Blanice-Kaplice-Rodl-Fault zone yielded intrusion ages of 270 Ma corresponding to this age of fault movements (**Kosler et al., 2001**)

Rb-Sr dating of muscovites from the southern part of the Rodl-Kaplice-Blanice-Fault Zone yielded ages of approximately 190 Ma, indicating partial Alpine rejuvenation of this ductile fault system (**Wallbrecher et al., 1993**).

An upper age limit for shear zone formation is given by Intrusion ages of 330 to 300 Ma for Late-Variscan granites as all shear zones crosscut various granite bodies (**Brandmayr et al., 1997**).

Two of the NNE-SSW striking shear zones (Rodl and Diendorf shear zone) extend further to the north merging with the NNE-striking Boskovice and Blanice Graben forming the Rodl-Kaplice-Blanice Fault zone and the Diendorf-Boskovice Fault zone. Extending from the east of Prague to Linz in Upper Austria, the Blanice-Kaplice-Rodl Fault zone is associated with a component of sinistral displacement of about 17 km (**Kosler, 2001**). A sinistral slip movement of at least 25 km is associated with the Diendorf-Boskovice Fault zone dissecting the Bruno-Vistulian Block from the Moravian Zone (**Mandl, 1999; Hejl et al., 2003**).

Shear zones are interpreted as corresponding kinematically to E/W oriented extension associated with N-S to NNW-SSE directed convergence.

3. Study Area

The area of interest is situated around the northeastern margin of the Budějovice Basin where the Hluboká Fault is featured as a linear topographic scarp with a height of up to about 80 m, extending over 15 km from Rudolfov in the Southeast to Mydlovary in the Northwest. Structural data were collected from 30 outcrops near the Hluboká and Zbudov fault scarp located in Moldanubian crystalline basement as well as Permocarboniferous, - Cretaceous and Miocene sedimentary deposits (**Fig. 13; Tab. 1**). The strategy of collecting structural data from rocks of different age should allow age dating of different deformation events with the “paleostress stratigraphy” method (**Kleinspehn et al., 1989**).

The inclination of the lowland area is directed south-eastwards with average elevations ranging from 395 m in the northwest to 375 m in the southeast, towards a basin with numerous lakes (**Vachal et al., 2010**).

From the southern edge of the basin two streams - Vltava and Malse - enter the lowlands and merge together in České Budějovice, leaving the basin at the northeastern margin near Hluboka nad Vltavou.

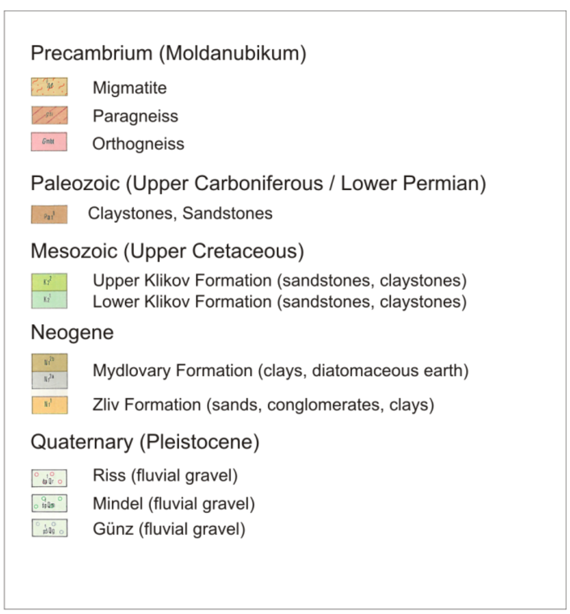

Fig.13: Left side and next page: Legend and geological map of study area with outcrops situated along the Hluboká Fault Zone.

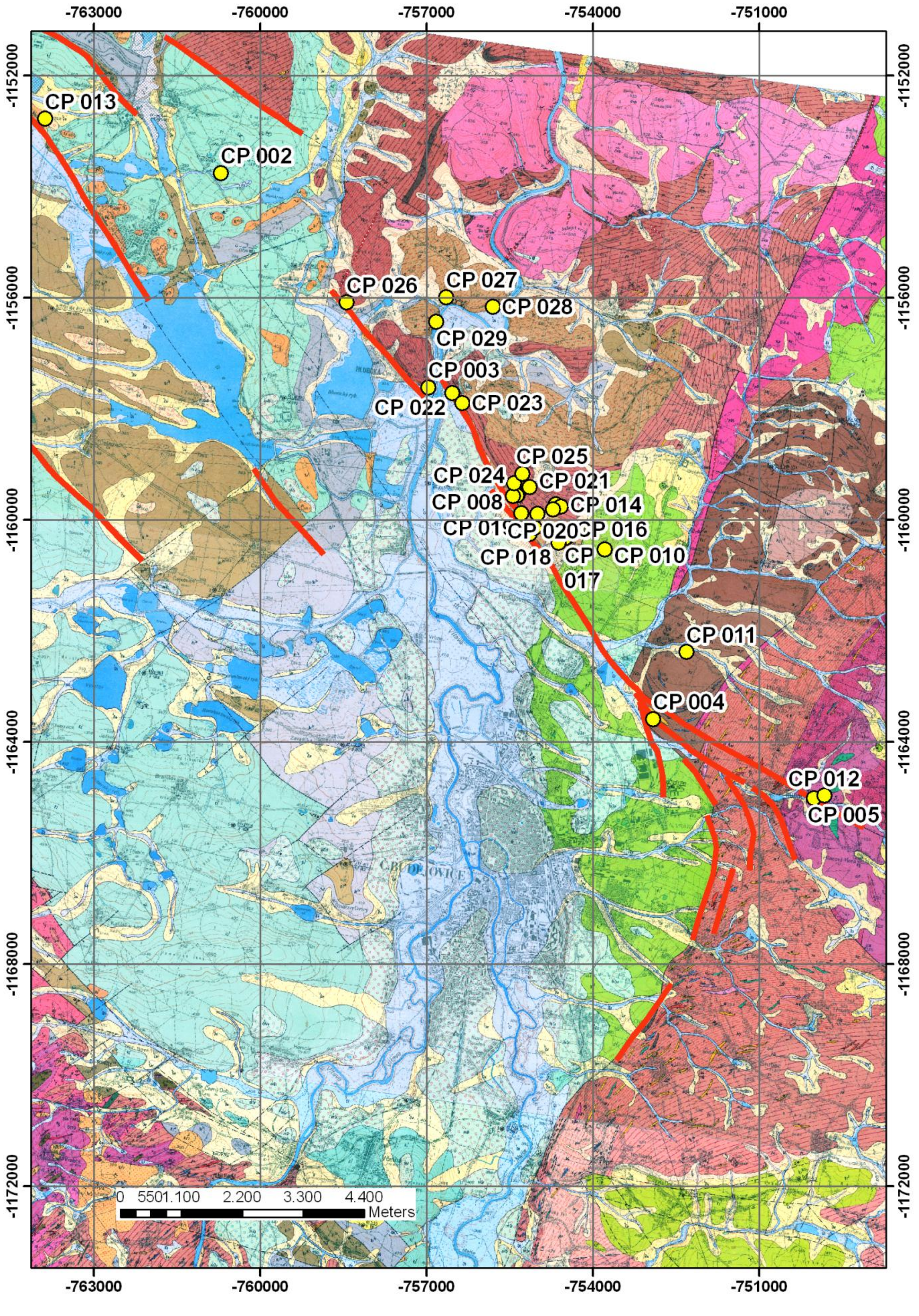
-763000
-760000
-757000
-754000
-751000
-1152000
-1156000
-1160000
-1164000
-1168000
-1172000
CP 013
CP 002
CP 026
CP 027
CP 028
CP 029
CP 003
CP 022
CP 023
CP 025
CP 024
CP 021
CP 008
CP 014
CP 01
CP 020
CP 016
CP 018
CP
017
CP 010
CP 011
CP 004
CP 012
CP 005
0 5501.100 2.200 3.300 4.400
Meters

Name	X	Y	Outcrop	Location	Tectonic Unit	Formation	Lithology	Remark
CP 001	49,03412	14,46845	Quarry	Hosín	Crystalline Basement	Variscan, Moldanubian crystalline	Phyllite, gneiss	Hluboka scarp
CP 002	49,07907	14,38524	Claypit	Munice	Budejovice basin	Klikov-Formation	Cretaceous sand, clay	
CP 003	49,04929	14,44304	Quarry	Hluboká nad Vltavou	Crystalline Basement	Variscan, Moldanubian crystalline	Phyllite, gneiss	
CP 004	49,00100	14,50897	Pit	Červený Vrch	Crystalline Basement	Variscan, Moldanubian crystalline	Amphibolite	
CP 005	48,99185	14,55086	Quarry	Rudolfov	Crystalline Basement	Variscan, Moldanubian crystalline	Amphibolite, Aplite	
CP 006	49,02799	14,47264	Quarry	Hosín	Crystalline Basement	Variscan, Moldanubian crystalline	Phyllite, gneiss	Hluboka scarp
CP 007	49,03388	14,46833	Creek	Hosín	Crystalline Basement	Variscan, Moldanubian crystalline	Phyllite, gneiss	Hluboka scarp
CP 008	49,03370	14,46731	Creek	Hosín	Crystalline Basement	Variscan, Moldanubian crystalline	Phyllite, gneiss	Hluboka scarp
CP 009	49,02914	14,47376	Quarry	Hosín	Crystalline Basement	Variscan, Moldanubian crystalline	Phyllite, gneiss	Hluboka scarp
CP 010	49,02713	14,49156	Sandpit	Hrdějovice	Budejovice basin	Klikov-Formation	Cretaceous quartz sand	
CP 011	49,01250	14,51491	Pond	Úsilné	Permocarboniferous basin		Permian - red shale and sandstone	
CP 012	48,99248	14,55334	Quarry	Rudolfov	Crystalline Basement	Variscan, Moldanubian crystalline	Amphibolite	
CP 013	49,08390	14,34033	Pit	Mydlovary	Budejovice basin	Mydlovary-Formation	Conglomerate	Zbudov fault
CP 013b	49,03333	14,47806	Creek	Hosín	Crystalline Basement	Variscan, Moldanubian crystalline	Phyllite, gneiss	Hluboka scarp
CP 014	49,03305	14,47944	Creek	Hosín	Crystalline Basement	Variscan, Moldanubian crystalline	Phyllite, gneiss	Hluboka scarp
CP 015	49,03250	14,47750	Creek	Hosín	Crystalline Basement	Variscan, Moldanubian crystalline	Phyllite, gneiss	Hluboka scarp
CP 016	49,02833	14,48194	Creek	Hrdějovice	Crystalline Basement	Variscan, Moldanubian crystalline	Phyllite, gneiss	Hluboka scarp
CP 017	49,02806	14,48139	Creek	Hrdějovice	Crystalline Basement	Variscan, Moldanubian crystalline	Phyllite, gneiss	Hluboka scarp
CP 018	49,02722	14,48000	Creek	Hrdějovice	Crystalline Basement	Variscan, Moldanubian crystalline	Phyllite, gneiss	Hluboka scarp
CP 019	49,03111	14,47000	Quarry	Hosín	Crystalline Basement	Variscan, Moldanubian crystalline	Phyllite, gneiss	Hluboka scarp
CP 020	49,03139	14,47389	Quarry	Hosín	Crystalline Basement	Variscan, Moldanubian crystalline	Phyllite, gneiss	Hluboka scarp
CP 021	49,03556	14,47111	Creek	Hosín	Crystalline Basement	Variscan, Moldanubian crystalline	Phyllite, gneiss	Hluboka scarp
CP 022	49,04889	14,44917	Quarry	Hluboká nad Vltavou	Crystalline Basement	Variscan, Moldanubian crystalline	Phyllite, gneiss	Hluboka scarp
CP 023	49,04750	14,45194	Quarry	Hluboká nad Vltavou	Crystalline Basement	Variscan, Moldanubian crystalline	Phyllite, gneiss	Hluboka scarp
CP 024	49,03583	14,46722	Creek	Hosín	Crystalline Basement	Variscan, Moldanubian crystalline	Phyllite, gneiss	Hluboka scarp
CP 025	49,03750	14,46889	Quarry	Hosín	Crystalline Basement	Variscan, Moldanubian crystalline	Phyllite, gneiss	Hluboka scarp
CP 026	49,06111	14,42028	Quarry	Munice	Crystalline Basement	Variscan, Moldanubian crystalline	Phyllite, gneiss	Hluboka scarp
CP 027	49,06417	14,44444	Quarry	Hluboká nad Vltavou	Crystalline Basement	Variscan, Moldanubian crystalline	Phyllite, gneiss	
CP 028	49,06361	14,45611	Quarry	Hluboká nad Vltavou	Crystalline Basement	Variscan, Moldanubian crystalline	Phyllite, gneiss	
CP 029	49,06000	14,44278	Quarry	Hluboká nad Vltavou	Crystalline Basement	Variscan, Moldanubian crystalline	Phyllite, gneiss	

Table 1: Complete outrcoplist

3.1. Structural data

Only a few of the investigated outcrops will be addressed in this chapter, due to the fact that most outcrops were extensively weathered lacking good structural data and particularly, fault slip data. In some cases only foliation and lithology could be recorded. Collected structural data are displayed in Schmidt equal area plots of the lower-hemisphere. For a better graphic discrimination between ductile and brittle features, ductile features like foliations, folds, ductile stretching lineations and crenulations are colored in red in contrast to brittle features indicated in black. Complete, polygenetic datasets were manually separated into cogenetic subsets potentially characterizing the same tectonic regime (**Fig. 14**).

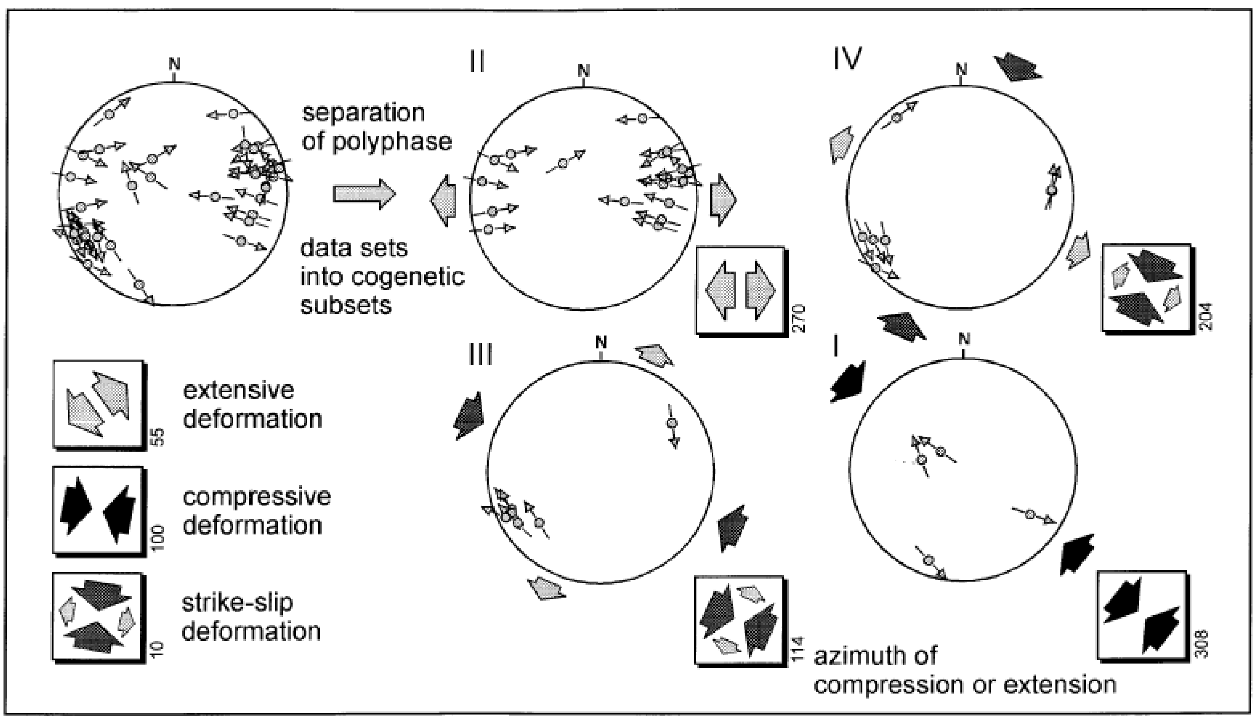

Fig. 14: Separation of polyphase datasets into cogenetic subsets (**from Peterek et al., 1997**)

Throughout the investigation area at the northeastern margin of the Budějovice Basin foliation of the Moldanubian basement strikes NW-SE, dipping steeply to SW towards the basin, suggesting that the orientation of the Hluboká Fault is predefined by Variscan structural anisotropies.

3.1.1. CP_001

Outcrop CP_001 is located southwest of Hosin in the crystalline basement at the starting point of the Hosin seismic 2D section (see chapter 4.2.). Even though deeply weathered a shear zone about 20 m in size striking parallel to the Hluboká Fault in NW-SE direction could be detected (**Fig. 15**). Measured faults could be separated into three different fault types, characterized by brittle NW-SE striking strike-slip faults with lunate fractures and syntethic Riedel shears indicating right lateral displacement; SW-dipping, ductile normal faults and NE-dipping, brittle normal faults (**Fig. 16**).

Lower greenschistfacies conditions are estimated for SW-dipping normal faults, which show ductile, synkinematic quartz depicting stretching lineations.

Fig. 15: Brittle fault zone in Bt-Ms-Paragneis with slightly W-dipping, sub-horizontal foliation (outcrop CP_001, Variscan, Moldanubian crystalline; viewing direction: SW).

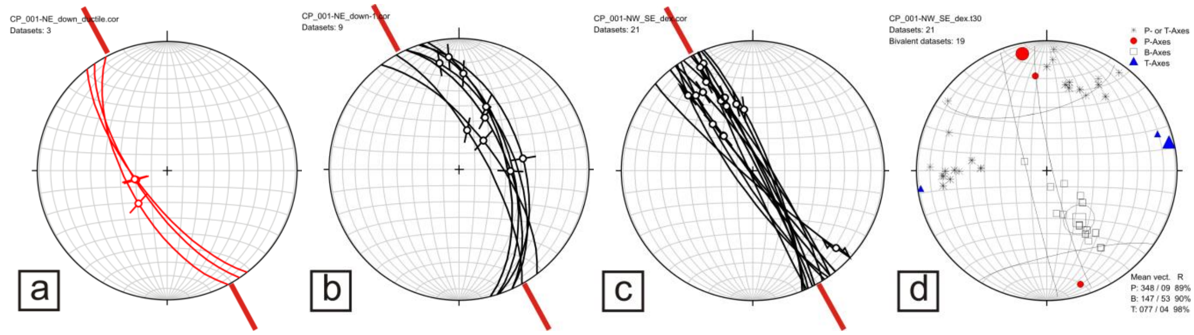

Fig.16: Sorted datasets displaying SW-directed, ductile extension (**a**), NE-directed, brittle extension (**b**), NW-striking, dextral strike-slip faulting (**c**), and calculated Pt-axes for dextral strike-slip faulting indicating subhorizontal NNW-directed shortening (**d**). (Outcrop CP_001, apparent strike of Hluboká Fault indicated by red lines).

3.1.2. CP_002

Outcrop CP_002 is located in a large claypit near Munice close to the presumed continuation of the Hluboká Fault to the NW. Grey, silty marls intercalated with red shale, 3 cm thick siltstone beds and 5-10 cm thick yellow-brownish middle sand layers are present, depicting the top section of the Upper Cretaceous Klikov Formation (**Fig. 17**; see also chapter 2). Abundant polished slickensides in shale show evidence for normal displacement mostly induced by gravitationally driven compaction. Nevertheless, two datasets indicating SW-NE directed extension by the presence of normal faults and NW-trending strike-slip faults could be recorded (**Fig.18**).

Fig. 17: Horizontally bedded clays, siltstones and middle sands of the Upper Klikov-Fm (oupcrop CP_002).

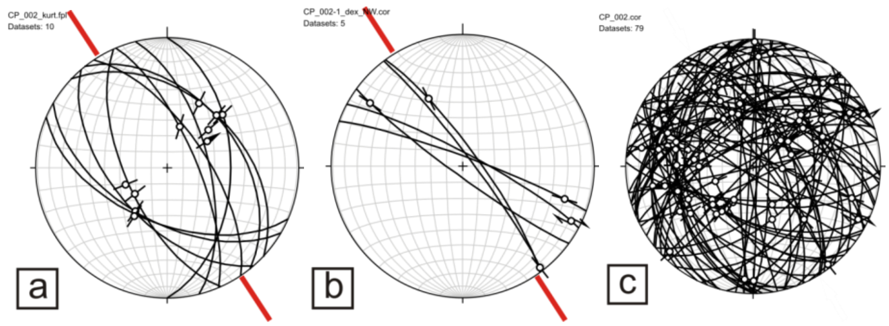

Fig. 18: NE-SW dipping normal faults (**a**) and two datasets indicating strike slip faulting (**b**), paralleling the strike of the Hluboká Fault, could be separated from the complete dataset (**c**), (outcrop CP_002).

3.1.3. CP_003

Located in the centre of Hluboká nad Vltavou and build up by micaschists, CP_003 is dominated by NW-striking, dextral strike-slip faults, paralleling the direction of ductile structures like chlorite stretching lineations and fold axes. A dataset of two slickensides indicates top-to-NE-directed normal faulting under greenschist facies conditions by the presence of chlorite stretching lineation. Several NE-SW striking faults are oriented parallel to a map scale fault, which probably displaces the Hluboká Fault for about 500m in southwestern direction and forming a passage way for the Vltava river (**Fig. 19; Fig. 20**).

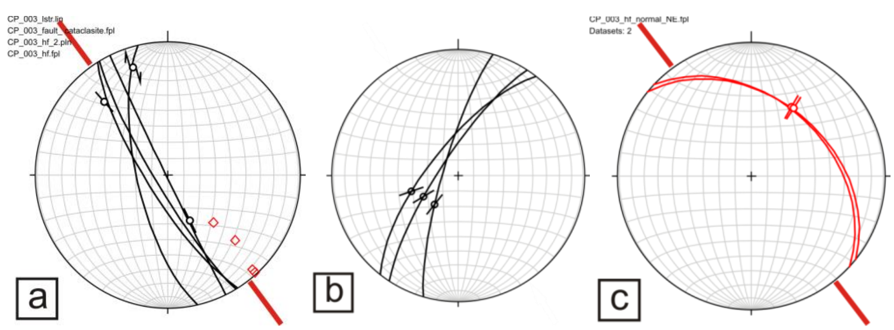

Fig. 19: Dextral strike-slip faults paralleling the strike of ductile stretching lineations (lstr, plotted as ◊) (**a**), NE-striking, sub-vertical faults associated with the possible displacement of the Hluboká Fault in southwestern direction (**b**), Greenschist facies, NE-dipping normal faults with Chl-mineralization (**c**), (outcrop CP_003).

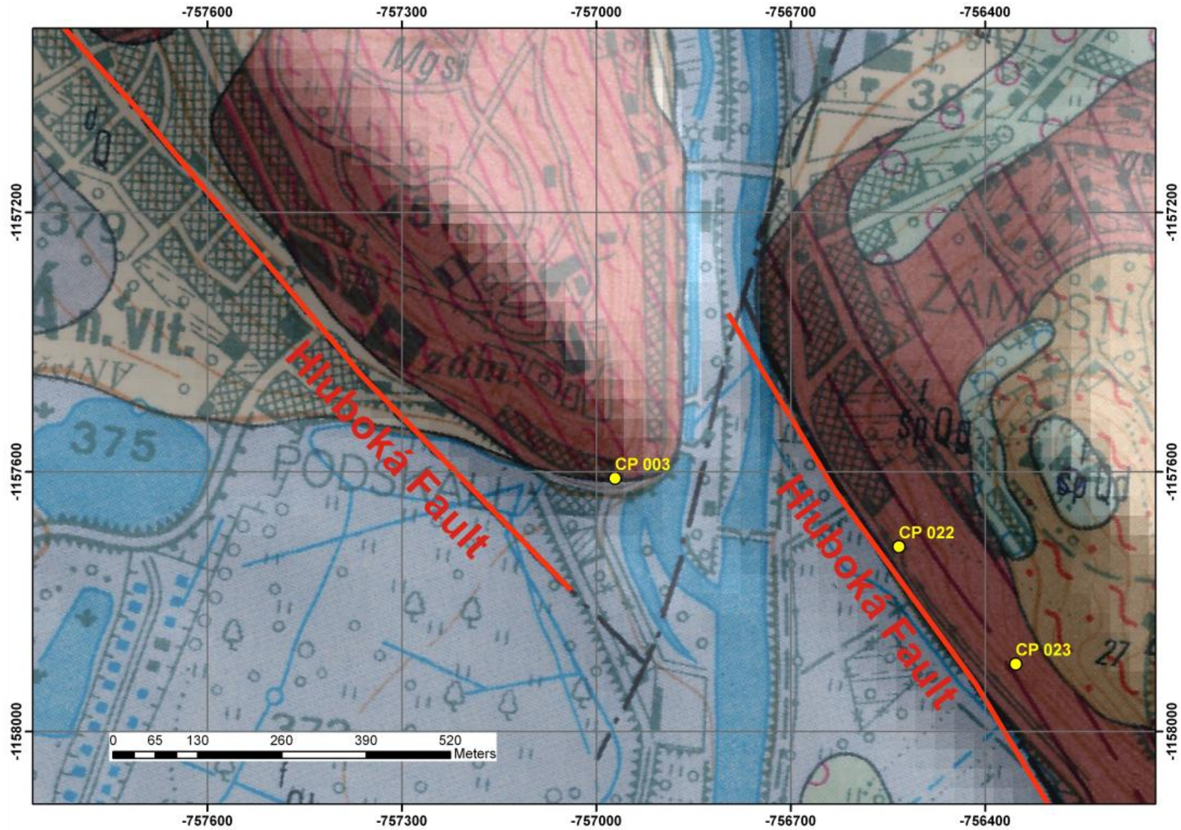

Fig. 20: Geological map displaying the location of CP_003 between the offset of the Hluboká Fault across the strike.

3.1.4. CP_004

CP_004 is located about 400 m SE of the Usilne seismic section (see chapter 4.1.) where the Hluboká Fault splits up into several splay faults, which are all associated with prominent morphological scarps. At the top of one of those scarps (Cherveny Vrch) the outcrop resides in the centre of a small, NW-trending tectonic window composed of amphibolites and aplites surrounded by Permocarboniferous deposits of the Lhotice Basin (see chapter 2.4.). Evidence for W-WSW directed extension is given by normal faults roughly trending N-S. Three fault planes striking NW-SE indicate oblique strike-slip shearing in this outcrop as well (**Fig. 21**).

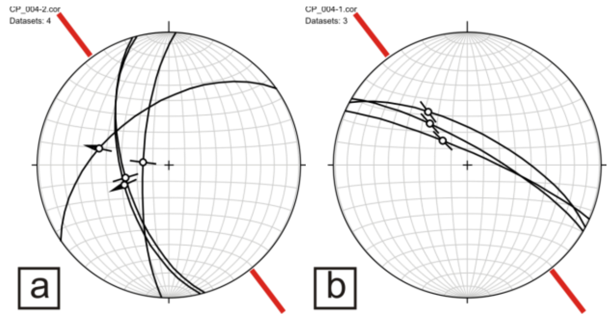

Fig. 21: Datasets reflecting W-WSW-directed extension (**a**) and NW-striking, oblique strike slip faults (**b**), (outcrop CP_004).

3.1.5. CP_005

Situated at the southeastern end of the investigation area near Rudolfov in Variscan crystalline basement close to CP_012 (**Fig. 13**), CP_005 exposes amphibolites and an aplitic intrusive dyke. Both lithologies are deliminated from each other by a ductile fault striking WNW-ESE (**Fig. 22/a**). Dextral offset of about 1 cm was observed at this shear zone. The outcrop also exposes two, apparently younger NE-SW-striking normal faults striking perpendicular to the dextral shear zone. Structures depict ductile faulting for these faults as well (**Fig. 22/b**). Furthermore, ductile stretching lineations in a shear band defined by elongated quartz and muscovite indicate greenschist facies metamorphic conditions associated with the late Variscan cooling phase of the Moldanubian units (**Fig. 22/b & Fig. 23**).

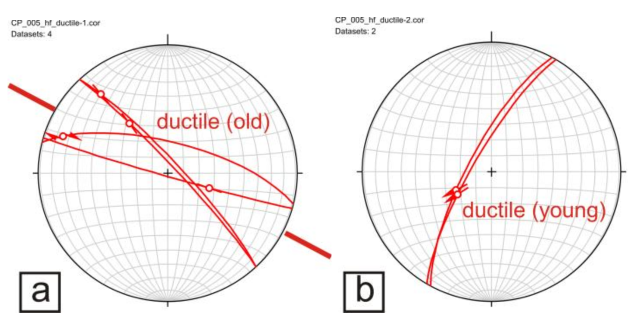

Fig. 22: Late variscan, ductile strike-slip faulting (**a**) and SW-directed normal faulting (**b**), (outcrop CP_005).

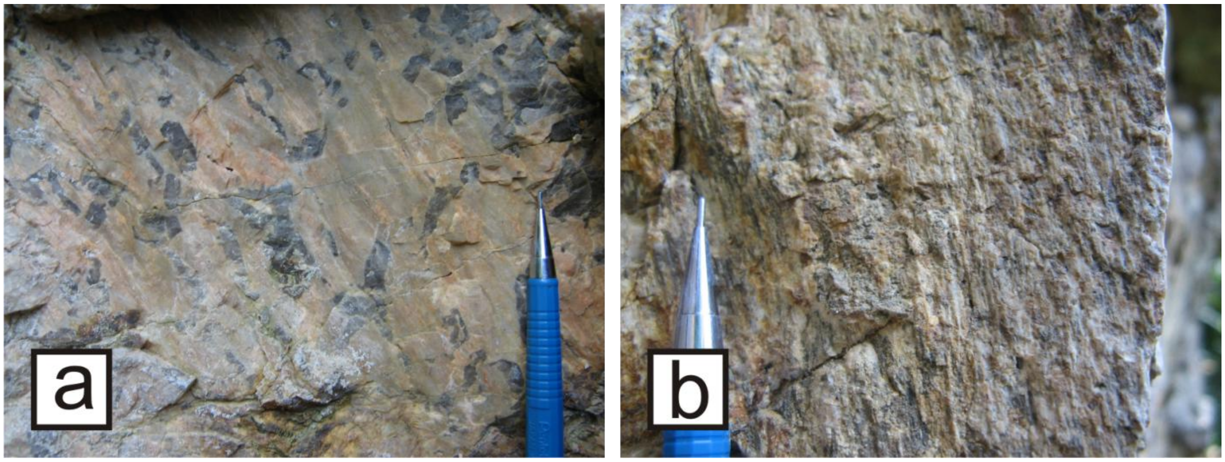

Fig.23: Aplitic intrusion with quartz (**a**) and shear band with ductile stretching lineations defined by quartz and muscovite (**b**), (outcrop CP_005, Variscan, Moldanubian crystalline).

3.1.6. CP_006

Located in Bt-Mu-Gneiss of the crystalline basement, three fault sets were discovered displaying brittle and ductile deformation in this outcrop. Ductile structures include muscovite stretching lineations suggesting NW-SE-directed extension (**Fig 24/a**). Idiomorphic quartz crystals grown into open tension gashes at a SW-dipping normal fault indicate late-Variscan SW-directed extension. Brittle deformation structures include SW-dipping normal faults (**Fig. 24/b**) and oblique dextral strike-slip faults striking NE-SW (**Fig. 24/c**). The former ones define a structure of two overstepping normal faults in some way resembling a breached relay ramp and marking the most striking feature in this outcrop (**Fig. 25**).

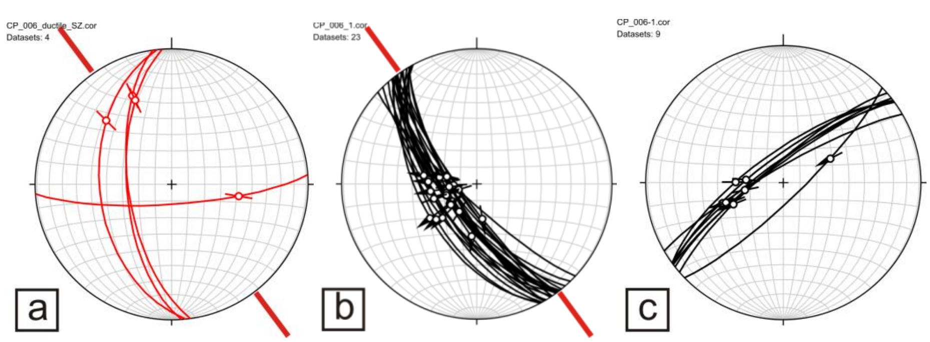

Fig. 24: Ductile normal faults related to NW-SE directed extension (**a**), SW-dipping, brittle normal faults (**b**) and oblique, dextral NE-directed strike-slip faults (**c**), (outcrop CP_006).

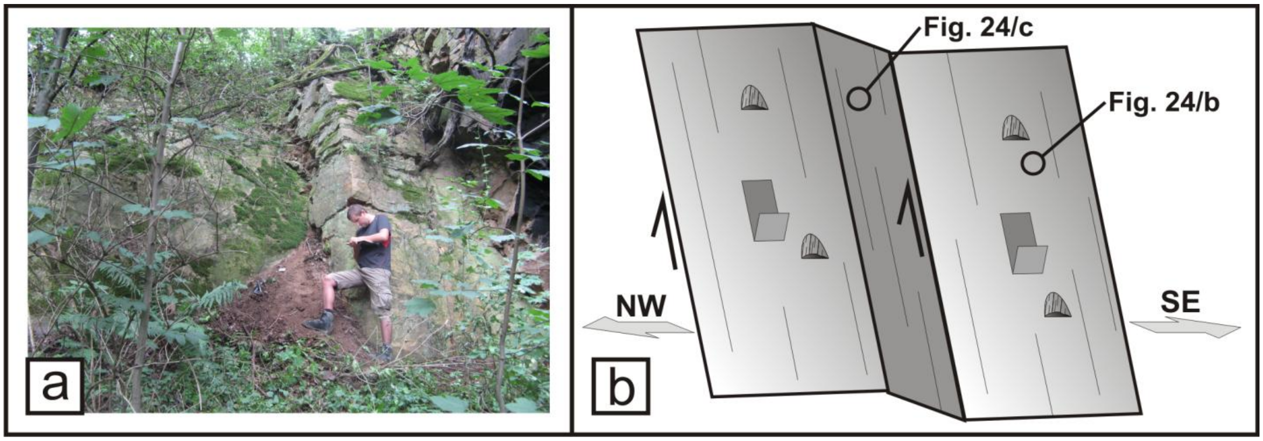

Fig. 25: Outcrop CP_006 (**a**) and sketch map of overstepping normal faults (**b; Fig. 24/b**). Lunate fractures give evidence for normal displacement (Variscan, Moldanubian crystalline).

3.1.7. CP_009

Located about 200 m further uphill to the NE of CP_006, this outcrop exposes a large SW-dipping brittle normal fault. The centre of the fault consists of a cataclasite-clay gouge band characterized by angular rock fragments in a light-grey shale matrix. Furthermore, the fault core hosts a mylonite composed mainly of quartz and associated with greenschistfacies metamorphic conditions (**Fig. 26,** see also chapter 3.2.)

Lineations and shear sense indicators were found in the cataclastic fault zone and in the mylonite, indicating two phases of fault activity. An older phase of ductile deformation is represented by the mylonite and gives evidence for normal faulting in northwestern direction. Information obtained from the cataclastic zone denotes subsequently brittle reactivation of ductile structures (shear bands) by normal faulting in southwestern direction (**Fig. 27/a**).

A feature worth mentioning beside the shear zone at this location is the presence of sub-vertical joints paralleling the strike of the Hluboká Fault. Unfortunately, their kinematics remained unresolved due to the absence of mineralizations and striations that would have been needed to assess their past tectonic activity.

Fig. 26: Shear zone at outcrop CP_009 in crystalline basement (**a**), cataclasite-clay gouge band (**b**) and mylonite (**c**), (outcrop CP_009, leucocratic Migmatite).

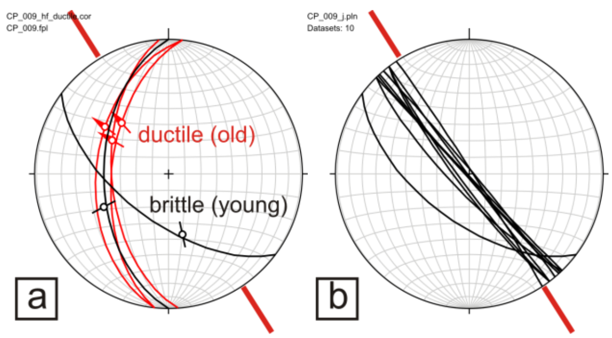

Fig.27: Ductile NW-directed and brittle SE-directed normal faulting (**a**). Sub-vertical joints striking NW-SE (**b**), (outcrop CP_009).

3.1.8. CP_010

CP_010 is located in a large sandpit in the forest northeast of Hrdejovice. Its sedimentary succession is dominated by poorly sorted, white-to white-grey, course grained sands and few conglomerate layers with components up to 4 cm in size. Components are exclusively angular to sub-rounded and well-rounded quartz grains are partly cemented by siderite and limonite. Sedimentary structures including large-scale cross-bedding indicate the formation under fluvial conditions, in this case depicting the lower part of the Upper Cretaceous Klikov-Formation (see chapter 2.).

Observed structural features include deformation bands and joints, both clearly discriminated from the surrounding white-grey sands by their dark red colors (**Fig. 28**). Joints are oriented at an angle of approximately 20° with respect to the strike of the

Hluboká Fault (**Fig. 29/a**). The geometry of the deformation bands is further compatible with the orientations of syn-and antithetic Riedel shears in a NW-striking, dextral shear zone. “Synthetic” deformation bands are paralleling the joints described above. Both sets are most likely associated with N-S directed compression (**Fig. 29/b**).

Fig. 28: Deformation bands in course grained conglomeratic sand (**a** & **b**) and sandstone block cemented by siderite/limonite (**c**), (outcrop CP_010, Lower Klikov Fm.).)

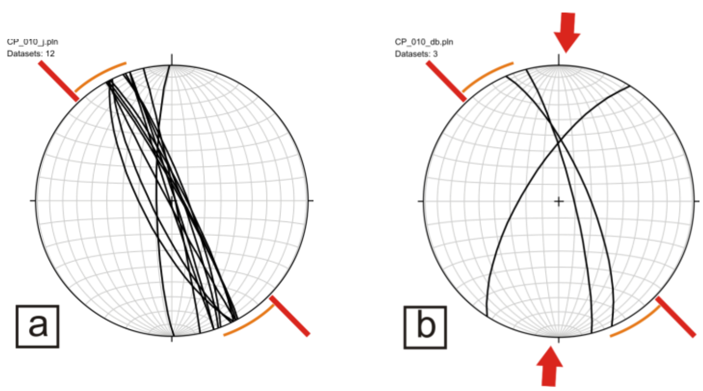

Fig. 29: Joints paralleling the strike of the Hluboká Fault (**a**). Conjugated set of deformation bands probably related to N-S directed compression (**b**), (outcrop CP_010).

3.1.9. CP_011

The only outcrop analysed from the Permocarboniferous shale-siltstone is located in the southwestern section of the Lhotice Basin (see chapter 2.4.). It contains structural features including calcite filled tension gashes, abundant normal faults with fibrous calcite slickensides and dextral strike-slip faults (**Fig. 30**).

SW-NE and SSW-NNE-directed extension is indicated by the orientation of tension gashes and normal faults, respectively (**Fig. 31/a & b**). The WNW-striking dextral faults are sub-parallel to the Hluboká Fault in this area (**Fig. 31/c**).

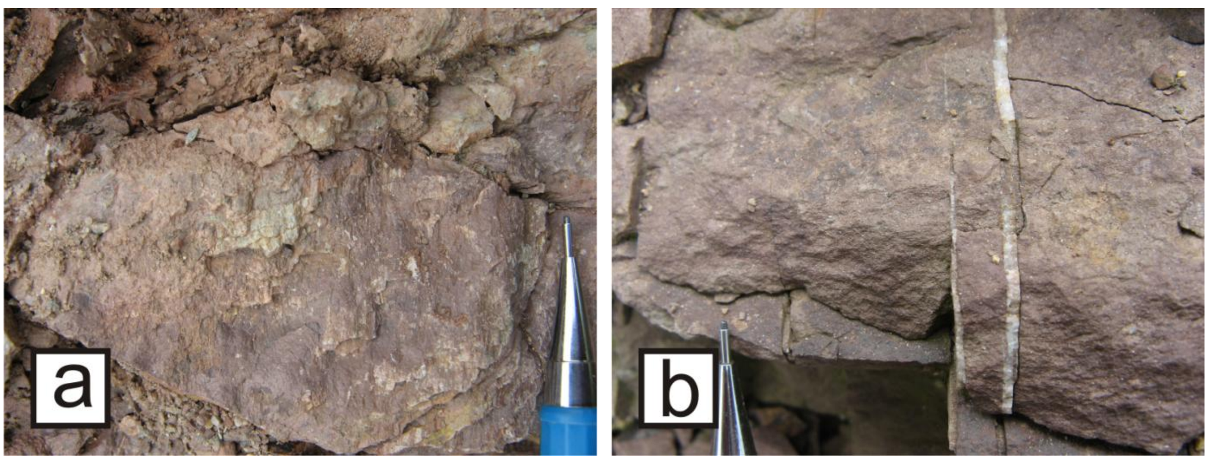

Fig. 30: Fibrous slickensides on a normal fault (**a**) and calcite filled tension gashes in Permocarboniferous siltstones (**b**), (outcrop CP_011).

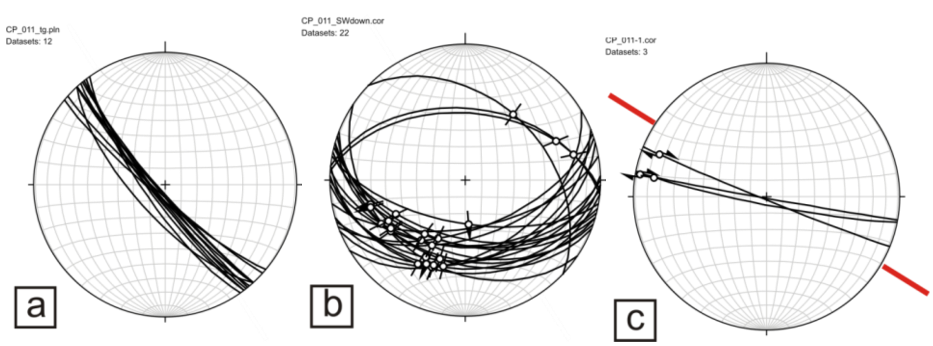

Fig. 31: Tension gashes (**a**), normal faults (**b**; also observed in outcrop Cp_012, Fig. 33/a) and dextral strike-slip faults (**c**), (outcrop CP_011).

3.1.10. CP_012

Located closely to the east of CP_005, the most striking feature in this outcrop is the presence of ductile and brittle-ductile faults. Mineralizations of quartz and chlorite along faults are significant for low metamorphic conditions ranging from greenschist facies to the brittle-ductile transition zone. Structural features in general include ductile strike-slip faults with dextral sense of shear striking NW- SE and E-W respectively, SE-dipping ductile faults with vertical striations and SW-dipping normal faults (also observed in CP_011, **Fig. 31/b**) partly overprinted by quartz slickenlines (**Fig. 32 & Fig 33**)

Two generations of quartz and chlorite stretching lineations further indicate an older stage of SW-directed extension subsequently followed by SSW-directed normal faulting.

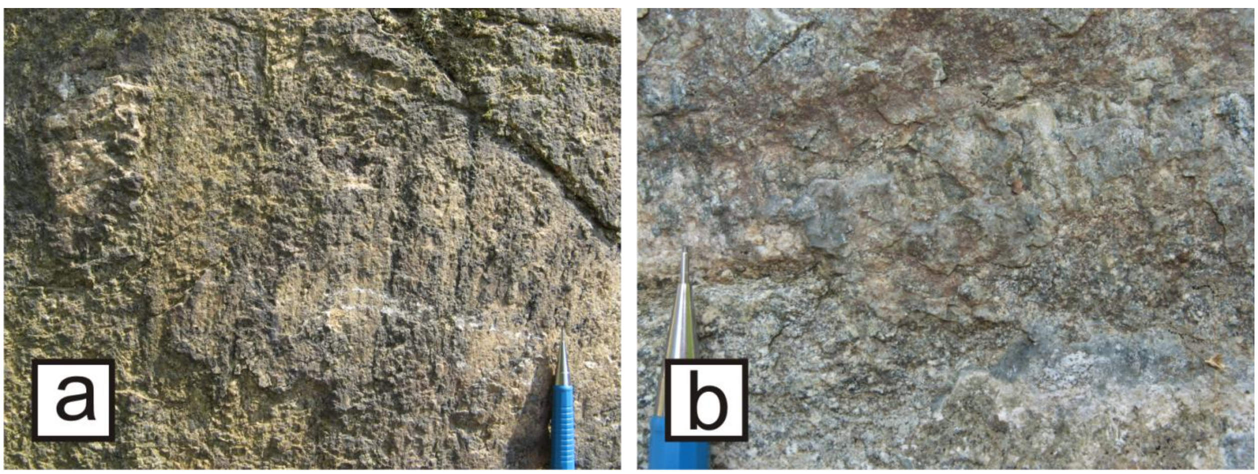

Fig. 32: Older stretching lineation (greenschistfacies) overprinted by younger quartz-slickenline (**a**), synkinematic quartz and chlorite on the slickenside of a brittle-ductile fault (**b**), (outcrop CP_012, Variscan, Moldanubian crystalline)

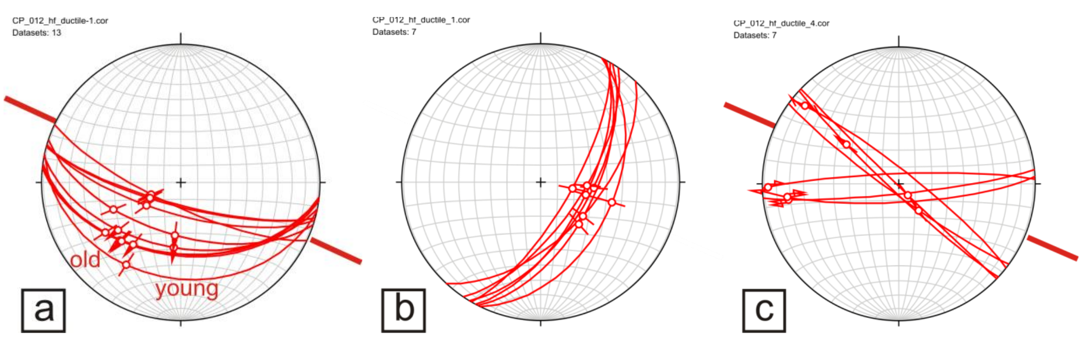

Fig. 33: SW-and SE-dipping ductile normal faults (**a** & **b**) and ductile, dextral strike-slip faults related to NW-directed compression (**c**), (outcrop CP_012).

3.1.11. CP_013

CP_013 is located near Mydlovary at the northwestern end of the investigation area. The small pit exposes conglomerate composed of well-rounded quartz components (0.5-2 cm) in a sandy matrix. Throughout the whole study area, CP_013 marks the only spot along the Hluboká and Zbudov Fault where structural data could be obtained from sediments of the Lower Miocene Zliv-Formation.

Recorded structures include steep vertical, NW-striking fault planes hosting a 2 cm thick cataclasite coated in red shale. Riedel shears denote right-lateral displacement, indicating dextral strike-slip faulting for the adjacent Zbudov Fault as well (**Fig. 34**)

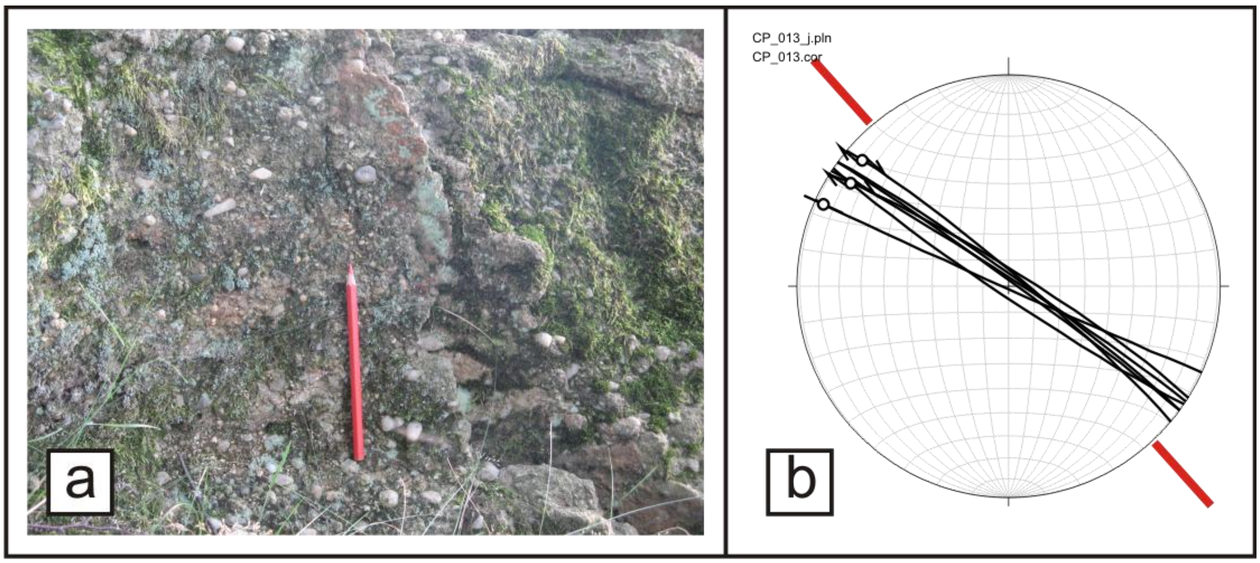

Fig. 34: Dextral strike-slip fault in Miocene conglomerate coated by reddish cataclasite (**a**). Dataset indicates strike-slip faulting in Miocene times as well (**b**), (outcrop CP_013; Zliv Fm., apparent strike of Zbudov Fault indicated by red lines).

3.2. Thin Section interpretation

Samples for thin sections were taken from 4 different outcrops (CP_001, CP_006, CP_007, CP_009), which are all situated in the Variscan crystalline basement southeast of Hluboká nad Vltavou near the village of Hosin. Orientated samples were cut in the XZ-plane of the mesoscopic structural framework, in which the XY-plane refers to the foliation or fault plane and X to the direction of the stretching lineation of the mylonites and slickensides, respectively. Micro-images of the thin sections were taken with a LEICA DM 4500 Microscope with a DCF 420 camera under bipolarized light.

Quartz, alkali feldspars and plagioclase are by far the most abundant mineral phases in all studied thin sections, followed by biotite, muscovite and chlorite in small amounts. Undulose extinction of quartz and partly of feldspar was observed in all thin sections. Dissolution of feldspar and subsequent formation of white mica as well as transition from muscovite to chlorite can be observed in nearly all samples.

However, except from thin sections taken from a mylonite in outcrop CP_009 (**Fig. 35**; see also chapter 3.1.7.), most samples were lacking good information concerning structural features and microtectonics.

Micro-images taken from this mylonite (outcrop CP_009, fault plane (276/45), lineation (306/40), normal fault) depict quartz as the predominant phase forming mylonitic trails bordered by partly broken feldspar grains (**Fig. 35/a**), providing a strong argument that high grade metamorphism above greenschist facies was not present. Although quartz grains in this shear zones depict shape preferred orientation, microscopic investigations under the wave plate revealed no alignment of quartz c-axes and accompanied crystal preferred orientation that would yield information about dextral or sinistral shearing. Nevertheless, top-to-NW shearing is indicated by slightly clockwise rotated feldspar clasts (**Fig. 35/b**).

Broken feldspar grains, which were observed throughout all thin sections from CP_009, strongly indicate a low temperature mylonite (300-450°C), (**Fig. 35/c & d**). Brittle behavior of feldspar, which was verified in all thin sections, as well as observations made in the field like synkinematic grown chlorite minerals along shear zones strongly suggest the formation under greenschist facies metamorphic conditions including NW and NE-striking normal faults as well as dextral, NW-striking strike-slip fault within the Hluboká Fault Zone.

Comparing the Hluboká Fault Zone with the parallel striking Pfahl and Danube shear zones at the southwestern border of the Bohemian Massif suggests that all three fault systems experienced a similar evolution concerning their microstructural and tectonic characteristics (**Brandmayr et al., 1995, 1997; Wallbrecher et al., 1993**).

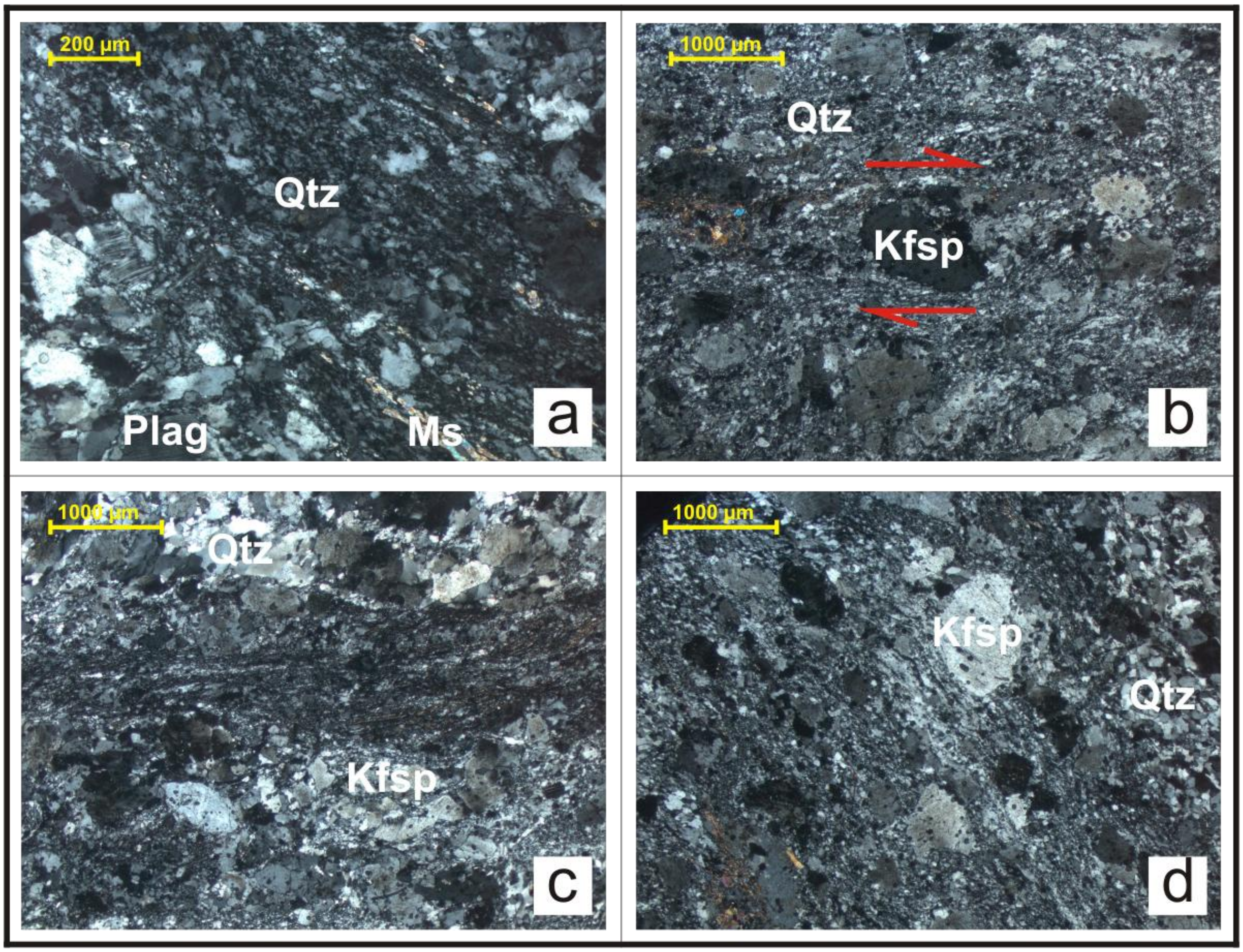

Fig.35: Oriented thin sections taken from mylonite in CP_009. **a)** Mylonitic zone with related muscovite migration along quartz-trails bordered by broken feldspar grains. **b)** Clockwise rotated feldspar-clast indicating top to NW normal faulting (see also **Fig. 27/a**). **c)** Brittle behavior of feldspar indicating a low temperature mylonite. **d)** Feldspar grains broken along high-grade quartz-veins**.**

3.3. Deformation history

The deformation history described below is based on the analysis of low-grade ductile and brittle deformation features, mostly faults and shear zones with shear sense indicators. The main problem therein is the age determination of brittle faulting events. In general it can be stated, that structures linked with a particular deformation phase are considered younger than the rocks deformed. Nevertheless, the investigation of the deformation history in the Bohemian Massif remains complicated due to the recurrence of similarly oriented paleostress fields throughout geologic history.

Taking into account all information obtained from structural field work including ductile and brittle deformation features as well as thin section analysis, four deformational phases have been reconstructed affecting all kinds of formations ranging from Variscan crystalline basement units to Lower Miocene deposits (**Fig. 40 & Fig. 41**).

Deformation D1: Variscan folding

Throughout the Variscan crystalline basement, ductile features including crenulation lineations, boudins, ductile stretching lineations, folds and foliations depict a paleostress field of NE-SW to NNE-SSW-directed shortening and NW-SE-directed stretching respectively, in this context referred to as D_1.

Foliation planes of crystalline basement units generally striking NW-SE parallel a large-scale, sub-horizontal fold axis (Fa 155/03), strongly suggesting that the regional fault strike of the Hluboká Fault is predefined by Variscan structures (**Fig. 36/a**).

Mesoscopic, NNW-trending fold axes measured in the field as well as ductile stretching and crenulation lineations contribute to the assumption of a paleostress field related to NE-SW to NNE-SSW-directed shortening (**Fig. 36/b**).

Associated mineralizations of ductile structures are indicative for greenschist facies metamorphic conditions, suggesting that D_1-deformation reflects the cooling stage of the Moldanubian crustal units during the late-phase of the Variscan orogeny.

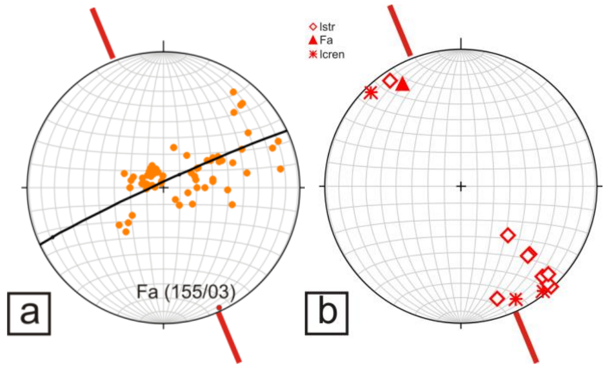

Fig. 36: Poles to Foliation pointing out NNW-SSE-trending Variscan fold axis (orientation of Fa: 155/03) paralleling the strike of the Hluboká Fault (**a**). Recorded crenulation lineations, ductile stretching lineations and fold axes (**b**). Summary plots from all outcrops in Variscan crystalline basement.

Deformation D2: Late-Variscan ductile normal-and strike-slip faulting

Structures linked to the second deformation stage include three kinds of ductile and brittle-ductile faults related to different kinematic regimes. D_2-features are characterized by NW-SE-striking normal faults (**D_{2A}; Fig. 37/a**), NE-SW-striking normal faults (**D_{2B}; Fig. 37/b**) and dextral strike-slip faults striking between NW-SE and E-W in Variscan crystalline basement (**D_{2C}; Fig. 37/c**), with the latter one probably linked to the first movement of the Hluboká Fault in Late-Variscan times

NW-and NE-striking ductile normal faults clearly postdate deformation phase D_1 by cutting older folds and foliations. In general, D_2 marks the transition from ductile to brittle deformation of the Variscan crystalline basement units. Brittle deformation of Permian sediments of the Lhotice Basin may have also occurred during D_2.

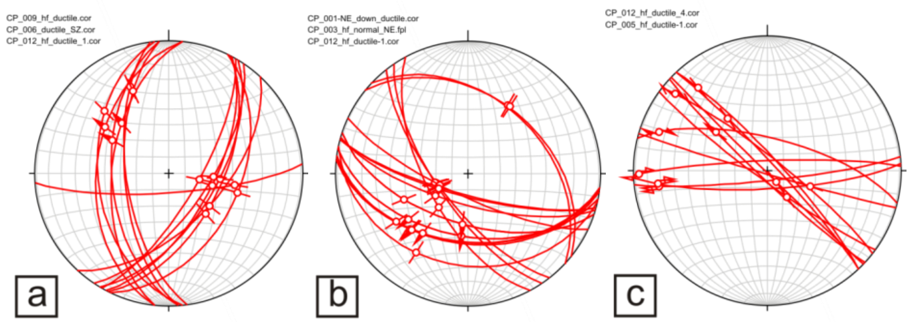

Fig. 37: Faults associated with deformation D_2. **D_{2A}**: NW and SE-dipping normal faults (**a**). **D_{2B}**: NE-SW-dipping normal faults (**b**). **D_{2C}**: dextral strike-slip faults striking between NW-SE and E-W in the southeastern section of the investigation area (**c**, see also **Fig. 13**, CP_005 & CP_012). Stereoplots combine data from different outcrops in crystalline basement.

Deformation D3: Brittle normal faulting

Brittle normal faults in crystalline basement rocks, Permian and Cretaceous sediments as well as calcite filled tension gashes observed in Permian shale deposits are significant for $D_{3.}$ All structures are related to an extensional stress field with SW-NE-directed extension (**Fig. 38**). Ductile normal faults referring to D_2 are partly overprinted by D_3-structures (e.g. CP_006, CP_009) leading to a relative age correlation of these deformation events. D_3-deformation features were not observed in Lower Miocene deposits, suggesting that D_3 terminated during the Upper Cretaceous or Paleogene.

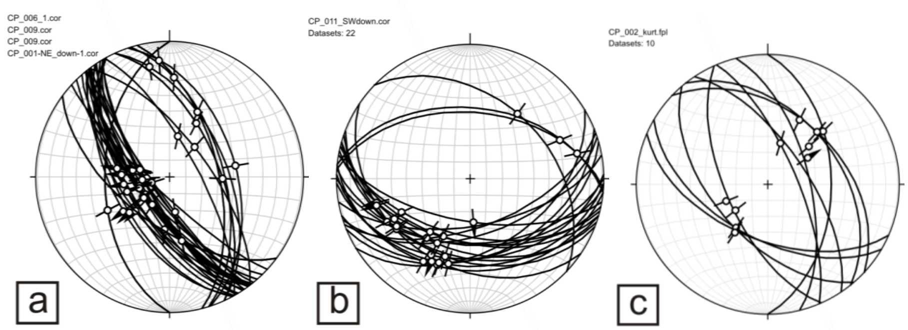

Fig. 38: Brittle normal faults in crystalline basement (**a**), Permian shale (**b**) and Upper Cretaceous sediments (**c**). Stereoplots combine data from different outcrops.

Deformation D4: Brittle strike-slip faulting

NW-striking, dextral strike-slip faults apparently related to the Hluboká represent the most abundant structures in the whole investigation area. Such faults have been observed in all units (Variscan basement; Permian, Cretaceous and Miocene sediments) suggesting a post-Miocene age for D_4 (**Fig. 39**). The overall characteristics of D_4-features in basement rocks are significant for brittle deformation. Unfortunately, cross-cutting relations as seen with D_1 and D_2 have not been observed with D_4, leaving the fact that D_3 features were not present in Lower Miocene deposits as the only criteria for D_4 post-dating D_3.

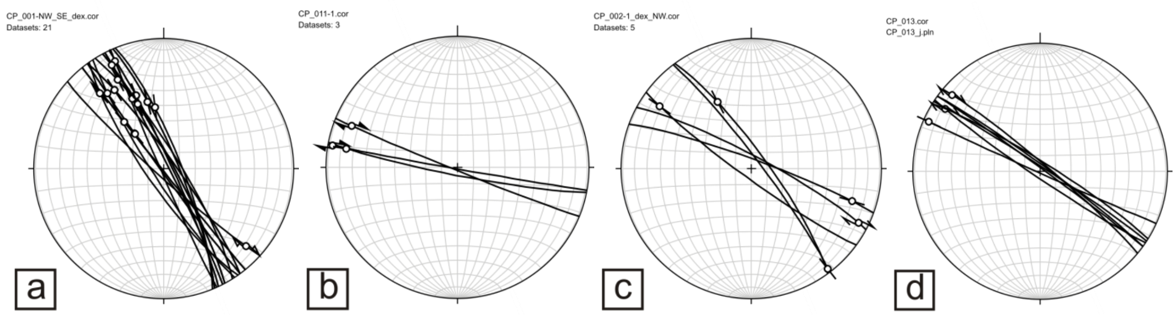

Fig. 39: Stereoplots depicting abundant dextral strike-slip faulting in crystalline basement (**a**), Permian shale (**b**), Upper Cretaceous (**c**) and Miocene sediments (**d**). Stereoplots combine data from different outcrops.

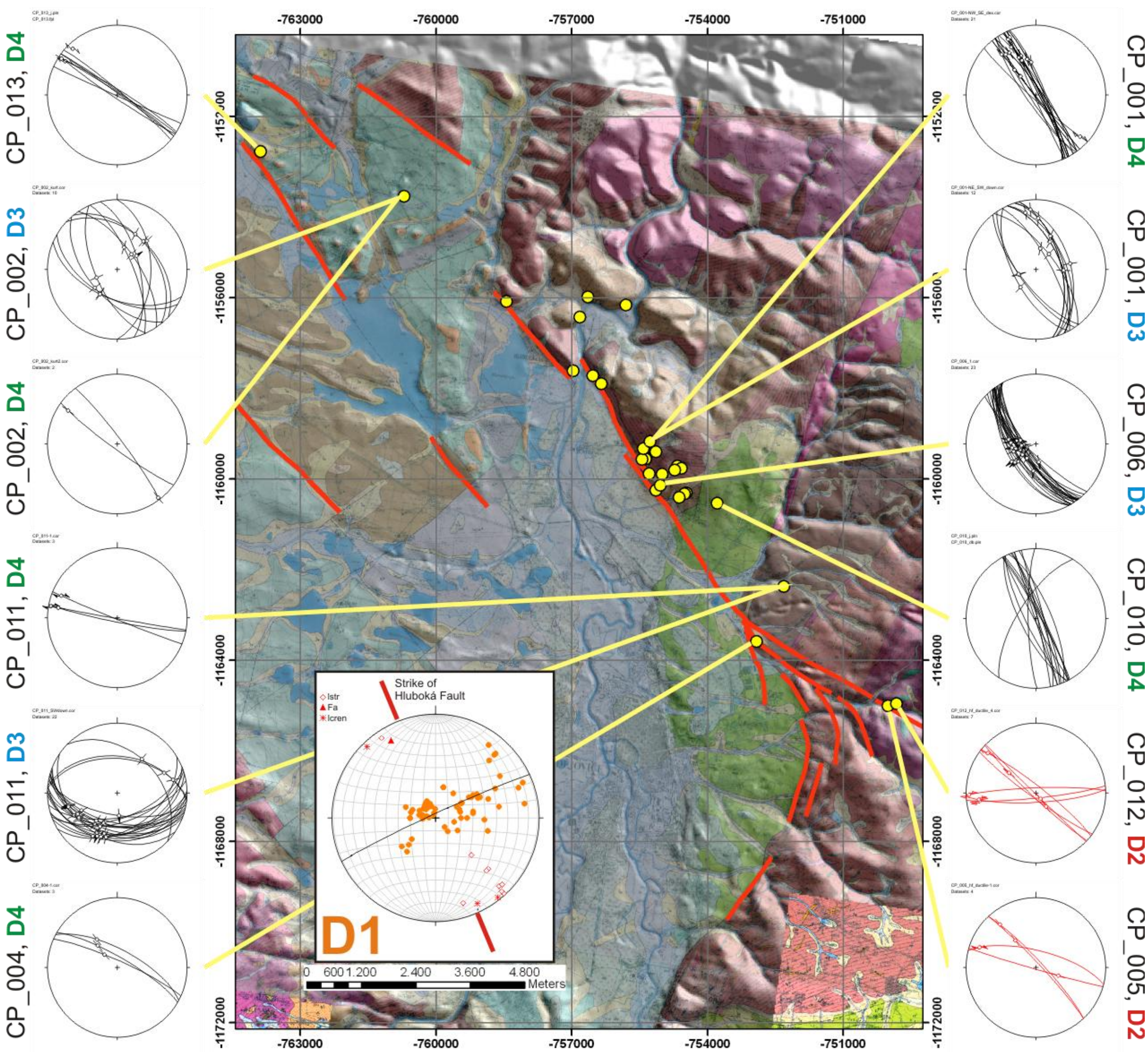

Fig. 40: Map view of investigation area. D_1 dataset combining foliation, crenulation, ductile stretching lineation and fold axes from different outcrops. D_2 and D_3 and D_4 datasets with related outcrops.

	Deformation Phase and Age	Related structures	Deformed Formations	Kinematics
Brittle	D4 Post-Miocene	- Dextral strike-slip faults	- Variscan Basement - Permian shale - Upper Cretaceous (Klikov Fm.) - Miocene conglomerate (ZlivFm.)	
Brittle	D3 Post-Cretaceous	- Tension gashes - SW & SSW dipping normal faults	- Variscan Basement - Permian shale - Upper Cretaeous (Klikov. Fm.)	
Ductile	D2 Late-Variscan D_{2A} D_{2B} D_{2C}	D_{2A} - SE & NW dipping normal faults D_{2B} - SW & NE dipping normal faults D_{2C} - NW-SE to E-W-striking dextral strike-slip faults	- Variscan Basement	D_{2A} D_{2B} D_{2C}
Ductile	D1 (Late)-Variscan	- Foliation - Folds with NW-trending fold-axes - Boudins - Crenulation - Stretching lineation	- Variscan Basement	

Fig. 41: Summary of reconstructed deformation phases with defining structural features.

4. Interpretation of 2D Seismic Profiles

Five seismic profiles have been recorded by the company Pöyry Engineering from June to September 2009 in order to assess the slip history and spatial geometry of the Hluboká Fault and the adjacent Zbudov Fault in the basin lowlands. All seismic sections roughly trend in NE-SW to ENE-WSW direction, with three of them covering the Hluboká Fault near the villages of Úsilné, Hosín and Munice from SE to NW. The profiles are spaced at distances of approximately 4.3 km. Two seismic profiles near Dasny and Mydlovary intersect the Zbudov Fault at a distance of approximately 8.3 km (**Fig. 42**). Each of the recorded sections has a length of 1.2 km summing up to a total length of 6 km of available reflection seismic.

A vacuum enhanced hammer (Vakimpac) was used as seismic energy source yielding an excitation frequency of 100-120 MHz for the seismic impulse (resolution limit: < 10 ms TWT ~ 2.5 – 3 m). Seismic processing and the conversion of seismic profiles from time to depth units were done exclusively by Werner Chwatal of the Technical University of Vienna. Seismic check shots for the Budejovice Basin were not available and calibration of seismic reflectors through well control was not useful due to mostly shallow drillings. However, comparison of the depth of crystalline basement rocks in wells near Hosin with depth converted seismic, prove that depth conversion leads to reasonable results (for post-stack/pre-migration data see attachment part 3: Seismic data).

The top of the crystalline Basement and Permian rocks underlying the Cretaceous basin fill are depicted in all seismic sections. They are marked as a band of three parallel reflectors characterized by high reflectivity situated in depths from about 400m (section Usilne) to 100m (section Mydlovary) below surface. Vertical offset of these reflectors along the northeastern basin margin to depths of about 400m is depicted in all sections covering the Hluboká Fault Zone.

Cretaceous sediments are characterized by reflectors of low and medium amplitudes, gently dipping SW at the northeastern basin margin and flattening towards the center of the basin. Miocene sediments in all seismic sections are depicted as sub-horizontal reflectors of medium to high amplitudes showing onlaps onto crystalline basement as seen in section Munice. In all sections covering the northeastern basin margin, interpreted faults coincide with the linear topographic scarp of the Hluboká Fault.

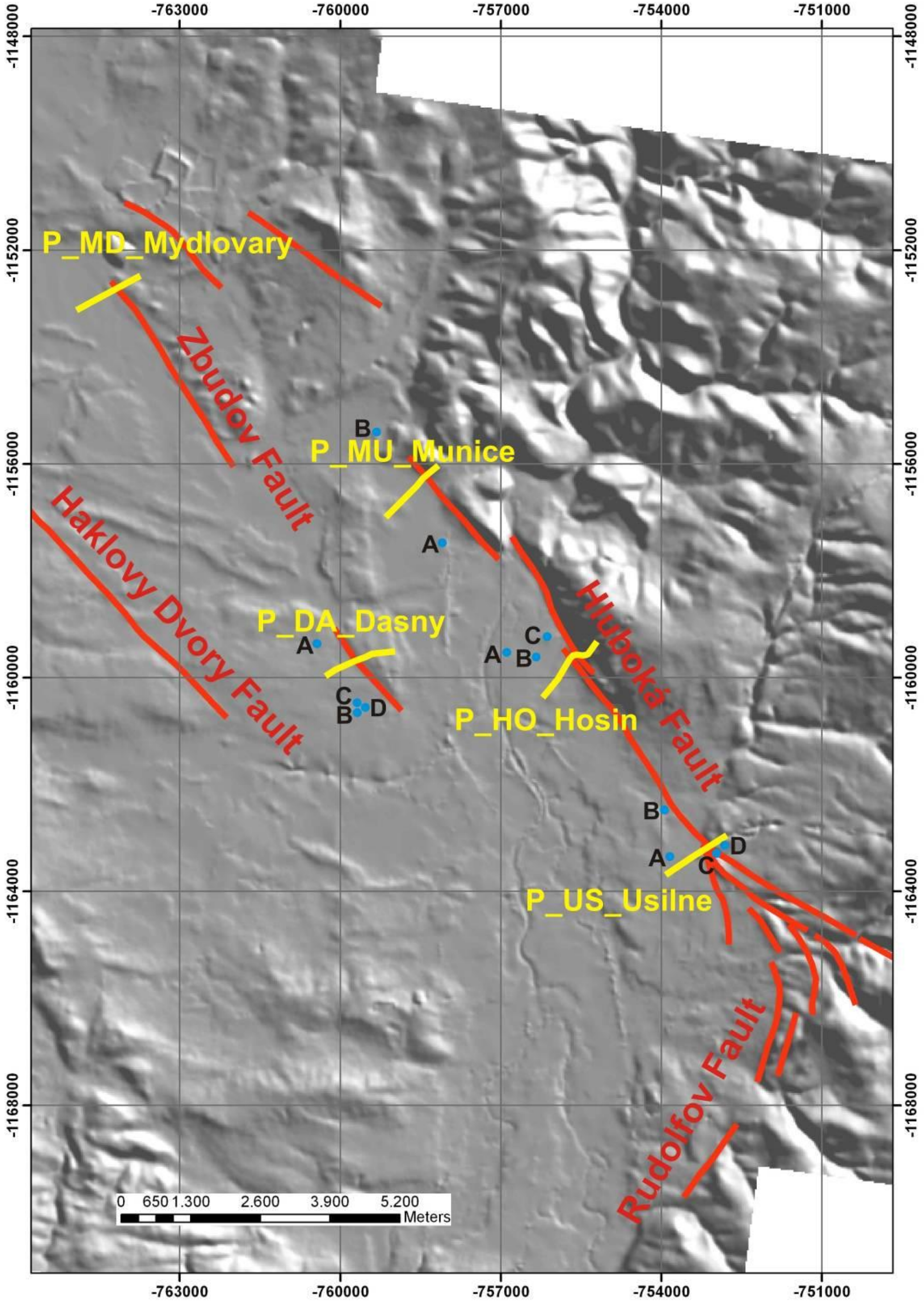

Fig.42: Location of 2D seismic profiles crossing the Hluboká Fault (Section P_US_Usilne, P_HO_Hosin, P_MU_Munice) and Zbudov Fault (P_DA_Dasny & P_MD_Mydlovary). Blue dots indicate drillings projected into seismic profiles.

4.1. Profile Usilne (P_US_Usilne)

Section P_US_Usilne depicts one master fault (**1**) and a couple of branch faults (**2** & **3**), partly accompanied by topopraphic expressions at the surface (**Fig. 43 & Table 2**). The master fault, representing the main branch of the Hluboká Fault, reaches the surface at geophone 184, offsetting the pre-Cretaceous basement to depths of about 400 m. At the surface the master fault coincides with a morphological scarp and forms the contact between Permian shale and siltstones of the Lhotice Basin in the northeast and Upper Cretaceous sediments of the Klikov Formation in the southwest. The presence of the master fault at this location was validated in the course of the first palaeoseismological trench at Usilne within the framework of CIP (**Špaček at al., 2011**).

In southwestern direction, three faults have been interpreted in this section branching off from the master fault and reaching the surface at geophone 197, 211 and 256, with the latter one coinciding with a second morphological scarp. Slight evidence for the presence of a fault at geophone 197 at the toe of the first morphological scarp also comes from field observations in outcrop CP_004 (Cherveny Vrch) about 400 m further southeast, showing a NW-striking fault (see chapter 3.1.4.).

Interpreted faults are also indicated by three marked steps in the diving wave velocity profile, with the first one delimiting high velocity Permian rocks and medium velocity Upper Cretaceous sediments and the latter ones confining an area of lower velocity in between, probably depicting an offset block of Upper Cretaceous sediments.

The southwestern section of P_US_Usilne is characterized by subhorizontal, slightly concave reflectors of Upper Cretaceous sediments gently dipping into southwestern direction and reflectors of high amplitudes depicting the pre-Cretaceous basement. It is not clear if top basement reflectors in this part of the basin depict the Variscan crystalline or Permian rocks forming the basin floor.

Upper Cretaceous sediments show constant thickness of about 370 m in the southwestern section. Growth strata geometries have not been observed, suggesting post-Cretaceous offset along the master fault.

The overall listric master fault geometry as well as offsets of Upper Cretaceous sediments along the branch faults might be connected with a releasing horsetail splay bending to the right and merging with the Rudolfov Fault (**Fig. 42**).

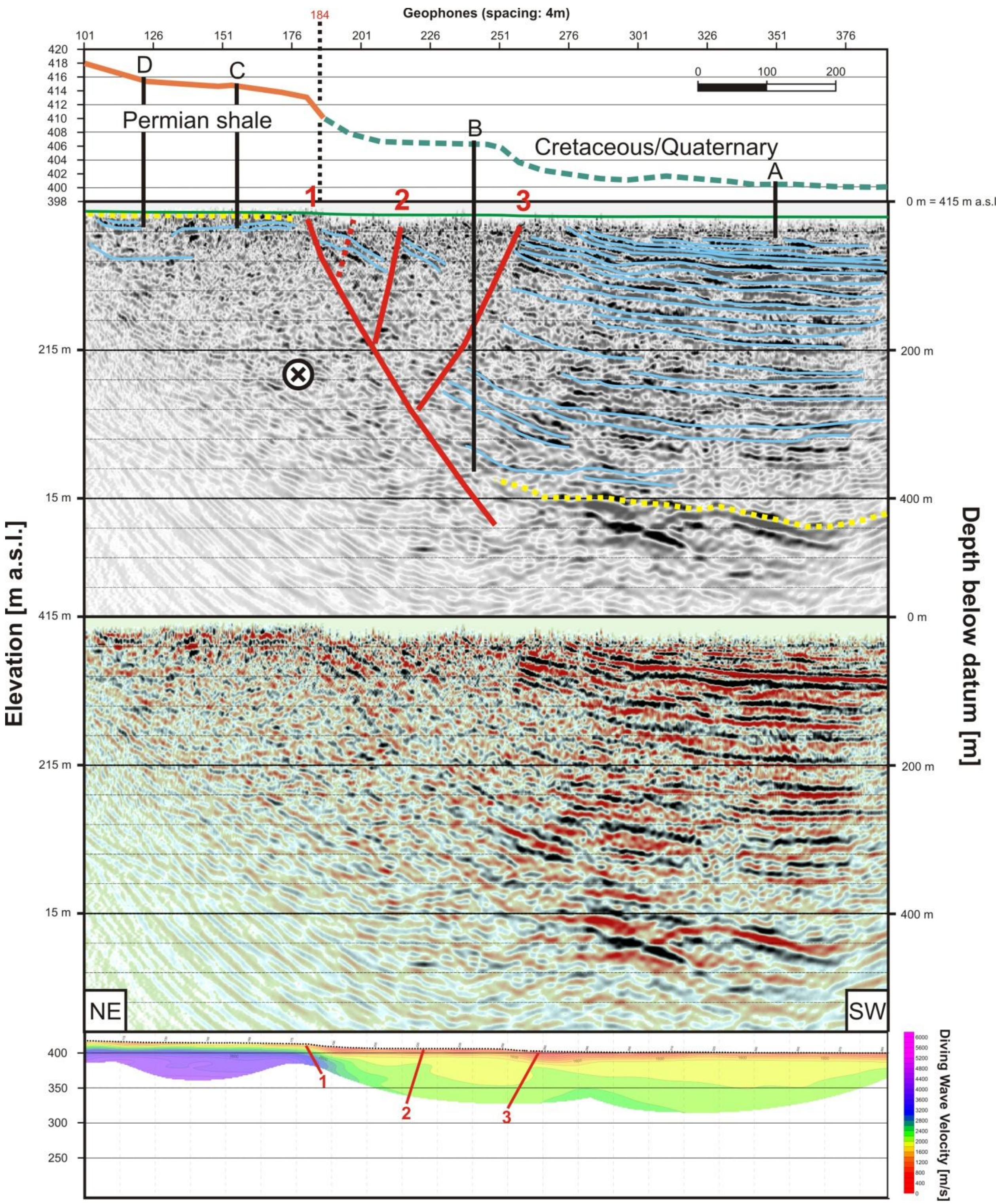

Fig. 43: Seismic profile P_US_Usilne. From top to bottom: Topographic profile; interpreted, migrated seismic depth section; uninterpreted seismic section and diving wave velocity profile. Top of pre-Cretaceous basement marked as dashed, yellow line. Reference level for seismic processing was picked at 415 m above sealevel.

	Wellname	Report Nr.	Depth	Projected from	Crystalline	Permian shale	Upper Cretaceous
A	1/40	V046625/046665	25 m	80 m NW			4,4 m
B	US 1	V070452	345 m	1180 m NW	330 m		4,5 m
C	JBV69	P059532	42 m	42 m SE		1,9 m	
D	JB72	P059532	13 m	13 m SE		3 m	

Table 2: Wells from Czech Geological Survey (Geofond Prague) displayed in **Fig. 43**.

4.2. Profile Hosin (P_HO_Hosin)

Profile Hosin depicts two sub-vertical, slightly SW-dipping faults at the toe of the morphological scarp at geophone 216 (**2**) and the second one located about 200 m further uphill (**1**), intercepting the crystalline basement reflectors at geophone 166 (**Fig. 44 & Table 3**). The steep dip of the main fault at geophone 216, which offsets the crystalline basement for about 300 m vertically, is constrained by the termination of basement reflectors northeast and southwest of the fault. Both faults are supported by the diving wave velocity profile, which shows two marked steps of the top of the high-velocity basement adjacent to the interpreted faults.

The image in the southwestern part of P_HO Hosin strongly resembles P_US_Usilne with horizontal reflectors of constant thickness, mostly associated with Upper Cretaceous sediments overlying the crystalline basement depicted as a prominent band of three parallel reflectors. An additional fault was assumed about 80 m southwest of the main fault slightly disrupting shallow reflectors of Upper Cretaceous sediments (**3**).

In general, the geometry of the sub-vertical fault (**2**) indicates strike-slip faulting with a high component of normal displacement.

	Wellname	Report Nr.	Depth	Projected from	Crystalline	Upper Cretaceous	Miocene
A	V904	P020833	8,5 m	900 m NW		5,8 m	
B	OH6	P012368	5 m	447 m NW			4,2 m
C	HL1	P018881	331 m	505 m NW	315,8 m	14,8	

Table 3: Wells from Czech Geological Survey (Geofond Prague) displayed in **Fig. 44**.

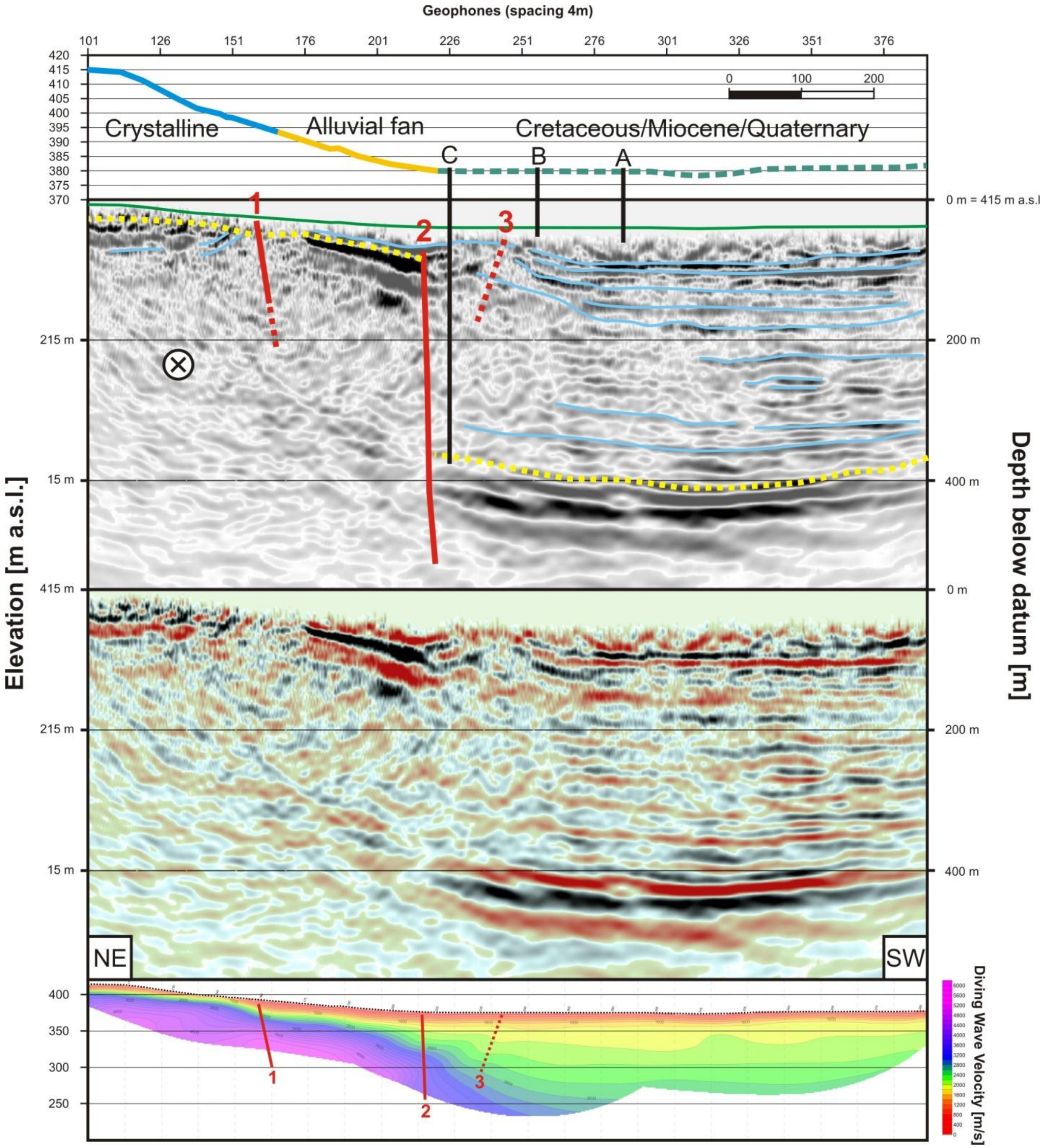

Fig. 44: Seismic profile P_HO Hosin. From top to bottom: Topographic profile; interpreted, migrated seismic depth section; uninterpreted seismic section and diving wave velocity profile. Top of pre-Cretaceous basement marked as dashed, yellow line. Reference level for seismic processing was picked at 415 m above sealevel.

4.3. Profile Munice (P_MU_Munice)

Section P_MU_Munice displays some similarities with P_HO_Hosin by the presence of two sub-vertical, slightly SW-dipping faults at geophone 172 (**1**) and 226 (**2**), also indicated by the top basement geometry in the diving wave velocity profile (**Fig. 45 & Table 4).** The fault interpreted in the northeastern part of the section coincides with the toe of a morphological scarp. The master fault accommodating the main vertical offset of the crystalline basement of 280 m is, however, not expressed by surface topography. Slight changes in topography can also be seen at geophone 251, coinciding with a suspected fault in the seismic section (**3**).

The image in the SW part of the section strongly resembles to what has been observed in section Hosin and Usilne showing concave reflectors of Upper Cretaceous sediments rising towards the margin of the basin, resulting in a large, synformal fold geometry with Cretaceous strata of approximately constant thickness. The upper part of the section displays sub-horizontal reflectors with onlaps onto the crystralline basement, consequently interpreted as sediments of the Mydlovary Formation of middle Miocene age (Karpatian - Lower Badenian) and separated from the underlying sediments by an angular unconformity. Offset of Miocene reflectors overlying fault 2 are not evident, leading to the assumption that activity of this fault terminated between the Upper Cretaceous and Miocene.

Growth strata geometries have neither been observed in Cretaceous nor Miocene sediments adjacent to the faults. Moreover, considering the large-scale fold geometry of Upper Cretaceous reflectors it is most likely that the Budejovice Basin emerged due to post-Cretaceous tilting and the subsequent formation of an angular unconformity between the Cretaceous and the overlying Miocene sediments.

	Wellname	Report Nr.	Depth	Projected from	Crystalline	Upper Cretaceous	Miocene
A	W1	V068630	5,1 m	1230 m SE			2,4 m
B	4H-087c	P119936	168 m	1315 m NW	144,4 m	0,8 m	

Table 4: Wells from Czech Geological Survey (Geofond Prague) displayed in **Fig. 45.**

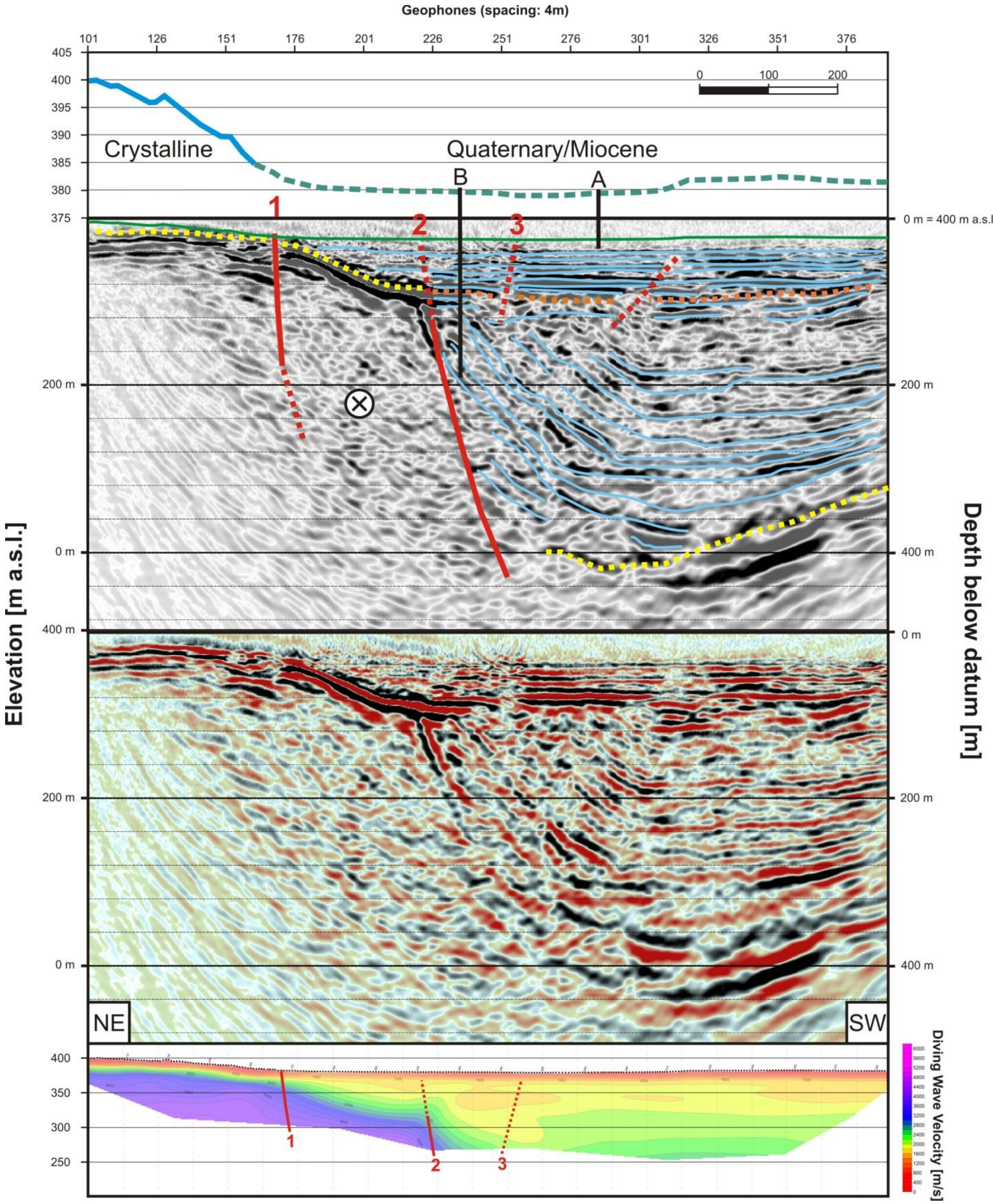

Fig. 45: Profile P_MU_Munice. From top to bottom: Topographic profile; interpreted, migrated seismic depth section; uninterpreted seismic section and diving wave velocity profile. Top of pre-Cretaceous basement marked as dashed, yellow line. Base Miocene marked as dashed, orange line. Reference level for seismic processing was picked at 400 m above sealevel.

4.4. Profile Dasny (P_DA_Dasny)

Sections P_DA_Dasny and P_MD_Mydlovary crossing the Zbudov Fault show a completely different picture than the previously described sections across the Hluboká Fault (**Fig 46 & Fig. 47**). Located in the basin lowlands, both sections depict two sub-vertical, nearly symmetrical faults.

P_DA_Dasny shows two steeply dipping planer faults, which converge to depth of about 330 m apparently merging into a principal displacement zone (PDZ) below the top of the pre-Cretaceous basement. The converging faults are clearly shown by the terminating and offset reflectors in the Upper Cretaceous and the offset basement reflectors. Fault 1 is also indicated by a marked step in the diving wave velocity profile. Larger offset of lower reflectors compared to smaller offset at shallow reflectors suggest the presence of a flower structure.

Intersecting with the upper layers at geophone 256 (**1**) and 305 (**2**), both faults are located close to the Zbudov scarp striking NE-SW (**Fig. 42**). Faults do not coincide with the mapped fault at the contact of Miocene and Upper Cretaceous sediments in the geological map at geophone 197 (**Fig. 13**).

The migrated seismic section displays a strong basement reflector slightly dipping from 200 m in the southwestern part to 250 m in the northeastern part showing vertical offsets of about 10 m at both faults. Concerning the overlying sediments, which are defined by sub-horizontal, slightly SW-dipping reflectors of medium amplitudes, it is hard to discern between Upper Cretaceous and Miocene strata, although at least the upper section seems to be composed of Miocene sediments of the Mydlovary Formation according to borehole information. Therefore, Miocene to post-Miocene fault activity would be indicated by the slight offset of shallow reflectors along the fault zone.

In the sedimentary successions on both sides of the Zbudov Fault, no growth strata geometries have been found (**Fig. 46 & Table 4**).

	Wellname	Report Nr.	Depth	Projected from	Crystalline	Upper Cretaceous	Miocene
A	SG29	P058157	31 m	586 m NW		27 m	0,5 m
B	4H-085c	P118880	195 m	830 m SE		47,5 m	2,5 m
C	HP-IX	P025997	199 m	830 m SE	195 m	14 m	1,8 m
D	4H-086b	P119935	60 m	830 m SE		48,7 m	2,4 m

Table 4: Wells from Czech Geological Survey (Geofond Prague) displayed in **Fig. 45.**

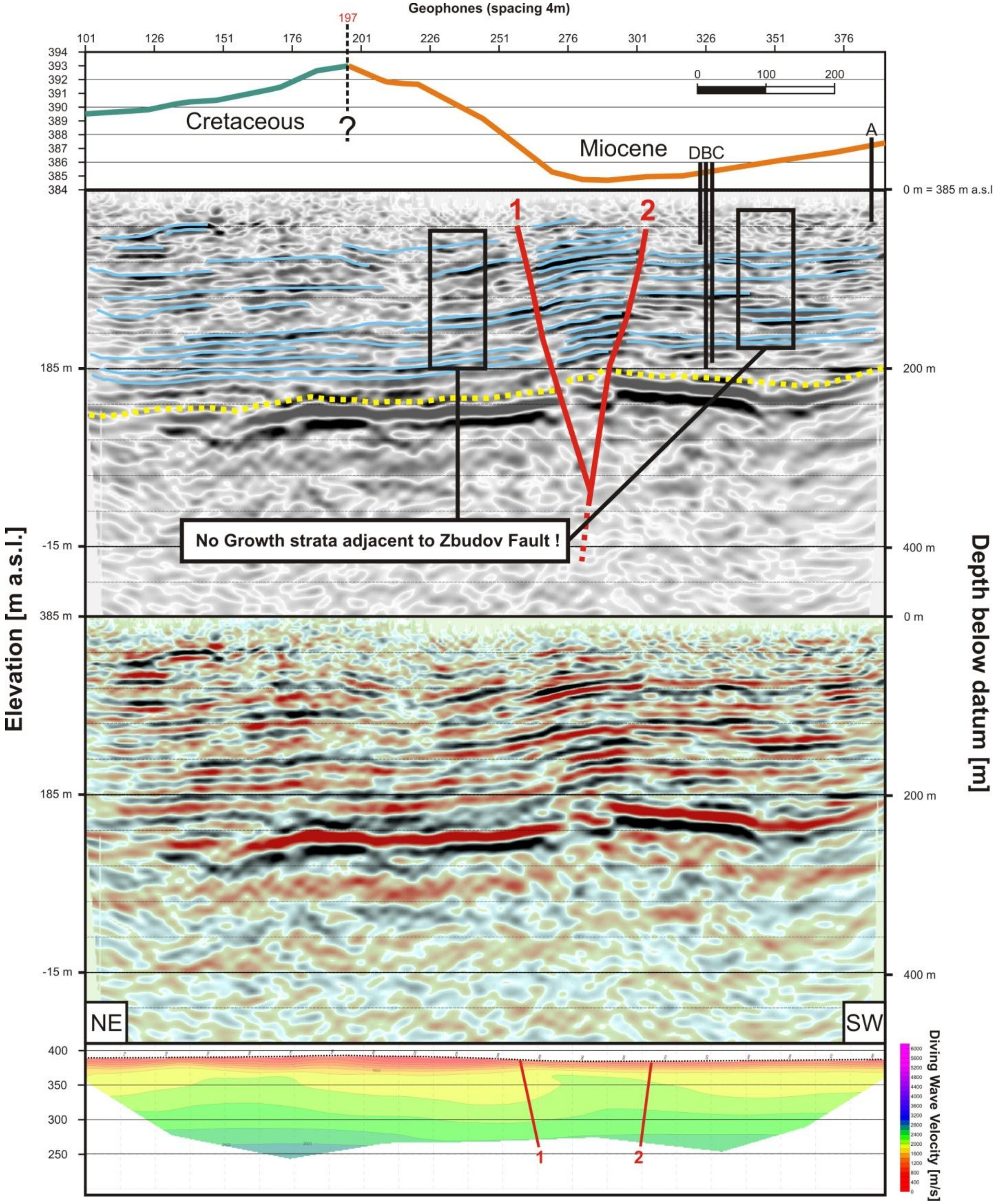

Fig. 46: Seismic Proflie P_DA_Dasny. From top to bottom: Topographic profile; interpreted, migrated seismic depth section; uninterpreted seismic section and diving wave velocity profile. Top of pre-Cretaceous basement marked as dashed, yellow line. Reference level for seismic processing was picked at 385 m above sealevel.

4.5. Profile Mydlovary (P_MD_Mydlovary)

Section P_MD_Mydlovary depicts two sub-vertical faults associated with the Zbudov Fault, comparable with the flower structure observed in section P_DA_Dasny. Whereas the upper sections of these faults are depicted by slightly disrupted reflectors of the sedimentary succession at geophone 230 (**1**) and 276 (**2**), the lower parts terminate a short band of three prominent reflectors at a depth of about 300 m, probably displaying an offset block within the crystalline basement. Structural data recorded in CP_013 next to the seismic profile in the Zliv Formation indicate dextral strike-slip movement as well as post-Miocene deformation age for the Zbudov Fault (**Fig. 13**). As already seen in section P_DA_Dasny, faults do not coincide with position of the mapped fault in the geological map at geophone 196 (**Fig. 13**).

The top of the crystalline basement can be traced along a sub-horizontal band of three parallel reflectors at a depth of 100 m covered by sediments of the Zliv Formation of Lower Miocene age (Ottnangian) in the northeastern and probably sediments of the Mydlovary Formation in the southwestern part of the section.

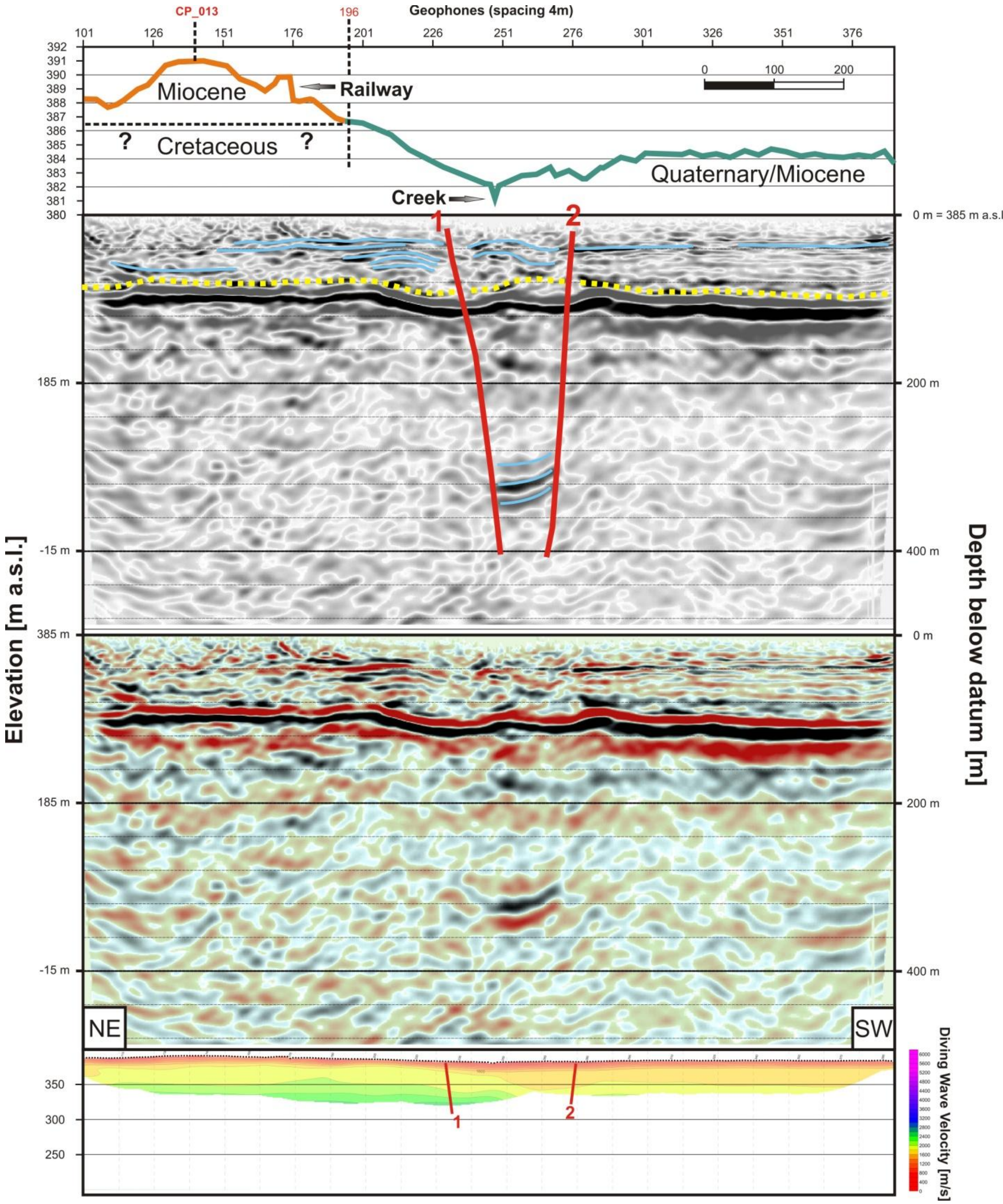

Fig 47: Seismic profile P_MD_Mydlovary. From top to bottom: Topographic profile; interpreted, migrated seismic depth section; uninterpreted seismic section and diving wave velocity profile. Top of pre-Cretaceous basement marked as dashed, yellow line. Reference level for seismic processing was picked at 385 m above sealevel. CP_013 projected from 180 m SE.

4.6. Summary seismic mapping

The absence of growth strata geometries in Upper Cretaceous and Miocene sediments adjacent to the Hluboká and Zbudov faults, which has been observed especially in section P_MU_Munice and P_DA_Dasny (see chapter **4.3.** & **4.4.**), indicates post-Cretaceous (Hluboká) and post - (Lower) Miocene (Zbudov) fault activity, respectively.

Reflectors of Upper Cretaceous sediments in P_US_Usilne, P_HO_Hosin and P_MU_Munice display concave-up, fold-like geometries most likely caused by post-Cretaceous tilting and the formation of an angular unconformity between the Cretaceous and the overlying Miocene sediments

Giving the fact that Hluboká and Zbudov Fault are characterized as dextral strike-slip faults paralleling each other at an average distance of about 3 km, it is most likely that both faults converge into a single principal displacement zone located within the crystalline basement. Moreover, fault geometries in section P_MU_Munice and P_HO_Hosin share geometrical similarities with a flower structure splitting up at higher depths.

Therefore, concerning the Haklovy Dvory Fault, paralleling the Zbudov Fault in southwestern direction at the mapped contact of Miocene and Upper Cretaceous sediments, dextral strike-slip faulting is suggested as well (**Fig.13 & Fig 42**). Unfortunately, structural or seismic data regarding the Haklovy Dvory Fault was not available.

Although highly speculative, all three faults might as well join into a deep-seated, lateral displacement zone associated with the Jáchymov Fault Zone.

5. 3D-Modeling of the Budějovice Basin

In order to supplement information obtained from seismic mapping, drilling reports of the investigation area were collected from the archive of the Czech Geological Survey (Geofond Prague). The construction of a consistent 3D model of the Budějovice Basin by the integration of information from various sources (seismic mapping, geological map, drilling reports etc.) was guided by two main objectives:

- Modeling of the 3D basin geometry should constrain the thickness and distribution of Upper Cretaceous and Miocene strata in order to identify depocenters, disrupted horizons and faults. Especially the reconstruction of post-Cretaceous and post-Miocene slip history along the Hluboká and Zbudov Fault was of main intererest.

- Work should supplement surface information from a terrain, which is rather poor in natural outcrops by intergrating subcrop data from drilling reports, in order to gain a better spatial overview of the geological features characterizing the Budějovice Basin.

5.1. Methodology

For computer aided modeling of the geological 3D model two software packages have been used:

- Adoption of geological features was done in an **ESRI ArcGIS 9.3.** project. This included contouring the distribution of formations characterizing the sedimentary basin infill as well as the course of the major fault zones present in the investigation area (Hluboká, Zbudov, Haklovy Dvory and Rudolfov Fault).

- Preliminary and final modeling was done by the means of **Paradigm GOCAD 2009.2.** Modeling included features pre-processed in ArcGIS 9.3. in order to visualize geological objects like faults, folds, sedimentary layers etc. in their spatial relation.

In detail, information that has been used for modeling are as follows:

- Topography based on the digital elevation model compiled within the framework of AIP by Dana Homolova (10 m ground resolution).

- Vectorized map items including mapped faults, contours of Upper Cretaceous and Miocene strata as well as Quaternary terraces adopted from the Czech geological maps (1:25000; map sheets: 22-434 “Netolice”; 22-443 ”Hluboká nad Vltavou”; 22-444 “Ševětin”; 32-212 “Nová Ves”; 32-221 ”České Budějovice”; 32-222 “Lišov”; 32-223 “Kamenný Ujezd” & 32-224 “Borovany”).

- Digitalized information obtained from 994 drilling reports from the Czech Geological Survey (Gefond Prague) containing geological information like sedimentological descriptions and stratigraphic interpretations (well list included in attachment part 4: Drillings for database).

- Five depth-converted, interpreted seismic cross-sections (see chapter 4) pre-processed by the Technical University of Vienna.

Out of 994 drillings, which are mostly located in the eastern part of the basin near the Hluboká Fault (**Fig. 48/a**), 981 reached the base of Quaternary terrace sediments of the Vltavou and Malše river, 212 the top of Miocene strata, 472 top of Upper Cretaceous sediments and 137 the top of the crystalline basement. Modeling of the base of Quaternary terrace sediments was included in the preliminary 3D model but not further processed as inaccuracies proofed to be too large for modeling a layer as thin as the Quaternary terrace deposits with a maximum thickness of only 10 m. Therefore, only 679 drillings remained in the model database including information on Upper

Cretaceous, Miocene and Crystalline units. Point informations of layer boundaries were calculated from the coordinates/elevations of drillings at the surface and the formation tops recorded in the well reports. The points were exported to GOCAD as XYZ-point files fitting the regional coordinate system, manually sorting out drillings not located within the crystalline basin border as well as borehole data with unlikely values caused by insufficent or wrong geological description. Data from drillings were further integrated with marker layers from seismic sections generating a triangulated surface depicting the boundary layers of Upper Cretaceous, Miocene and Crystalline units. In another step, surface edges were stitched with mapped geological contacts between different formations (**Fig. 48/b & Fig. 49**). Finally, generated surfaces were smoothed manually by deleting or relocating outliers of nodes from the triangulated surface.

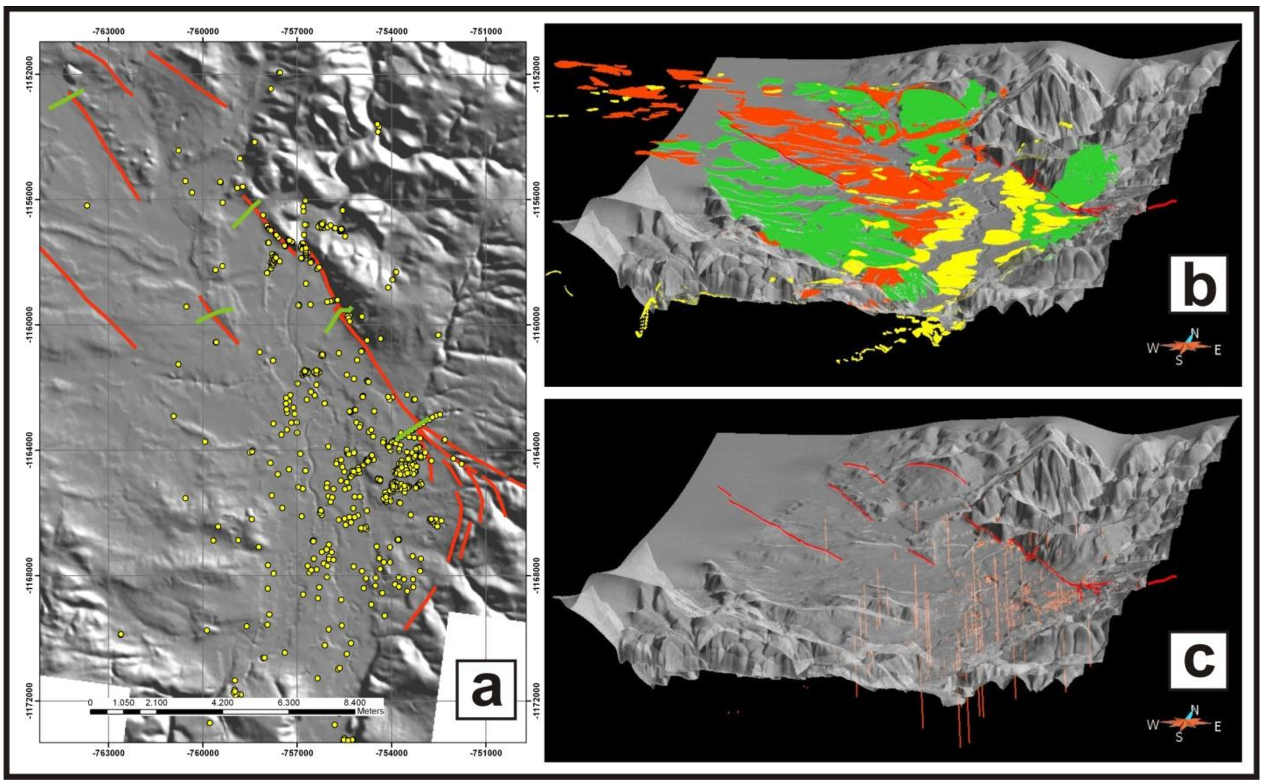

Fig. 48: a) Hillshade model derived from DEM of the Budějovice Basin showing drillings used for 3D-modeling as well as seismic sections depicted as green lines. **b)** Distribution of Upper Cretaceous (green), Miocene (orange) and Quaternary terrace sediments (yellow) characterizing the basins infill (adopted from geological map 1: 25 000). **c)** Wellpaths showing depth of Geofond drillings in the basin (Vertical exaggeration of 1:12 in **b** and **c**).

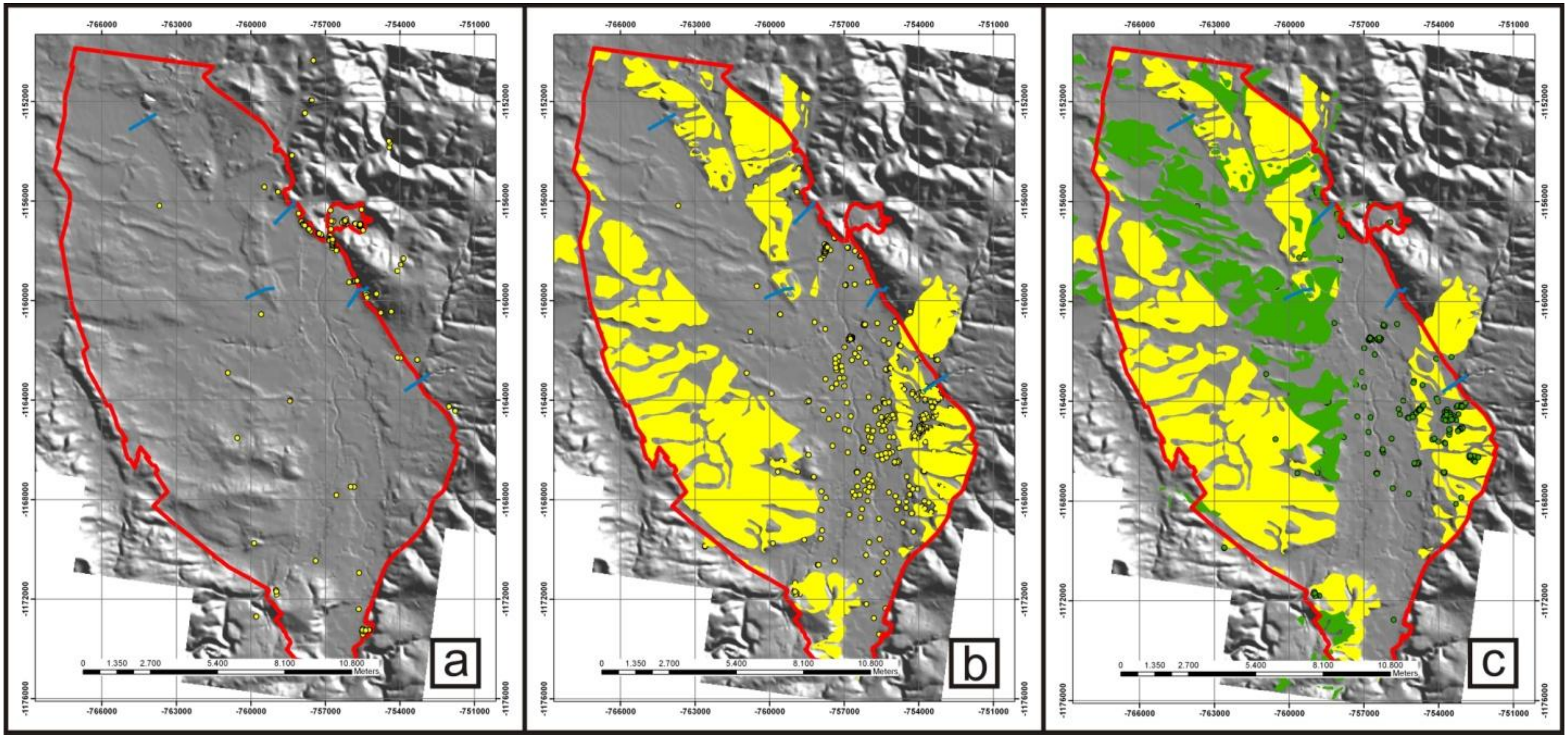

Fig. 49: Map views showing the distribution of drillings that have been used for modeling the subsurface horizons of crystalline, Upper Cretaceous and Miocene units. **a)** Crystalline outline of the Budéjovice Basin (red), seismic sections (light blue) and drillings reaching the crystalline basement **b)** Upper Cretaceous sediments cropping out at the surface (yellow areas) and drillings reaching the top of cretaceous sediments**. c)** Miocene deposits at the surface (green areas) and drillings reaching the top of Miocene sediments.

5.2. Top Crystalline Basement

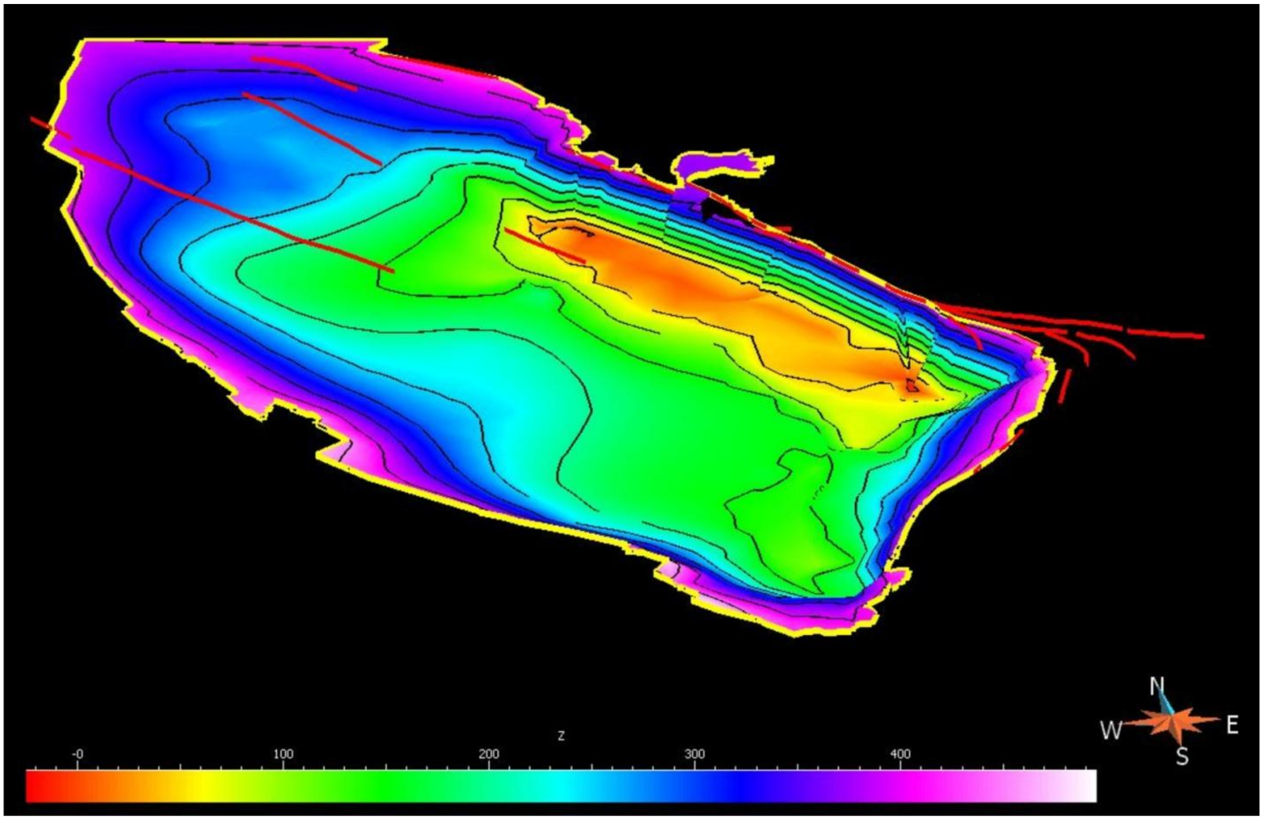

Fig. 50: Horizon Top Crystalline Basement depicting basin flanks of medium dip at SW and NW border and high-angle dips at SE and NE border (Vertical exaggeration: 1:5. Color bar denotes elevation in meters above sealevel).

The top of the crystalline basement clearly depicts the asymmetry of the Budějovice Basin (**Fig. 50**). The basin floor gently plunges towards the eastern border of the basin with a dip of approximately 5°. At the northeastern margin of the basin the Hluboká Fault steeply offsets crystalline basement units for up to about 380 m, indicating that the basins formation was mainly influenced by the activity of the Hluboka Fault.

The southeastern corner of the Budějovice Basin is highlighted by the termination of the Hluboká Fault at the southwestern end of the Lhotice Basin (see chapter 2.4. and 4.1.) splitting up into several splay faults, all of which depicted by minor morphological scarps partly bending to SW and merging with the NNE-striking Rudolfov Fault (see also chapter 3.1.4.). The depocenter of the Budéjovice Basin is located in the southeastern part of the basin (ca. 390 m below surface) adjacent to the intersection of the NNE-striking Blanice-Kaplice-Rodl-Fault zone and the Hluboká Fault zone.

5.3. Top Upper Cretaceous

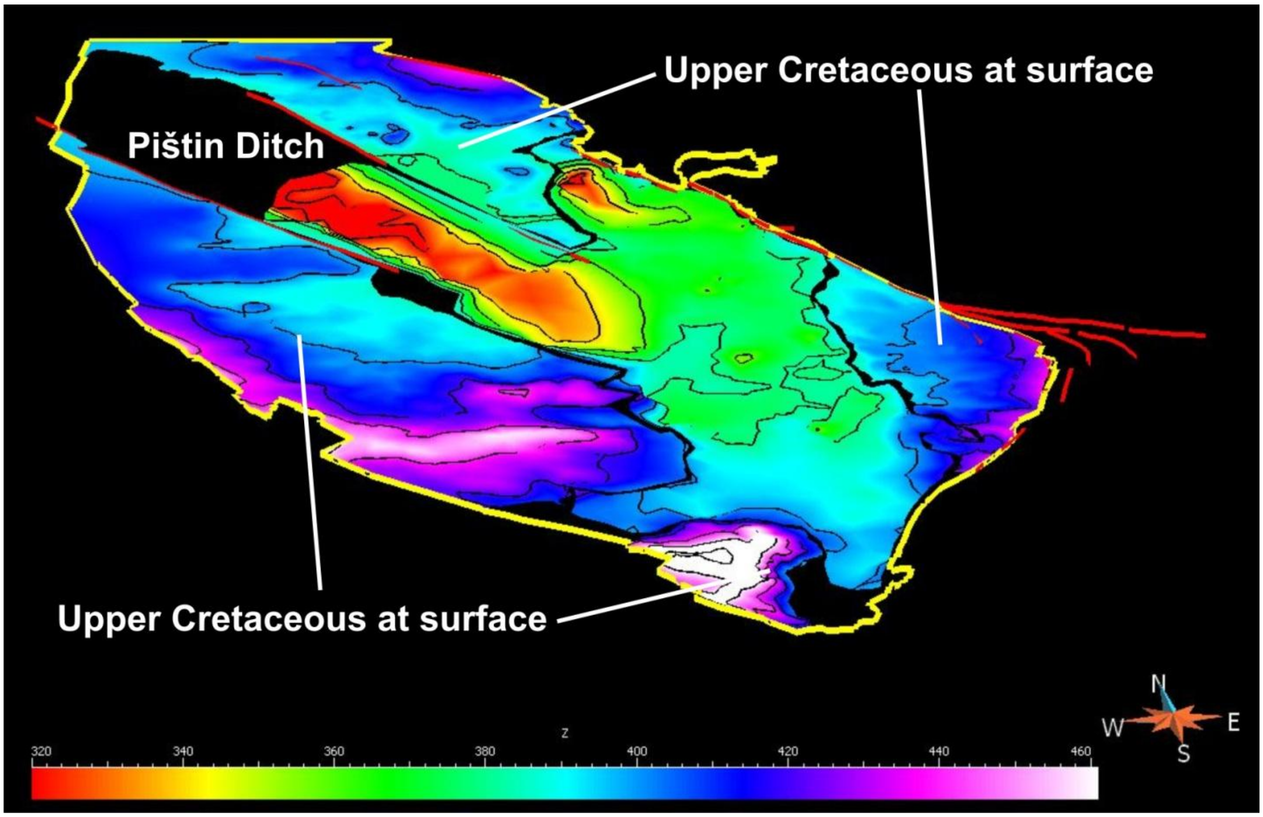

Fig.51: Horizon Top of Upper Cretaceous sediments (Vertical exaggeration: 1:5. Color bar denotes elevation in meters above sealevel).

According to the regional geological maps (1:25 000), Upper Cretaceous sediments of the Klikov Formation crop out at the eastern and southern corner of the basin, but also cover large areas close to the southwestern and northeastern basin margin (**Fig. 51**). The constructed sub-surface horizon - moslty corresponding to the base of Miocene sediments - covers the area around the Vltavou and Malše river (**Fig.13**). The main depression of the horizon Top Upper Cretaceous is located between the Zbudov and Haklovy Dvory Fault at about 320 m a.s.l. The depression is filled with Miocene sediments reaching up to the surface. Another, much smaller depression is located near seismic profile P_MU_Munice (see chapter 4.3.) to the NW of Hluboka nad Vltavou, probably related to a previous Tertiary fluvial channel, also called the “northern river channel”) passing from E to W to the north of the Hluboká hill (**Špaček at al., 2011; Fig. 52**).

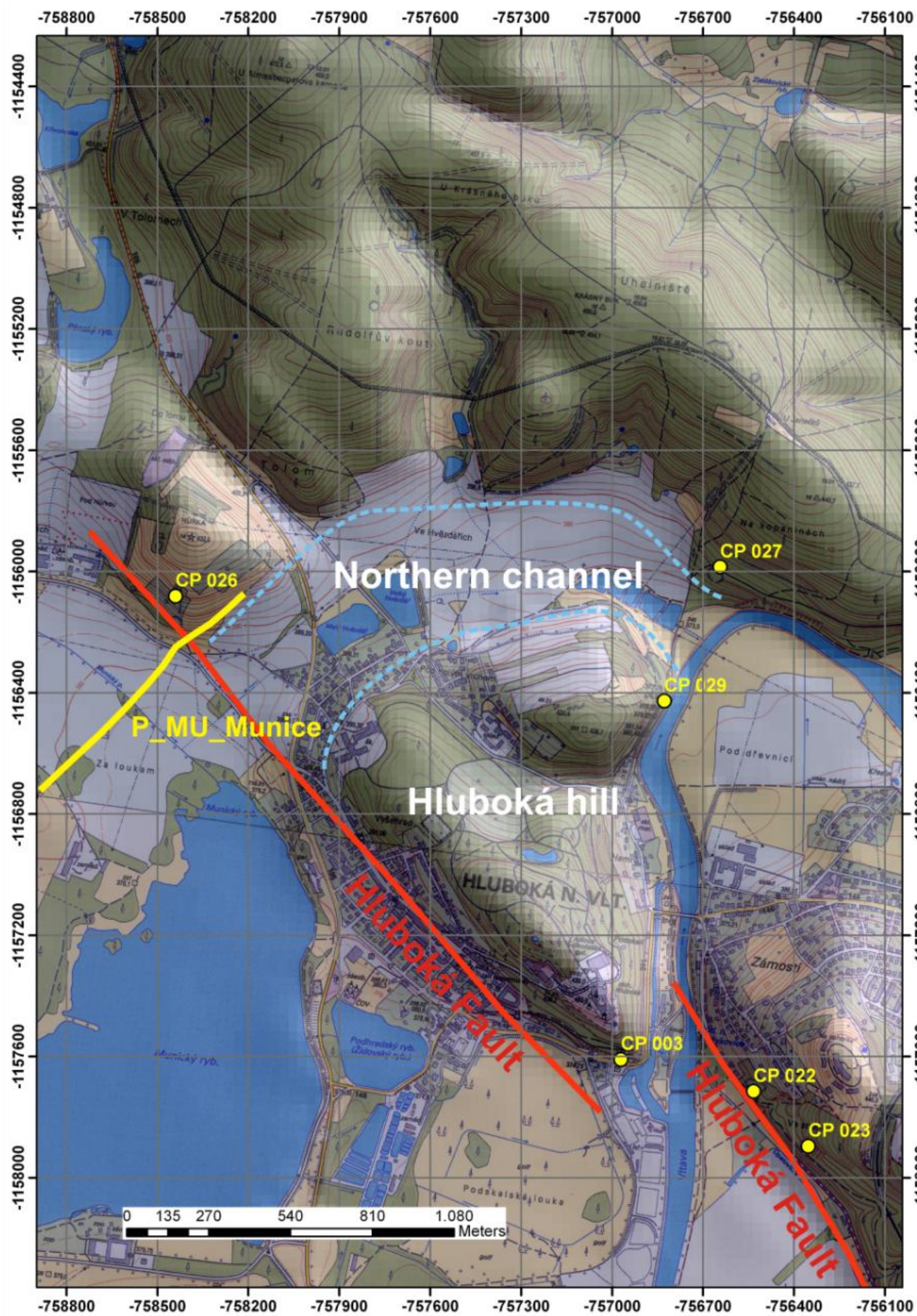

Fig. 52: Tertiary “northern channel” connecting the Budéjovice Basin in the west with the ox bow of the Vltavou north of Hluboka nad Vltavou in the east.

5.4. Top Miocene

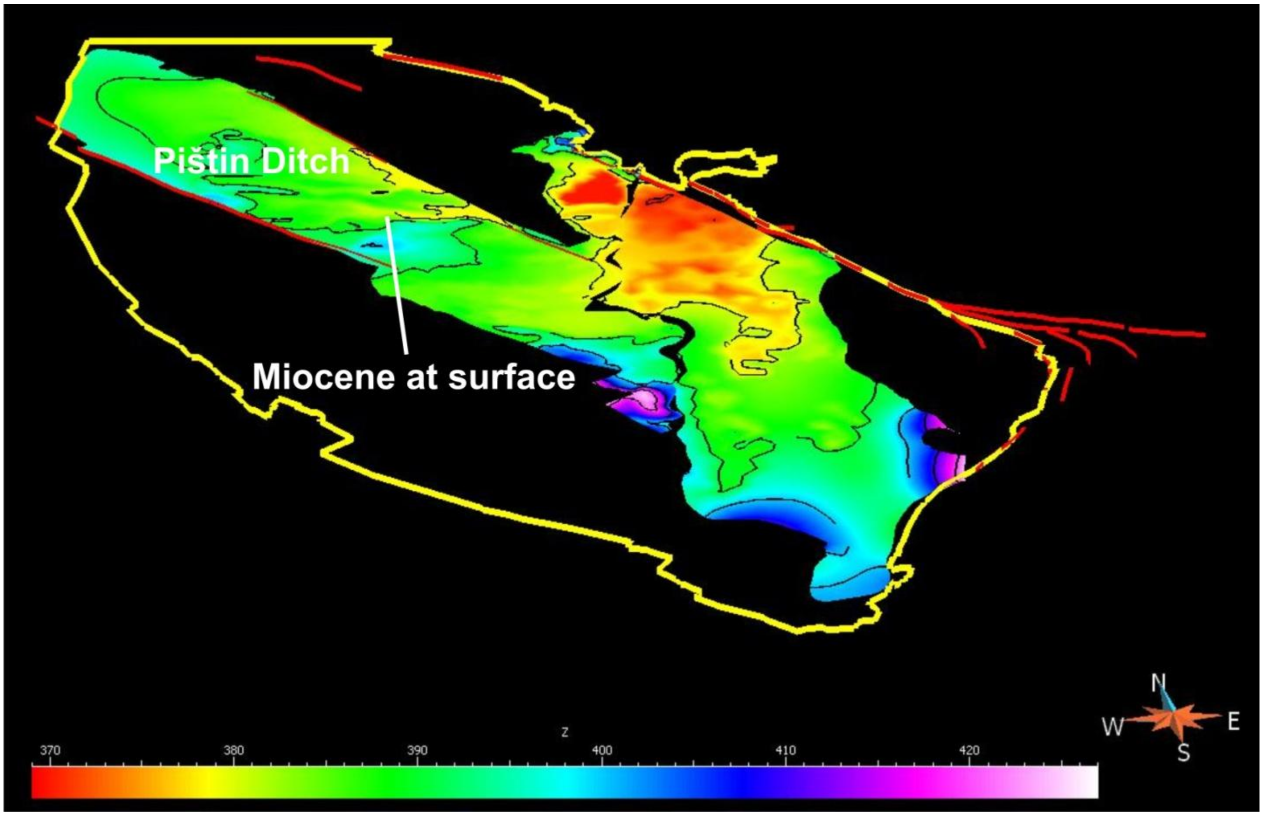

Fig.53: Horizon Top of Miocene sediments (Vertical exaggeration: 1:5. Color bar denotes elevation in meters above sealevel).

Miocene sediments crop out at the surface mostly in a 3 km broad zone between the Zbudov Fault in the NE and the Haklovy Dvory Fault in the SW (**Fig. 53**). Well data and information obtained from seismic sections P_MD_Mydlovary and P_DA_Dasny further indicate that Miocene sediments - mostly belonging to the Mydlovary Formation - completely fill up the northwestern part of this area down to the crystalline basin floor, also known as Pištin Ditch. In general, Miocene sediments are restricted to the central areas of the Budejovice Basin with the deepest part located in the northeastern section around Hluboka nad Vltavou.

The average thickness of Neogene strata is about 20 to 30 m. Neogene and Quarternary deposits therefore contribute only minor volumes to the basin fill.

5.5. Summary 3D-Modeling

The sedimentary infill of the Budějovice Basin mostly consists of Upper Cretaceous sediments of the Klikov-Formation increasing in thickness from west to east, predominantly overlain by Lower to Middle Miocene sediments of the Mydlovary Formation in the Pištin Ditch and, with lower thickness, in the Vltava and Malše flood plain area. The asymmetric basin shape geometry shown by the horizon Top Crystalline Basement in some ways resembles a terrestrial half-graben with comparable sediment forming conditions, which are divided into a high energy sedimentary facies (alluvial fans at the eastern margin) and a low energy sedimentary facies with lacustrine and fluvial sediments in the center of the Budějovice Basin. Another typical feature for such kind of setting is the presence of lakes and/or draining rivers in the area of the basin associated with the largest subsidence rate. In case of the Budějovice Basin this scheme is given by the course of the river Vltava and its tributary, the river Malše, entering the basin from the south and running close to the eastern part to the north, abandoning the basin east of Hluboká nad Vltavou.

With respect to the rhombic crystalline outline geometry, the Budějovice Basin most likely developed as a fault bounded basin along the right-lateral, NW-striking Jáchymov Fault Zone (**Fig. 54**). In this context, the Pištin Ditch could have been developed as a smaller, interior sub-pull-apart basin which opened later on during the Lower Miocene, filled with sediments of the Mydlovary Formation. This assumption would also imply that the Zbudov and Haklovy Dvory Fault would have to be regarded younger than the Hluboká and Dubné Fault, delimiting the basin to NE and SW. A comparison of the seismic profiles P_MU_Munice and P_DA_Dasny (see chapter 4.3. & 4.4.) shows that the Hluboká Fault terminates below Miocene deposits near Munice, whereas the Zbudov Fault cleary disrupts Miocene sediments at the surface. Unfortunately, fault characteristics for the Haklovy Dvory and Dubné Fault could not be acquired. Concerning the Rudolfov Fault at the southeastern margin of the basin normal faulting is strongly assumed from the image given in seismic section P_US_Usilne (see chapter 4.1.) and from the apparent dip of the crystalline basement between 50° to 60° shown in the 3D basin model.

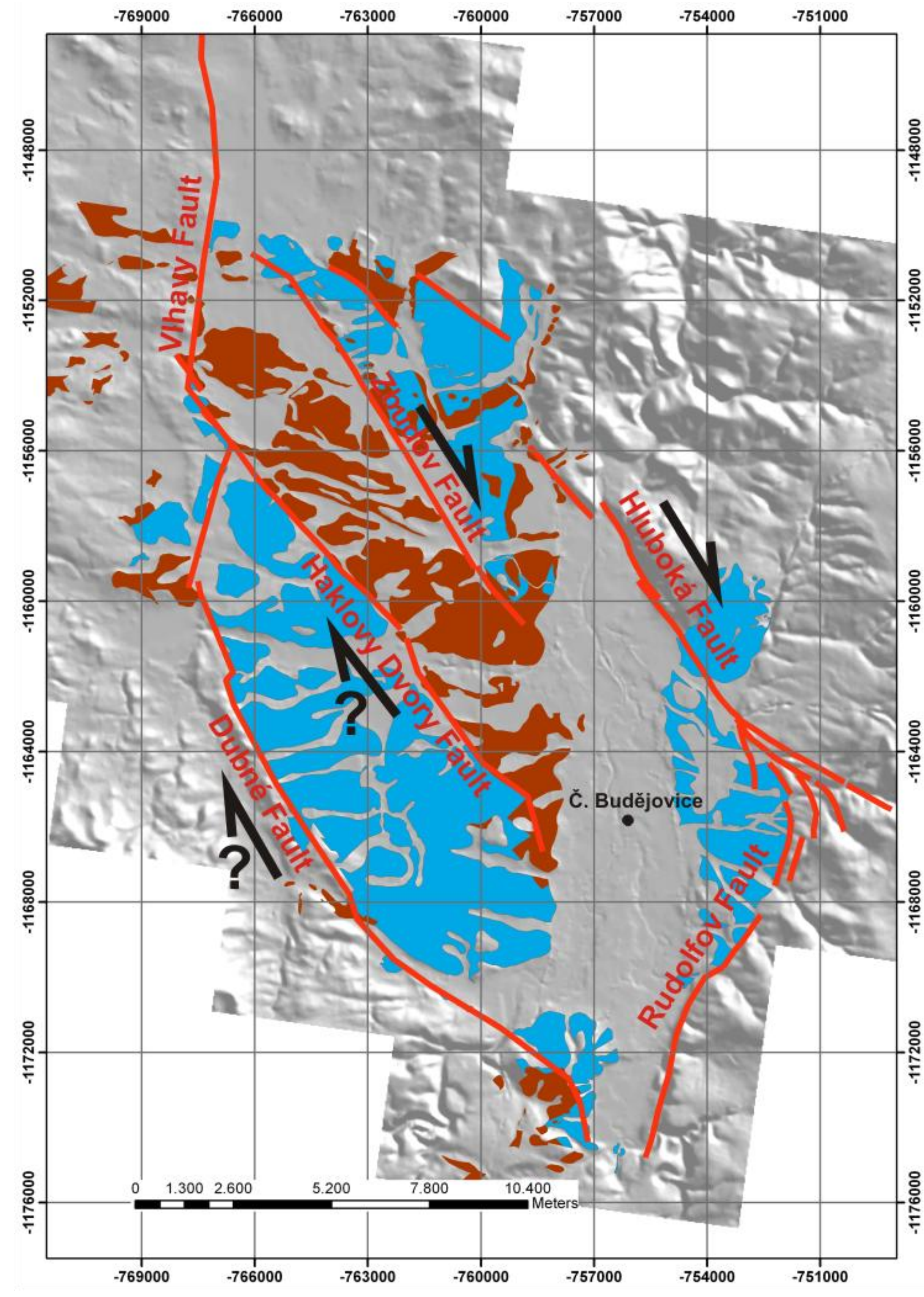

Fig. 54: Fault map of the Budějovice basin with the main sedimentary formation indicated in blue (Upper Cretaceous Klikov Fm.) and brown (Lower to Middle Miocene deposits).

6. Conclusion

In the course of this master thesis the following conclusion have been made:

The Hluboká Fault developed parallel to pre-existing Variscan ductile foliation and folds, which are characterized as deformation $\mathbf{D_1}$. The first movement of the Hluboká Fault took place in late-Variscan times under low to very low greenschist facies metamorphic conditions ($\mathbf{D_{2C}}$). Late-Variscan tectonics at low metamorphic conditions further include two extensional deformations with distinct stretching directions ($\mathbf{D_{2A}}$ - NW-SE-directed extension; $\mathbf{D_{2B}}$ - NE-SW-directed extension). No consistent age relations could be established between these deformations and ductile strike-slip faulting.

Ductile deformation structures are overprinted and reactivated by the following brittle structures:

- Brittle, NW-striking normal faults provide evidence for dominantly SW-directed extension ($\mathbf{D_3}$). The ages of deformed sediments from field and seismic investigation suggest post-Cretaceous to pre-Miocene age for $\mathbf{D_3}$.
- Sub-vertical, dextral strike-slip faults striking parallel to the Hluboká fault ($\mathbf{D_4}$). Faults correlated to this deformation occur in crystalline basement units, Permian deposits as well as in the Upper Cretaceous and Miocene basin fill suggesting post-Miocene age for $\mathbf{D_4}$.

Structures generally proof polyphase brittle deformation between the late Variscan orogeny and post-Miocene times. Structural data characterize both, the Hluboká and Zbudov Fault as dextral strike-slip faults.

Seismic data depict the Hluboká Fault as a sub-vertical, steeply SW-dipping strike-slip fault with a large component of normal displacement, offsetting crystalline basement units for up to 380 m. The fault offsets Cretaceous strata, which are folded into a large-scale asymmetrical syncline adjacent to the fault (P_HO_Hosin and P_US_Usilne). Seismic data provide no evidence for Cretaceous growth strata. The sections further exhibit a marked angular unconformity between the folded Cretaceous sediments and the overlying horizontal Miocene strata. Section P_MU_Munice shows that the main fault branch of the Hluboká Fault terminates at the Cretaceous-Miocene unconformity, not offsetting overlying Miocene sediments.

Sections across the parallel Zbudov Fault (P_DA_Dasny, P_MD_Mydlovary) display flower structures with two symmetrical fault branches cutting the Miocene sedimentary fill of the Budějovice Basin. These faults apparently converge into a single displacement zone within the crystalline basement. The migrated seismic depth sections proof that the Zbudov Fault is younger than Miocene. Evidence for the displacement of Miocene sediments at the Hluboká Fault has not been observed. The analyzed geological data indicates that the main subsidence in the eastern part of the Budéjovice Basin occurred due to post-Cretaceous tilting.
3D-Modeling of lithological and lithostratigraphical boundaries resulted in the construction of three surfaces (Top Crystalline Basement, Top Upper Cretaceous, Top Miocene), which are correlated across the entire Budějovice Basin. The horizon Top Crystalline Basement delineates an asymmetrical basin with a smooth basin floor gently dipping with about 5° towards NE and E. The NE basin margin is formed by the sub-vertical Hluboká Fault, the SE basin margin coincides with the Rudolfov Fault. Modeling indicates that the latter dips with about 50° towards the basin. Comparison of the horizons Top Upper Cretaceous and Top Miocene indicates that most of the basin fill is made up by Cretaceous strata. Miocene sediments reach their maximum thickness of about 80 m in the NNE-trending Pistin Ditch, which is delimited by the Zbudov and Haklovy Dvory Fault to the NE and SW, respectively.

Considering the spatial fault geometries of the Hluboká and Zbudov strike-slip faults, which parallel each other at distance of about 3 km, it appears likely that both faults join into a single deep-seated, right-lateral displacement zone associated with the Jáchymov Fault Zone.

7. References

ADAMOVIČ, J. & COUBAL, M. (1999) Intrusive Geometries and Cenozoic Stress History of the Northern Part of the Bohemian Massif. Geolines, Praha, 9: 5-14.

BRANDMAYR, M. DALLMEYER, R. D. HANDLER, R. & WALLBRECHER, E. (1995) Conjugate shear zones in the Southern Bohemian Massif (Austria): implications for Variscan and Alpine tectonothermal activity. Tectonophysics, 248: 97-116.

BRANDMAYR, M. LOIZENBAUER, J. & WALLBRECHER, E. (1997) Contrasting P-T conditions during conjugate shear zone development in the Southern Bohemian Massif, Austria. Mitt. Österr. Geol. Ges., 90: 11-29.

BÜTTNER, S. KRUHL, J. H. (1997) The evolution of a late-Variscan high-T/low-P region: the southeastern margin of the Bohemian massif. International Journal of Earth Sciences (Geol. Rundsch.), 86: 21-38.

BÜTTNER, S. (2007) Late Variscan stress-field rotation initiating escape tectonics in the south-western Bohemian Massif: a far field response to late-orogenic extension. Journal of Geosciences, 52: 29-43.

CHLUPÁČ, I. & VRÁNA, S. (Editors), (1994) Regional Geological subdivision of the Bohemian Massif on the territory of the Czech Republic. Report of the Working Group for the Regional Geological Classification of the Bohemian Massif at the former Czechoslovak Stratigraphic Commission. Journal of the Czech Geological Survey, 39/1: 18.

FALKE, H. (Editor), (1972) Rotliegend: Essays on European Lower Permian. Band 15, 299.

FALKE, H. (Editor), (1975) The Continental Permian in Central, West, and South Europe. Proceedings of the NATO Advanced Study Institute held at the Johannes Gutenberg University, Mainz

FINGER, F. GERDES, A. JANOUŠEK, V. RENÉ , M. & RIEGLER, G. (2007) Resolving the Variscan evolution of the Moldanubian sector of the Bohemian Massif: the significance of the Bavarian and the Moravo–Moldanubian tectonometamorphic phases. Journal of Geosciences, 52: 9–28.

FRITZ, H. (1991) Strukturelle Entwicklung am Südostrand der böhmischen Masse. Arbeitstagung Geol. B.-A., Geologie am Ostrand der Böhmischen Masse in Niederösterreich, Wien, S. 89-97.

FRITZ, H. (1996) Geodynamic and tectonic evolution of the southeastern Bohemian Massif: the Thaya section (Austria). Mineralogy and Petrology, 58: 253-278.

FRITZ, H. DALLMEYER, R. D. & NEUBAUER, F. (1996) Thick-skinned versus thin-skinned thrusting: Rheology controlled thrust propagation in the Variscan collisional belt (The southeastern Bohemian Massif, Czech Republic-Austria). Tectonics, Vol. 15, No. 6, 1389-1413.

FRITZ, H. & NEUBAUER, F. (1993) Kinematics of crustal stacking and dispersion in the south-eastern Bohemian Massif. Geol. Rundschau., 82: 556-565.

FUCHS, G. (1991) Das Bild der Böhmischen Masse im Umbruch. Jb. Geol. B.-A., Band 134, Heft 4, 701-710.

HAVÍŘ, J. (2000) Stress analyses in the epicentral area of Nový Kostel (Western Bohemia). Studia geoph. et geod., 44: 522-536.

HAVÍŘ, J. (2005) Orientations of the principal paleostresses in the Western Bohemia seismoactive region and their comparision with the recent stresses. Journal of the Czech Geological Society, 50: 3-4, 133-142.

HEJL, E. SEKYRA, G. & FRIEDL, G. (2003) Fission-track dating of the south-eastern Bohemian massif (Waldviertel, Austria): thermochronology and long-term erosion. International Journal of Earth Sciences, 92: 677–690.

HOLUB, V. & TÁSLER. R. (1978) Filling of the Late Palaeozoic basins in the Bohemian Massif as a record of their palaeogeographical development. International Journal of Earth Sciences (Geol. Rundsch.), 67/1: 91-109.

HUBER, K. H. (2003) Some Field Observations and Remarks on the Gmünd Beds of the Northwestern Waldviertel Region (Lower Austria). Jb. Geol. B.-A., Band 143, Heft 4, 543-566.

JINDRICH, V. (1971) New Views in Tectonic Significance of Platform Sediments in the Bohemian Massif, Czechoslovakia. Geological Society of America Bulletin, 82: 763-768.

KLEINSPEHN, K.L. PERSHING, J. & TEYSSIER, C. (1989) Paleostress stratigraphy: A new technique for analyzing tectonic control on sedimentary-basin subsidence. Geology, Vol. 17, No. 3, 253-256.

KOŠLER, J. KELLEY, S. P. & VRÁNA, S. (2001) $^{40}Ar/^{39}Ar$ hornblende dating of a microgranodiorite dyke: implications for early Permian extension in the Moldanubian Zone of the Bohemain Massif. International Journal of Earth Sciences (Geol. Rundsch.), 90: 379-385.

MALKOVSKÝ , M. (1987) The Mesozoic and Tertiary basins of the Bohemian Massif and their Evolution. Tectonophysics, 137: 31-42.

MALLARD, D.J. (1991) Learning to cope with faults. In: B. Mohammadioun (ed.), Proceedings of the International Conference “Seismic Hazard Determinations in Areas with Moderate Seismicity”, Quest Editions, Presses Academiques.

MANDL, G. (Editor), (1999) Field trip guide: Vienna - Dachstein - Hallstatt - Salzkammergut (UNESCO World Heritage Area). FOREGS '99 Vienna, 113.

MATTE, Ph. MALUSKI, H. RAJLICH, P. & FRANKE, W. (1990) Terrane boundaries in the Bohemian Massif: Result of large-scale Variscian shearing. Tectonophysics, 177: 151-170.

MATURA, A. (2003) Zur tektonischen Gliederung der variszischen Metamorphite im Waldviertel Niederösterreichs. Jb. Geol. B.-A., Band 143, Heft 2, 221-225.

MCCANN, T. (Editor), (2008) The Geology of Central Europe. Volume 2: Mesozoic and Cenozoic. The Geological Society of London, 1449.

PEŠKOVA, I. HÓK, J. ŠTĚPANČÍKOVÁ, P. STEMBERG, J. & VOJTKO, R. (2010) Results of stress analysis inferred from fault slip data along the Sudetic Marginal Fault (NE part of Bohemian Massif). Acta Geologica Slovaca, 2,1,: 11-16.

PETEREK, A. RAUCHE, H. SCHRÖDER, B. FRANZKE, H.-J. BANKWITZ, P. & BANKWITZ, E. (1997) The late-and post-Variscan tectonic evolution of the Western Border fault zone of the Bohemian massif (WBZ). Geol. Rundschau., 86: 191-202.

PITRA, P. BURG, J.-P. & GUIRAUD, M. (1999) Late Variscian strike-slip tectonics between the Teplá-Barrandian and Moldanubian terranes (Czech Bohemian Massif): petrostructural evidence. Journal of the Geological Society, London. Vol. 156: 1003-1020.

ŠIMŮNEK, P. PRACHAŘ, I. BARTÁK, V. DOMÁCÍ, L. & PISKAČ, J. (1995) NPP Temelín Construction Site. Supplementary geological and seismological surveys. Part A: Tectonics. Part B: Seismic risk. MS, Energoprůzkum, Prague.

SLÁNSKÁ, J. (1976) A Red-Bed Formation in the South Bohemian Basins, Czechoslovakia. Sedimentary Geology, 15: 135-164.

ŠPAČEK, P. PRACHAŘ, I. VALENTA, J. ŠTĚPANČÍKOVÁ, P. ŠVANCARA, J. PAZDÍRKOVÁ, R. HANŽLOVÁ, J. HAVÍŘ, J. & MÁLEK (2011) Quaternary activity of the Hluboká Fault. – Unpublished report MU Brno, 199pp + appendices.

SUK, M. (1984) Geological history of the territory of the Czech Socialist Republic. Geological Survey, Prague, 396.

VÁCHAL, J. ŠKODA, S. POPP, F. VÁCHALOVÁ, R. MORALOVÁ, J. & KOUPILOVÁ, M. (2010) The Hluboká tectonic break – a significant geofactor of Hluboká nad Vltavou. Journal of Landscape Studies, 2: 89 – 95.

VÁCHOVÁ, Z. & KVAČEK, J. (2009) Paleoclimate analysis of the Klikov Formation, Upper Cretaceous, Czech Republic. Bulletin of Geosciences, 84/2: 257-268.

WALLBRECHER, E. BRANDMAYR, M. HANDLER, R. LOITZENBAUER, J. MADERBACHER, F. & PLATZER, R. (1993) Konjugierte Scherzonen in der südlichen Böhmischen Masse: Variszische und alpidische kinematische Entwicklungen. Mitt. Österr. Miner. Ges., 138: 237-252.

WALTER, R. (2007) Geologie von Mitteleuropa. E. Schweizerbart'sche Verlagsbuchhandlung (Nägele u. Obermiller), Stuttgart, 7. Auflage, 511.

WESSELY, G. (2006) Geologie der Österreichischen Bundesländer: Niederösterreich. Geologische Bundesanstalt, Wien, 416.

ZIEGLER, P. A. (1990) Geological Atlas of the Central and Western Europe. Shell Internationale Petroleum Maatschappij B.V., Band 2, 239.

ZIEGLER, P. A. & DÈZES, P. (2007) Cenozoic uplift of Variscan Massifs in the Alpine foreland: Timing and controlling mechanisms. Global and Planetary Change, 58: 237–269.

ZULAUF, G. DÖRR, W. FIALA, J. & VEJNAR, Z. (1997) Late Cadomian crustal tilting and Cambrian transtension in the Teplá-Barrandian unit (Bohemian Massif, Central European Variscides). Geol. Rundsch., 86: 571-584.

ZULAUF, G. (2001) Structural style, deformation mechanisms and paleodifferential stress along an exposed crustal section: constraints on the rheology of quartzofeldspathic rocks at supra- and infrastructural levels (Bohemian Massif). Tectonopysics, 332: 211-237.

Attachments

1. Map system properties for all map images displayed in this master thesis:

Projected Coordinate System: S-JTSK_Krovak_East_North

Projection: Krovak
False Easting: 0,00000000
False Northig: 0,00000000
Pseudo Standard Parallel 1: 78,50000000
Scale Factor: 0,99990000
Azimuth: 30,28813975
Longitude of Center: 24,83333333
Latitude of Center: 49,50000000
X Scale: -1,00000000
Y Scale: 1,00000000
XY Plane Rotation: 90,00000000
Linear Unit: Meter

Geographic Coordinate System: GCS_S_JTSK

Datum: D_S_JTSK
Prime Median: Greenwich
Angular Unit: Degree

Sheroid Name: Bessel

2. Complete structural Datasets:

Name	X (Lat.)	Y(Long.)	Outcrop	Lithology/Unit	Complete Dataset
CP_001	49,03412	14,46845	Quarry	Phyllite, Gneiss/Crystalline Basement	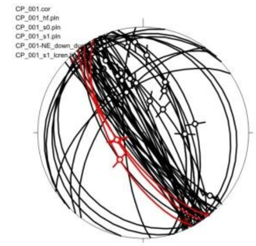
CP_002	49,07907	14,38524	Claypit	Upper Cretaceous clay and sand/Budějovice Basin	
CP_003	49,04929	14,44304	Quarry	Phyllite, Gneiss/Crystalline Basement	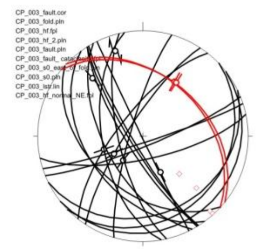
CP_004	49,00100	14,50897	Pit	Amphibolite/ Crystalline Basement	
CP_005	48,99185	14,55086	Quarry	Amphibolite, Aplite/ Crystalline Basement	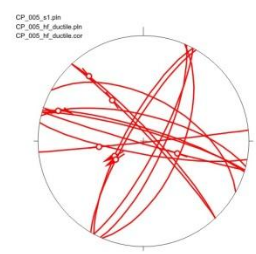

Name	X (Lat.)	Y(Long.)	Outcrop	Lithology/Unit	Complete Dataset
CP_006	49,02799	14,47264	Quarry	Phyllite, Gneiss/Crystalline Basement	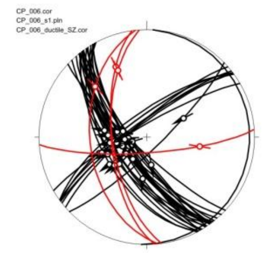
CP_007	49,03388	14,46833	Creek	Phyllite, Gneiss/Crystalline Basement	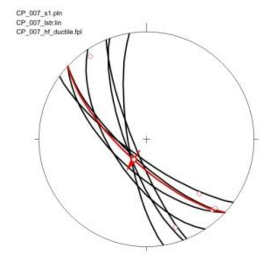
CP_008	49,03370	14,46731	Creek	Phyllite, Gneiss/Crystalline Basement	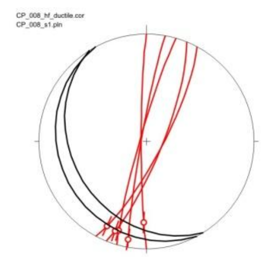
CP_009	49,02914	14,47376	Quarry	Phyllite, Gneiss/Crystalline Basement	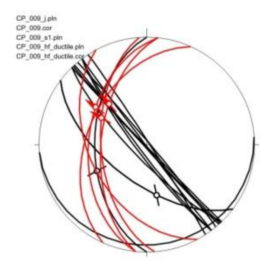
CP_010	49,02713	14,49156	Sandpit	Upper Cretaceous quartz sand/ Budějovice Basin	

Name	X (Lat.)	Y(Long.)	Outcrop	Lithology/Unit	Complete Dataset
CP_011	49,01250	14,51491	Pond	Permian shale and siltstones/ Lhotice Basin	
CP_012	48,99248	14,55334	Quarry	Amphibolite/ Crystalline Basement	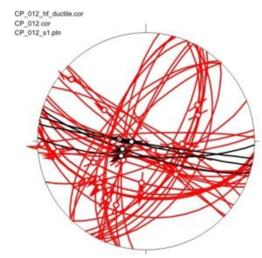
CP_013	49,08390	14,34033	Pit	Conglomerate/ Budějovice Basin	
CP_013b	49,03333	14,47806	Creek	Phyllite, Gneiss/Crystalline Basement	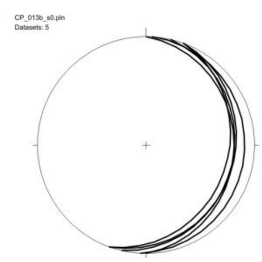
CP_014	49,03305	14,47944	Creek	Phyllite, Gneiss/Crystalline Basement	

Name	X (Lat.)	Y(Long.)	Outcrop	Lithology/Unit	Complete Dataset
CP_015	49,03250	14,47750	Creek	Phyllite, Gneiss/Crystalline Basement	
CP_016	49,02833	14,48194	Creek	Phyllite, Gneiss/Crystalline Basement	
CP_017	49,02806	14,48139	Creek	Phyllite, Gneiss/Crystalline Basement	
CP_018	49,02722	14,48000	Creek	Phyllite, Gneiss/Crystalline Basement	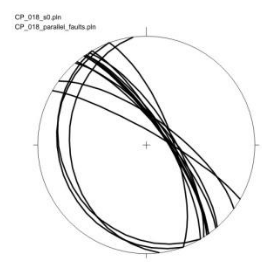
CP_019	49,03111	14,47000	Quarry	Phyllite, Gneiss/Crystalline Basement	

Name	X (Lat.)	Y(Long.)	Outcrop	Lithology/Unit	Complete Dataset
CP_020	49,03139	14,47389	Quarry	Phyllite, Gneiss/Crystalline Basement	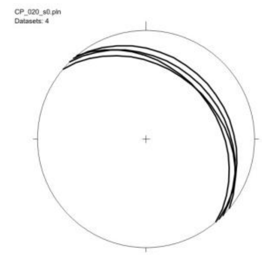
CP_021	49,03556	14,47111	Creek	Phyllite, Gneiss/Crystalline Basement	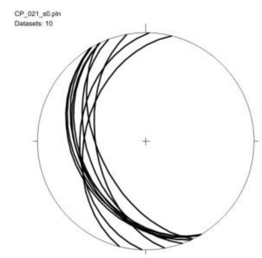
CP_022	49,04889	14,44917	Quarry	Phyllite, Gneiss/Crystalline Basement	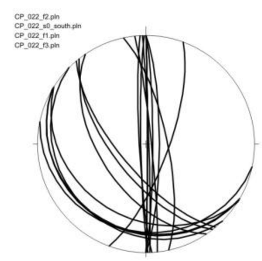
CP_023	49,04750	14,45194	Quarry	Phyllite, Gneiss/Crystalline Basement	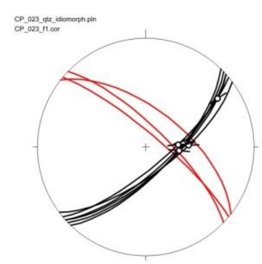
CP_024	49,03583	14,46722	Creek	Phyllite, Gneiss/Crystalline Basement	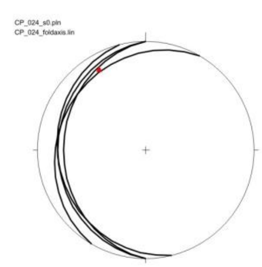

Name	X (Lat.)	Y(Long.)	Outcrop	Lithology/Unit	Complete Dataset
CP_025	49,03750	14,46889	Quarry	Phyllite, Gneiss/Crystalline Basement	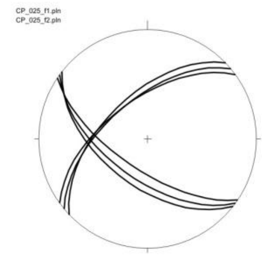
CP_026	49,06111	14,42028	Quarry	Phyllite, Gneiss/Crystalline Basement	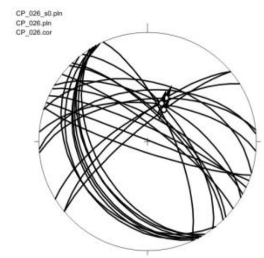
CP_027	49,06417	14,44444	Quarry	Phyllite, Gneiss/Crystalline Basement	
CP_028	49,06361	14,45611	Quarry	Phyllite, Gneiss/Crystalline Basement	
CP_029	49,06000	14,44278	Quarry	Phyllite, Gneiss/Crystalline Basement	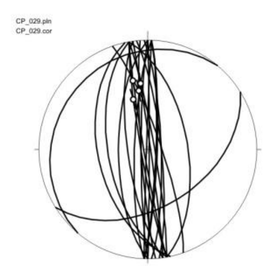

3. Seismic data:

Post-stack/pre-migration data of seismic profile **P_US_Usilne.**

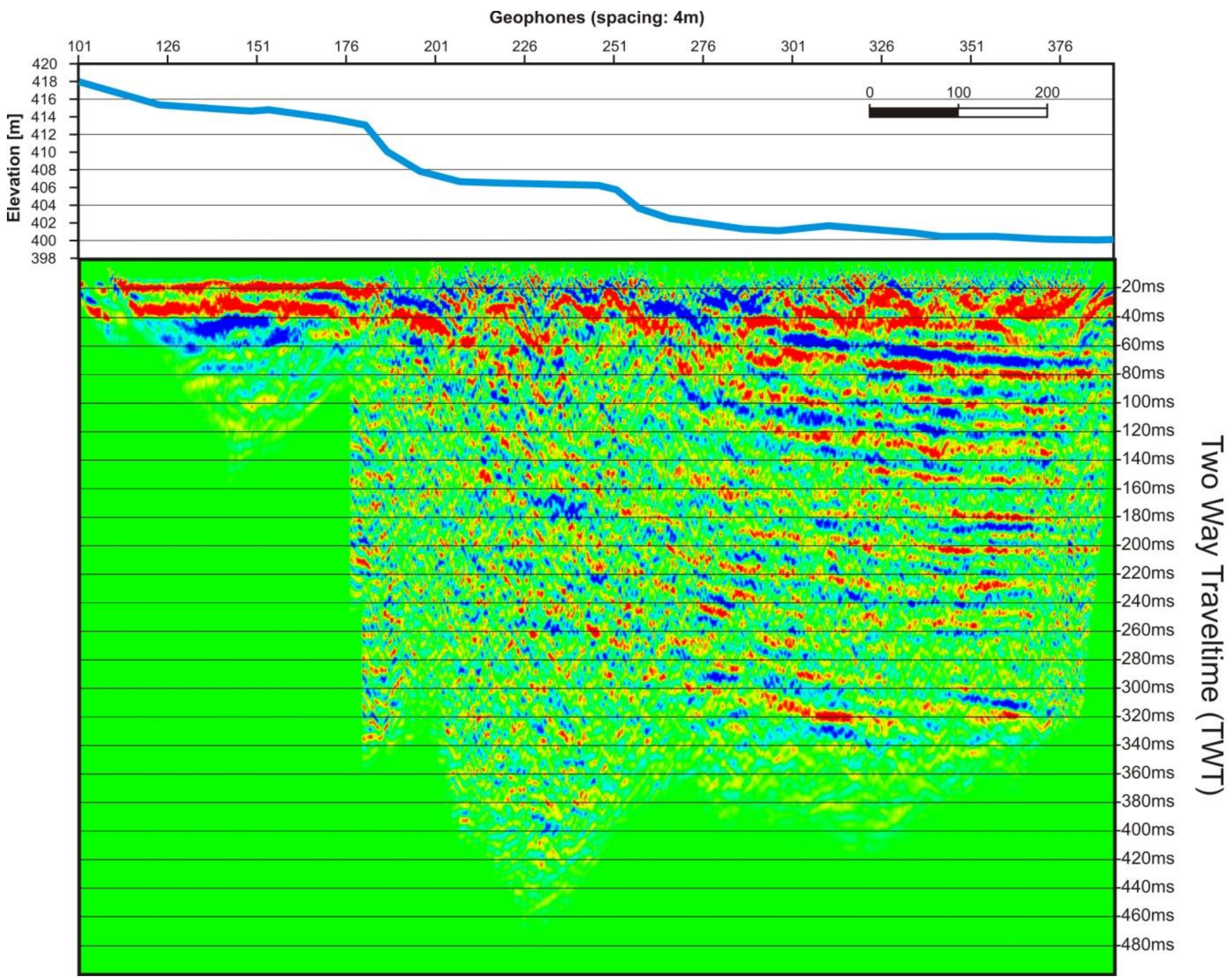

Post-stack/pre-migration data of seismic profile **P_HO_Hosin.**

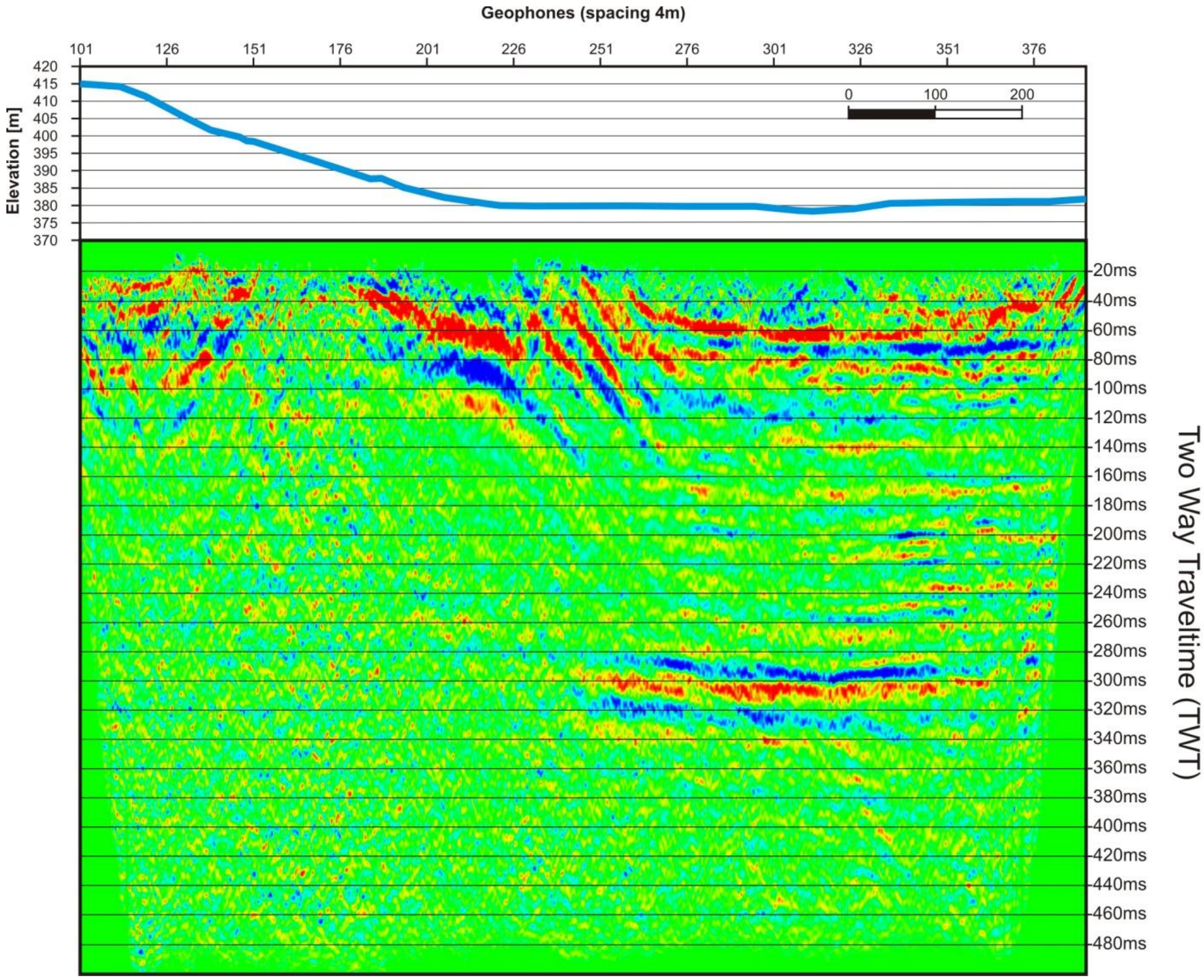

Post-stack/pre-migration data of seismic profile **P_MU_Munice.**

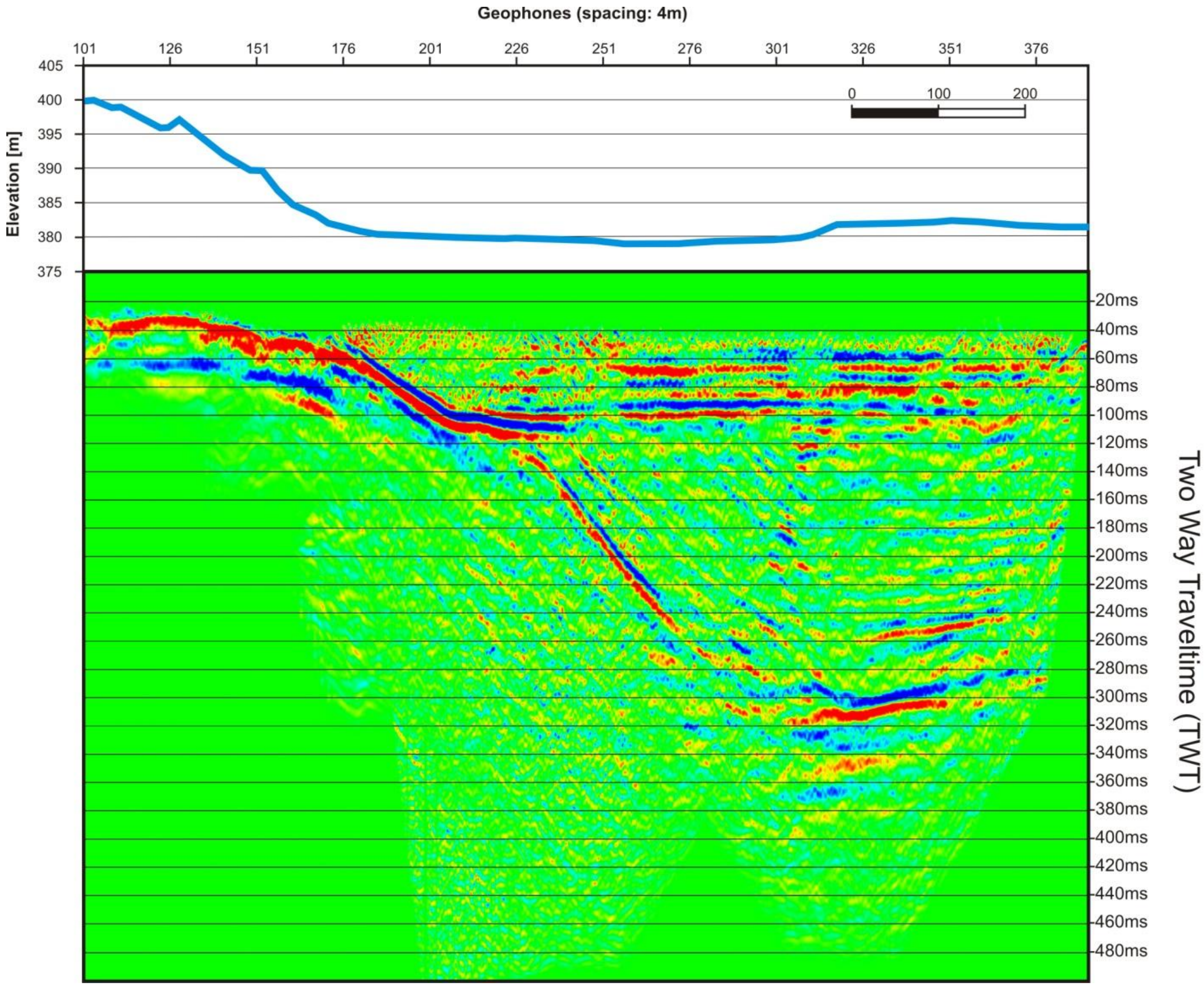

Post-stack/pre-migration data of seismic profile **P_DA_Dasny.**

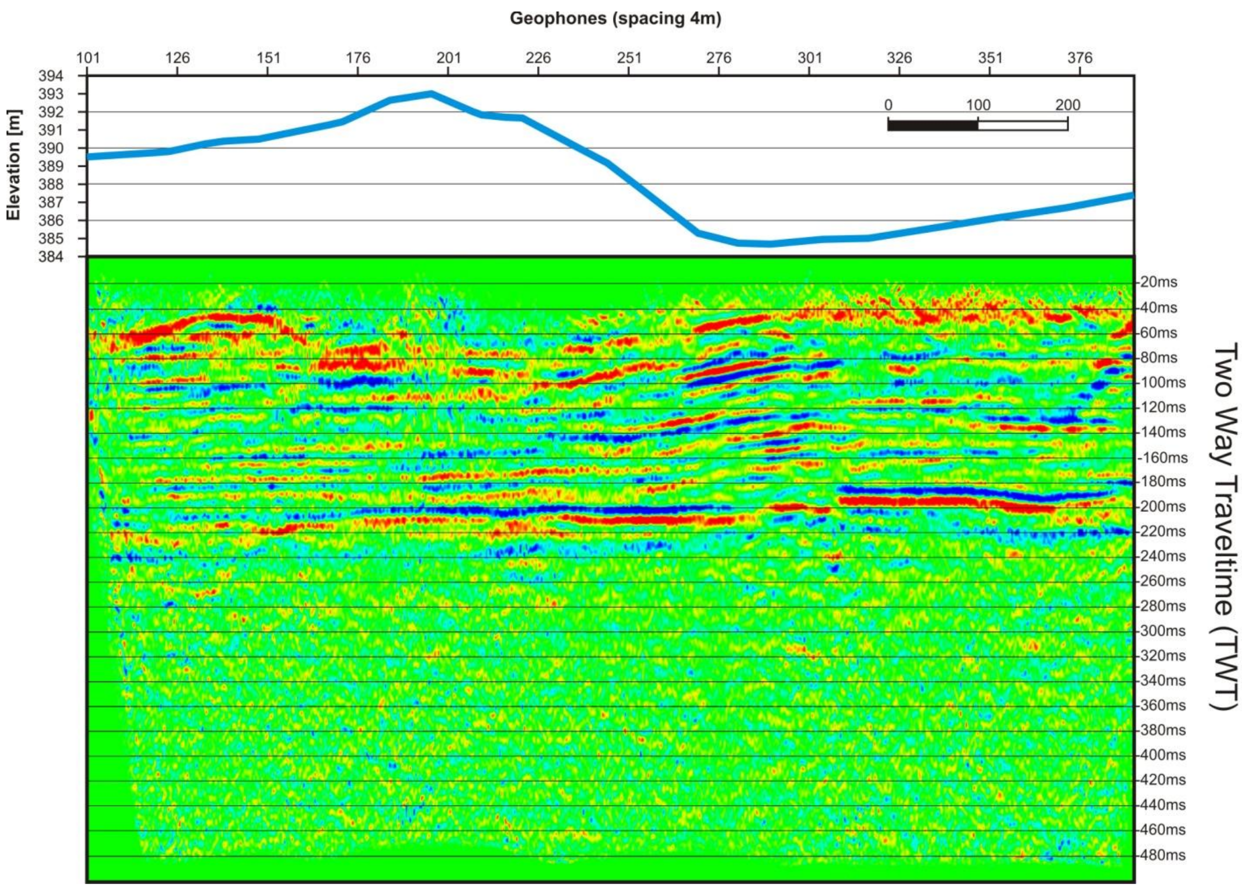

Post-stack/pre-migration data of seismic profile **P_MD_Mydlovary.**

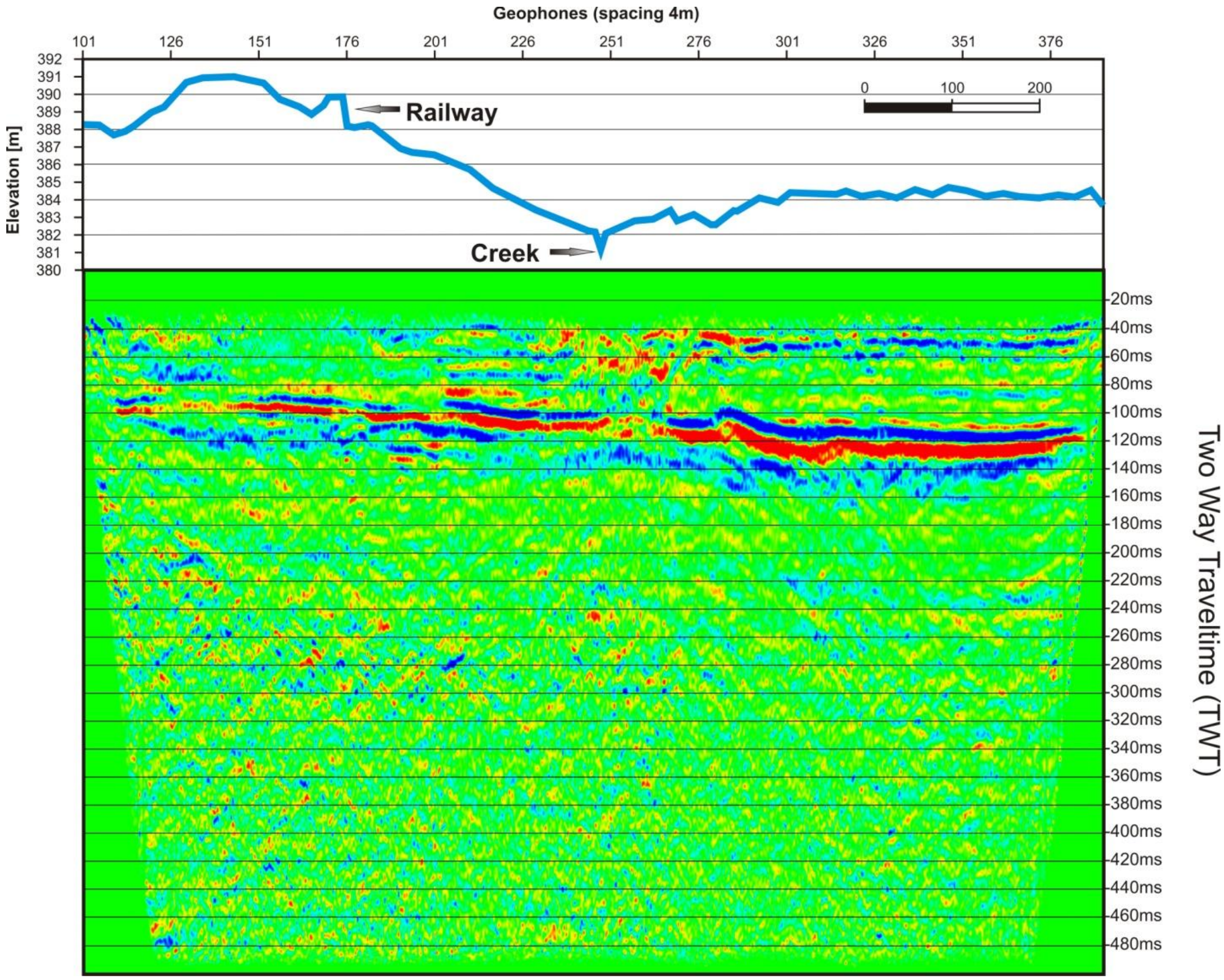

4. Drillings for database:

ID	Geofond_Nr.	Drilling_name	Report_Nr.	X [m]	Y [m]	XY from:	Elevation [m]	Elevation from:	Depth [m]
1		OP1	CIP-drilling	-755936,16	-1159246,21	differ. GPS	374,44	differ. GPS	6,0
2		OP2	CIP-drilling	-755893,99	-1159223,93	differ. GPS	374,24	differ. GPS	10,0
3		HR1	CIP-drilling	-754930,64	-1160824,02	differ. GPS	387,32	differ. GPS	6,0
4		HR2	CIP-drilling	-754958,48	-1160849,40	differ. GPS	386,59	differ. GPS	9,6
5		OP3	CIP-drilling	-755816,00	-1159217,99	differ. GPS	374,33	differ. GPS	3,5
6		OP4	CIP-drilling	-755803,71	-1159214,36	differ. GPS	375,06	differ. GPS	3,8
7		OP5	CIP-drilling	-755736,26	-1159207,88	differ. GPS	388,47	differ. GPS	12,7
8		OP6	CIP-drilling	-755720,51	-1159203,54	differ. GPS	391,22	differ. GPS	5,0
9		HL4	CIP-drilling	-756523,77	-1157955,09	differ. GPS	373,15	differ. GPS	5,0
10		HL5	CIP-drilling	-756556,03	-1157984,79	differ. GPS	373,44	differ. GPS	8,0
11		HL6	CIP-drilling	-756571,13	-1158006,69	differ. GPS	373,21	differ. GPS	7,2
12		HL 12	CIP-drilling	-756361,53	-1158220,30	hand GPS	373,40	differ. GPS	8,0
13		HL 13	CIP-drilling	-756347,46	-1158209,14	hand GPS	373,40	differ. GPS	10,0
14		HL 14	CIP-drilling	-756305,90	-1158166,19	hand GPS	373,50	Map 1:10	10,0
15		HL 10	CIP-drilling	-756695,43	-1156810,64	hand GPS	373,30	Map 1:10	4,0
16		HL 11	CIP-drilling	-756754,31	-1156800,69	hand GPS	373,30	Map 1:10	5,0
17		HL 8	CIP-drilling	-756651,99	-1158528,44	hand GPS	373,50	differ. GPS	7,6
18		HL 9	CIP-drilling	-756576,11	-1158441,56	hand GPS	373,50	Map 1:10	7,0
19		M3	CIP-drilling	-758077,95	-1156501,05	differ. GPS	387,53	differ. GPS	10,0
20		MUN1	CIP-drilling	-758729,68	-1155589,56	differ. GPS	404,55	differ. GPS	23,5
21		MUN2	CIP-drilling	-758904,74	-1155628,80	differ. GPS	403,15	differ. GPS	10,0
22	646301	VO-76/P	FZ005230	-752637,05	-1166291,72	measured	415,26	measured	15,4
23	646319	VO-85/HV	FZ005230	-752741,95	-1166263,32	measured	412,40	measured	13,0
24	646323	VO-81/P	FZ005230	-752615,63	-1166375,79	measured	417,27	measured	14,0
25	646331	VO-63SI	FZ005230	-752775,59	-1166187,53	measured	411,93	measured	10,0
26	646351	VO-69Sc	FZ005230	-752651,09	-1166260,44	measured	415,06	measured	23,0
27	646352	VO-70	FZ005230	-752510,57	-1166266,84	measured	417,62	measured	22,7
28	646353	VO-71	FZ005230	-752540,50	-1166426,11	measured	420,04	measured	22,0
29	646354	VO-74/P	FZ005230	-752771,58	-1166255,57	measured	411,27	measured	15,0
30	646356	VO-72	FZ005230	-752585,96	-1166200,97	measured	414,96	measured	20,0
31	646357	VO-75/P	FZ005230	-752692,90	-1166276,70	measured	413,73	measured	16,0
32	646358	VO-77	FZ005230	-752409,59	-1166244,89	measured	419,29	measured	18,0
33	646359	VO-79/P	FZ005230	-752737,93	-1166229,40	measured	412,92	measured	18,0
34	646360	VO-78/P	FZ005230	-752733,75	-1166191,41	measured	412,15	measured	20,5
35	509132	GB3	P012010	-760554,70	-1165525,50	measured	411,90	measured	190,0
36	385418	OH3	P012368	-755672,00	-1160903,00	measured	382,00	measured	6,0
37	507095	B1	P012368	-756998,00	-1163435,00	measured	385,50	measured	5,0
38	507096	B2	P012368	-757082,00	-1162840,00	measured	381,20	measured	5,0
39	507102	B8	P012368	-756434,00	-1162247,00	measured	378,50	measured	7,5
40	507103	B9	P012368	-757763,00	-1161137,00	measured	376,40	measured	6,0
41	507108	B14	P012368	-758187,00	-1160867,00	measured	378,00	measured	7,0
42	507113	OH8	P012368	-755415,00	-1161589,00	measured	384,20	measured	7,0
43	507116	R4	P012368	-755287,60	-1170156,70	measured	390,00	measured	6,0
44	507118	R6	P012368	-755577,70	-1169592,50	measured	393,50	measured	7,0
45	507119	R7	P012368	-755600,00	-1168769,00	measured	390,00	measured	6,0
46	511446	PL5	P012368	-755809,00	-1172761,50	measured	398,60	measured	7,4
47		B3	P012368	-757215,00	-1162393,00	measured	379,80	measured	5,7
48		B4	P012368	-756896,00	-1162200,00	measured	378,80	measured	7,0
49		B5	P012368	-756496,00	-1162854,00	measured	380,20	measured	7,6
50		B6	P012368	-756101,00	-1162865,00	measured	379,70	measured	7,0
51		B7	P012368	-757232,00	-1161554,00	measured	377,20	measured	6,0
52		B11	P012368	-755550,00	-1162925,00	measured	379,70	measured	6,3
53		B12	P012368	-756452,00	-1163502,00	measured	380,00	measured	7,0
54		B13	P012368	-756025,00	-1163558,00	measured	381,00	measured	8,0
55		B15	P012368	-758279,00	-1161365,00	measured	378,50	measured	9,0
56		OH1	P012368	-755220,00	-1162100,00	measured	386,00	measured	6,0
57		OH2	P012368	-755180,00	-1161116,00	measured	384,00	measured	6,0
58	385419	OH4	P012368	-755642,00	-1160237,00	measured	382,50	measured	5,0
59		OH5	P012368	-756260,00	-1160025,00	measured	373,80	measured	6,0
60	385421	OH6	P012368	-756158,00	-1159518,00	measured	374,90	measured	5,0

61		OH7	P012368	-755865,00	-1161678,00	measured	382,10	measured	8,0
62		PI1	P012368	-756264,34	-1173827,78	measured	402,00	measured	5,5
63		PI2	P012368	-756025,06	-1173551,59	measured	401,12	measured	5,0
64		PI3	P012368	-755716,91	-1173207,60	measured	401,63	measured	8,9
65		PI4	P012368	-756112,86	-1172946,11	measured	399,79	measured	11,5
66		PI5	P012368	-755809,02	-1172761,55	measured	398,62	measured	7,4
67		PI6	P012368	-755583,45	-1172581,90	measured	398,67	measured	8,1
68		PI7	P012368	-755756,31	-1172482,68	measured	397,88	measured	7,0
69		PI8	P012368	-755533,30	-1172318,53	measured	396,89	measured	6,0
70		PI9	P012368	-755384,67	-1172037,35	measured	396,27	measured	8,0
71		PI10	P012368	-755294,27	-1171709,38	measured	396,31	measured	6,0
72		PI11	P012368	-754930,00	-1170957,00	measured	393,00	measured	6,8
73		PI12	P012368	-755196,50	-1170893,50	measured	392,50	measured	7,0
74		PI13	P012368	-756370,38	-1173431,33	measured	401,24	measured	6,5
75		PI14	P012368	-756658,56	-1173100,25	measured	400,23	measured	6,0
76		PI15	P012368	-756657,02	-1172883,19	measured	400,00	measured	9,5
77		PI16	P012368	-756336,01	-1172549,31	measured	400,04	measured	7,4
78		V3	P012368	-754153,00	-1168321,00	measured	411,00	measured	10,0
79		V4	P012368	-754173,00	-1168430,00	measured	407,50	measured	11,0
80		R2	P012368	-756014,00	-1169398,00	measured	396,00	measured	3,0
81		R3	P012368	-755007,50	-1170483,00	measured	392,50	measured	5,0
82		R4	P012368	-755287,57	-1170156,73	measured	390,00	measured	6,0
83		R5	P012368	-755711,28	-1170164,74	measured	394,00	measured	6,7
84		R6	P012368	-755577,66	-1169592,52	measured	393,50	measured	7,0
85		R7	P012368	-755600,00	-1168769,00	measured	390,00	measured	6,0
86	506961	BR14	P012694	-759930,00	-1163726,80	measured	391,80	measured	80,4
87	506819	V16	P013074	-756820,00	-1161590,00	map	377,90	measured	20,0
88	506821	VP18	P013074	-756750,00	-1161555,00	map	377,30	measured	9,0
89	506823	VP21	P013074	-756660,00	-1161515,00	map	377,30	measured	18,0
90	506824	V22	P013074	-756830,00	-1161535,00	map	377,50	measured	20,0
91	506825	VP23	P013074	-756780,00	-1161520,00	map	376,50	measured	20,0
92	506826	VP24	P013074	-756760,00	-1161500,00	map	377,00	measured	16,0
93	506827	VP26	P013074	-756720,00	-1161480,00	map	377,30	measured	25,0
94	506828	V27	P013074	-756675,00	-1161465,00	map	377,80	measured	20,0
95	506829	VP28	P013074	-756755,00	-1161430,00	map	378,00	measured	17,0
96	506830	VC19	P013074	-756720,00	-1161540,00	map	377,38	measured	6,0
97	506831	VC25	P013074	-756740,00	-1161490,00	map	377,27	measured	20,0
98	506839	P7A	P013074	-756737,00	-1161495,00	map	377,30	measured	16,2
99	506842	P10	P013074	-756748,00	-1161469,00	map	377,20	measured	16,0
100	506843	P11	P013074	-756750,00	-1161475,00	map	377,20	measured	16,0
101	510302	K1	P016805	-753767,00	-1166849,00	map	399,50	map	7,4
102	510303	K2	P016805	-753766,00	-1166845,00	map	399,60	map	7,2
103	510304	V11	P016805	-753814,00	-1166857,50	map	398,20	map	11,0
104	510306	V13	P016805	-753762,00	-1166840,00	map	399,60	map	7,4
105	510307	V14	P016805	-753770,00	-1166872,00	map	399,30	map	6,2
106	510308	V15	P016805	-753782,00	-1166871,00	map	398,70	map	6,9
107	510309	V16	P016805	-753787,00	-1166847,00	map	398,80	map	9,2
108	507920	CB1	P018879	-758440,00	-1166200,00	map	425,00	map	56,0
109	507921	CB2	P018879	-758504,00	-1164068,50	measured	390,20	measured	252,0
110	385293	HL1	P018881	-756042,59	-1159261,79	measured	374,44	measured	331,0
111	506909	HL2	P018881	-760774,46	-1161255,28	measured	386,88	measured	180,4
112	506034	V902	P020833	-756110,00	-1163865,00	map	381,28	measured	8,5
113	511947	Vi1	P022238	-755661,97	-1172403,81	measured	397,40	measured	233,0
114	509141	DB21	P023688	-760922,33	-1162909,57	measured	386,13	measured	171,0
115	506910	HP-III	P025997	-758415,60	-1164009,47	measured	389,54	measured	223,5
116	506913	HP-IX	P025997	-759588,52	-1160549,36	measured	383,65	measured	199,0
117	511461	HP-I	P025997	-758990,31	-1171642,95	measured	428,49	measured	76,5
118	511382	HV1	P031266	-758790,20	-1171791,80	measured	440,28	measured	50,5
119	511384	HV3	P031266	-758903,50	-1171777,30	measured	437,51	measured	50,0
120	511385	HV4	P031266	-758958,40	-1171814,40	measured	438,50	measured	40,0

121	511386	HV5	P031266	-759028,60	-1171731,40	measured	436,01	measured	37,0
122	511389	HJ8	P031266	-758976,20	-1171695,90	measured	432,30	measured	50,0
123	508288	J1	P031783	-756490,20	-1166870,00	measured	385,90	measured	12,0
124	508289	J2	P031783	-756476,90	-1166883,00	measured	385,90	measured	12,8
125	508290	J3	P031783	-756506,90	-1166889,20	measured	385,60	measured	13,0
126	508291	J4	P031783	-756484,40	-1166904,20	measured	385,60	measured	12,2
127		V 501	P034617	-756849,10	-1157488,70	measured	374,08	measured	6,7
128		V 502	P034617	-756828,50	-1157476,50	measured	374,04	measured	6,5
129	506285	HV1	P037401	-759664,80	-1166880,00	measured	408,58	measured	50,0
130	506496	V1	P045955	-757807,00	-1165440,00	map	388,70	measured	9,0
131	506497	V2	P045955	-757810,00	-1165470,00	map	388,60	measured	9,0
132	506498	V3	P045955	-757820,00	-1165450,00	map	388,70	measured	9,0
133	506500	V5	P045955	-757820,00	-1165455,00	map	388,70	measured	9,0
134	506503	V7	P045955	-757840,00	-1165400,00	map	388,50	measured	8,0
135	506897	HP1	P046334	-756820,00	-1165230,30	measured	382,72	measured	100,0
136	506898	HP2	P046334	-756729,00	-1164649,00	measured	382,38	measured	84,0
137	509584	V10	P046834	-753496,10	-1162227,80	measured	394,40	measured	3,0
138	506480	W1	P046999	-756181,10	-1166915,50	measured	386,90	measured	4,8
139	506481	W2	P046999	-756199,10	-1166924,90	measured	387,00	measured	4,2
140	506482	W3	P046999	-756198,00	-1166897,60	measured	387,20	measured	4,5
141	506483	W4	P046999	-756179,70	-1166893,20	measured	387,10	measured	4,7
142	507958	V9	P057396	-756223,00	-1166062,00	map	385,50	measured	8,0
143	507961	V12	P057396	-756267,00	-1165989,00	map	384,50	measured	8,0
144	507965	V16	P057396	-756256,00	-1165922,00	map	385,20	measured	9,0
145	507966	V17	P057396	-756251,00	-1165904,00	map	385,30	measured	8,0
146	507967	V18	P057396	-756229,00	-1165941,00	map	385,30	measured	8,0
147	507968	V19	P057396	-756242,00	-1165925,00	map	385,30	measured	9,0
148	385914	SG29	P058157	-760520,00	-1159420,00	map	389,00	map	31,0
149	385982	HJ1	P063920	-759593,90	-1158242,70	measured	393,53	measured	14,0
150	511951	J15	P064218	-762607,60	-1169891,30	measured	434,80	measured	5,0
151	511952	J16	P064218	-762598,80	-1169865,70	measured	434,60	measured	5,0
152	511214	J21	P072430	-753076,55	-1165023,31	measured	406,10	measured	4,0
153	511216	J26	P072430	-753145,10	-1165092,99	measured	405,65	measured	3,5
154	511217	J16	P072430	-753088,05	-1165131,98	measured	406,74	measured	3,0
155	511219	J18	P072430	-753040,55	-1165088,01	measured	406,33	measured	3,0
156	511224	J12	P072430	-753138,88	-1165121,23	measured	406,14	measured	3,0
157	511229	J5	P072430	-753197,18	-1165178,19	measured	405,86	measured	5,0
158	511230	J4	P072430	-753213,57	-1165161,84	measured	405,74	measured	5,0
159	511231	J3	P072430	-753234,13	-1165176,89	measured	405,89	measured	5,0
160	511232	J2	P072430	-753224,98	-1165196,96	measured	405,85	measured	5,0
161	511280	V1	P073873	-753770,00	-1165660,00	measured	401,90	map	8,0
162	511281	V2	P073873	-753730,00	-1165680,00	measured	401,90	map	6,5
163	509140	HV3	P074222	-755419,50	-1163976,70	measured	383,88	measured	312,0
164	634939	HV2	P074683	-755845,00	-1167494,00	measured	387,29	measured	274,0
165	509280	V1	P081852	-755890,00	-1165500,00	map	384,80	measured	12,0
166	509281	V2	P081852	-755890,00	-1165505,00	map	385,00	measured	10,5
167	509285	V4	P081862	-755250,00	-1164655,00	map	383,70	measured	6,0
168	567948	CB1	P088401	-755200,00	-1167710,00	map	389,00	map	32,0
169	603271	V9	P092301	-755604,00	-1164307,00	map	383,20	measured	15,0
170	637262	V1	P099250	-756564,00	-1162132,00	map	379,00	map	9,0
171	637212	V4	P099288	-756220,00	-1160947,00	map	377,00	map	8,0
172	637214	V3	P099288	-756227,00	-1160980,00	map	377,20	map	8,0
173	637255	V1	P099288	-756171,00	-1160989,00	map	377,30	map	8,0
174	637256	V5	P099288	-756198,00	-1160949,00	map	377,20	map	8,0
175	657984	V101	P106755	-754792,10	-1166512,20	map	389,42	measured	20,0
176	657985	V102	P106755	-754960,90	-1166529,80	map	388,64	measured	18,0
177	657986	V103	P106755	-754821,80	-1166448,50	map	389,88	measured	20,0
178	657987	V104	P106755	-754869,50	-1166484,80	map	389,15	measured	20,0
179	657988	V105	P106755	-754970,30	-1166480,40	map	388,85	measured	20,0
180	682112	4H-092b	P118196	-758429,21	-1164049,14	measured	398,50	measured	52,4

181	686605	HV8	P118472	-758222,00	-1167082,00	map	410,00	map	41,0
182	684643	4H-085c	P118880	-759574,64	-1160562,41	measured	383,70	measured	195,0
183	687079	4H-086b	P119935	-759570,22	-1160553,10	measured	383,67	measured	60,0
184	687082	4H-093c	P119940	-757953,45	-1158335,29	measured	375,85	measured	305,8
185	687083	4H-094b	P119941	-757958,46	-1158344,71	measured	375,71	measured	61,4
186	695653	4H-091c	P124241	-758427,39	-1164037,60	measured	389,43	measured	221,9
187	695986	V3	P122244	-756854,00	-1166104,00	map	386,08	measured	6,0
188	696172	V1018	P122300	-757264,19	-1164612,00	measured	388,46	measured	10,0
189	506778	8/128	V046625	-757320,00	-1163340,00	map	385,00	map	9,8
190	385564	HV1	V067186	-759372,00	-1158126,00	measured	386,28	measured	62,0
191	510404	W14	V068451	-753578,10	-1165341,10	measured	401,80	measured	5,0
192	510416	W35	V068451	-753618,70	-1164729,60	measured	402,30	measured	8,0
193	507199	HV1	V071221	-756988,50	-1161872,30	measured	377,30	measured	65,0
194	507872	V205	V074279	-756323,04	-1165745,27	measured	382,10	measured	5,5
195	507873	V206	V074279	-756324,81	-1165715,15	measured	381,93	measured	5,0
196	507874	V207	V074279	-756355,74	-1165713,29	measured	381,74	measured	5,0
197	507875	V208	V074279	-756419,17	-1165703,45	measured	384,45	measured	9,0
198	507877	V217	V074279	-756829,18	-1163993,12	measured	383,57	measured	9,5
199	507878	V218	V074279	-756725,74	-1164067,64	measured	381,80	measured	6,0
200	507879	V219	V074279	-756668,33	-1163996,94	measured	381,43	measured	7,5
201	507880	V220	V074279	-756673,25	-1164036,75	measured	381,48	measured	7,0
202	507881	V221	V074279	-756577,00	-1163926,00	measured	382,15	measured	8,0
203	507882	V222	V074279	-756582,00	-1163977,00	measured	383,01	measured	8,0
204	507403	V240	V074279	-757073,08	-1161720,25	measured	377,49	measured	7,5
205	507883	V243	V074279	-757674,70	-1161233,03	measured	377,08	measured	8,0
206	507884	V244	V074279	-757687,33	-1161221,66	measured	377,15	measured	10,0
207	507885	PV247	V074279	-757864,40	-1161286,69	measured	377,27	measured	7,5
208	507404	V248	V074279	-757903,11	-1161339,07	measured	377,57	measured	8,0
209	507887	V250	V074279	-757948,37	-1161145,46	measured	378,80	measured	10,0
210	507405	V251	V074279	-757987,18	-1161143,80	measured	378,70	measured	13,0
211	508927	HV1	V075502	-758869,50	-1166872,50	measured	408,74	measured	31,0
212		W2	V075892	-754905,56	-1161080,00	measured	386,55	measured	4,5
213		W10	V075892	-754882,19	-1161691,89	measured	386,04	measured	4,0
214	506596	V311	V076292	-756437,40	-1161958,50	measured	379,40	measured	7,5
215	506597	V312	V076292	-756393,30	-1161916,80	measured	377,90	measured	6,0
216	511979	HV1	V078994	-758079,00	-1170631,00	measured	396,30	measured	9,5
217	511980	HV2	V078994	-758037,20	-1170622,70	measured	396,47	measured	7,0
218	509681	W33	V079237	-753087,50	-1167858,70	measured	419,60	measured	4,5
219	509683	W41	V079237	-753308,30	-1168120,00	measured	426,60	measured	3,3
220	506947	903-B	P46014	-755196,00	-1161722,00	map	385,50	Map 1:10	10,0
221	507869	PV202	V074279	-756517,00	-1165711,00	map	384,97	measured	9,0
222	507870	V203	V074279	-756410,00	-1165741,00	map	383,09	measured	6,0
223	507871	V204	V074279	-756355,00	-1165746,00	map	381,90	measured	5,5
224		PV503	P034617	-756848,70	-1157447,00	measured	373,80	measured	6,5
225		PV504	P034617	-756833,60	-1157445,80	measured	374,13	measured	7,0
226		PV505	P034617	-756817,70	-1157444,80	measured	374,20	measured	6,8
227		V506	P034617	-756844,50	-1157402,90	measured	373,68	measured	7,0
228		V507	P034617	-756831,20	-1157401,60	measured	373,99	measured	7,0
229		V508	P034617	-756819,90	-1157401,00	measured	374,13	measured	6,8
230		V509	P034617	-756687,40	-1157702,70	measured	374,71	measured	7,3
231		V510	P034617	-756657,60	-1157684,80	measured	374,65	measured	7,0
232		PW511	P034617	-756679,70	-1157711,60	measured	374,94	measured	5,6
233		W531	P034617	-755549,90	-1156343,20	measured	380,32	measured	3,2
234		K544	P034617	-754422,80	-1153839,00	measured	373,13	measured	2,2
235		K547	P034617	-754399,70	-1153669,40	measured	373,19	measured	1,2
236		K548	P034617	-754443,40	-1153592,70	measured	381,50	measured	2,4
237		W554	P034617	-756800,80	-1156370,30	measured	372,53	measured	2,3
238		PW555	P034617	-756806,20	-1156215,80	measured	375,07	measured	6,0
239		W556	P034617	-756741,10	-1156031,00	measured	378,94	measured	6,0
240		V561	P034617	-756876,60	-1157501,40	measured	374,34	measured	7,2

241		V562	P034617	-756829,40	-1157522,00	measured	374,46	measured	7,6
242		V563	P034617	-756815,10	-1157529,00	measured	374,57	measured	7,4
243		Sonda 1	P043456	-755811,00	-1156901,00	map (Prachar)	380,00	map (Prachar)	8,0
244		Sonda 2	P043456	-755815,00	-1156907,00	map (Prachar)	380,00	map (Prachar)	8,0
245		Sonda 3	P043456	-755795,00	-1156908,00	map (Prachar)	380,00	map (Prachar)	8,0
246	507391	S1	V039457	-756375,00	-1161576,00	map	377,89	measured	5,5
247	507392	S2	V039457	-756305,00	-1161501,00	map	377,53	measured	6,0
248	507393	S3	V039457	-756445,00	-1161539,00	map	377,79	measured	7,0
249	507394	S4	V039457	-756352,00	-1161462,00	map	377,50	measured	6,0
250	507395	S5	V039457	-756455,00	-1161500,00	map	377,75	measured	6,0
251	507396	S6	V039457	-756390,00	-1161526,00	map	377,57	measured	7,0
252	507397	S7	V039457	-756387,00	-1161452,00	map	377,50	measured	7,5
253		S1	V052185	-756774,00	-1161554,00	map	380,00	map	17,0
254		S2	V052185	-756666,00	-1161505,00	map	380,00	map	18,0
255		S3	V052185	-756703,00	-1161528,00	map	380,00	map	12,0
256		S4	V052185	-756717,00	-1161531,00	map	380,00	map	10,7
257		S5	V052185	-756721,00	-1161533,00	map	380,00	map	10,7
258		S6	V052185	-756730,00	-1161538,00	map	380,00	map	11,0
259		S7	V052185	-756739,00	-1161541,00	map	380,00	map	10,7
260		S8	V052185	-756748,00	-1161545,00	map	380,00	map	10,7
261	506033	V901	P020833	-756568,00	-1166312,00	map	385,00	map 1:10	8,5
262	506035	V903	P020833	-756693,00	-1162385,00	map	378,70	map 1:10	7,7
263	384472	V904	P020833	-756580,00	-1159348,00	map	378,80	map 1:10	8,5
264	384473	V905	P020833	-757549,00	-1157971,00	map	373,00	map 1:10	8,5
265	384533	S7	P040773	-758347,00	-1154168,00	map	403,10	map	9,5
266	384537	S10A	P040773	-757830,00	-1152463,00	map	419,10	map	3,5
267	384538	S11	P040773	-757580,00	-1151953,00	map	422,50	map	6,5
268	384539	S11A	P040773	-757544,00	-1151951,00	map	421,50	map	6,5
269	382762	S14	P040773	-757478,00	-1150352,00	map	463,20	map	2,0
270	384545	V3	P043441	-757709,00	-1157932,00	map	374,12	measured	8,0
271	384546	V4	P043441	-757819,00	-1158100,00	map	374,98	measured	8,0
272	384682	V1	P045945	-758820,00	-1154680,00	map	396,90	map	10,0
273	384683	V2	P045945	-758816,00	-1154692,00	map	397,30	map	10,0
274	385040	Sonda 1	P029743	-761095,00	-1155069,00	map	403,60	map	5,0
275	385041	Sonda 2	P029743	-761170,00	-1155020,00	map	405,90	map	5,0
276	385042	Sonda 3	P029743	-760968,00	-1155033,00	map	402,80	map	5,0
277		V-1	P046834	-752725,60	-1164336,70	map	412,10	map	3,0
278		V-2	P046834	-752755,30	-1164158,30	map	412,10	map	2,0
279		V-3	P046834	-752772,90	-1164011,00	map	411,70	map	2,0
280		V-4	P046834	-752935,30	-1163797,00	map	408,60	map	2,0
281		V-11	P046834	-753525,00	-1161951,00	map	398,20	map	3,0
282		V-12	P046834	-753521,20	-1161934,60	map	398,80	map	3,0
283		V-14	P046834	-753742,90	-1161810,20	map	400,90	map	3,0
284		V-15	P046834	-753706,30	-1161711,80	map	402,70	map	2,0
285		V-16	P046834	-754068,50	-1161401,90	map	399,90	map	2,0
286		V-17	P046834	-754288,60	-1161213,20	map	399,30	map	2,0
287		V-18	P046834	-754490,00	-1161007,60	map	399,40	map	3,0
288		V-34	P046834	-756754,40	-1158277,80	map	373,40	map	8,0
289		V-35	P046834	-756858,10	-1158257,60	map	374,80	map	8,0
290		V-36	P046834	-757002,20	-1158230,70	map	372,40	map	3,0
291		V-45	P046834	-758609,20	-1158323,00	map	378,60	map	2,0
292		V-46	P046834	-758811,80	-1158285,50	map	379,60	map	3,0
293		V-47	P046834	-758816,10	-1158256,60	map	379,50	map	3,0
294		V-48	P046834	-759071,10	-1158185,30	map	378,20	map	2,0
295		V-49	P046834	-759254,40	-1157992,10	map	380,40	map	2,0
296		V-52	P046834	-759811,60	-1157388,10	map	394,20	map	2,0
297		V-53	P046834	-759932,00	-1157266,70	map	391,40	map	2,0
298		V-55	P046834	-760177,20	-1156531,60	map	391,10	map	2,0
299		V-58	P046834	-760673,10	-1155712,00	map	384,00	map	4,0
300		V-59	P046834	-760548,80	-1155421,40	map	383,30	map	2,0

301		V-60	P046834	-760855,50	-1155390,40	map	383,20	map	2,0
302		V-61	P046834	-760974,10	-1155043,20	map	388,00	map	2,0
303		V-63	P046834	-761263,10	-1154386,10	map	388,10	map	2,0
304		V-64	P046834	-761284,60	-1154389,90	map	388,00	map	2,0
305		V-66	P046834	-761833,60	-1154319,10	map	398,17	map	3,0
306		V-67	P046834	-761849,20	-1154293,60	map	397,70	map	3,0
307		V-68	P046834	-762173,00	-1154429,30	map	395,00	map	2,2
308		V-70	P046834	-762586,70	-1154196,70	map	395,20	map	2,0
309		V-71	P046834	-762627,80	-1154177,90	map	394,20	map	2,0
310		V-72	P046834	-762675,00	-1154329,40	map	391,00	map	3,0
311		V-73	P046834	-762691,70	-1154339,00	map	391,10	map	3,0
312		S1	P047243	-757131,00	-1157657,00	measured	371,48	measured	3,8
313		W-3	P047243	-759371,30	-1156094,80	measured	384,16	measured	5,0
314		W-4	P047243	-760343,10	-1155775,80	measured	385,25	measured	4,8
315		W-5	P047243	-760942,30	-1155145,90	measured	384,50	measured	3,0
316		W-6	P047243	-760557,20	-1155405,20	measured	382,97	measured	3,7
317		S-7	P047243	-761086,80	-1155147,60	measured	383,15	measured	3,2
318	510730	PJ-2	P058529	-752325,70	-1163702,30	measured	423,80	measured	5,0
319	510731	J-3	P058529	-752297,20	-1163657,10	measured	424,50	measured	5,0
320		JB 65	P059532	-753465,80	-1163429,70	measured	400,30	measured	6,0
321	510770	JB 66	P059532	-753362,70	-1163360,80	measured	400,10	measured	6,0
322	510771	JB 67	P059532	-753235,60	-1163278,70	measured	400,60	measured	6,0
323	510772	JB 68	P059532	-753110,00	-1163199,70	measured	402,40	measured	7,0
324	510773	JBV69	P059532	-752984,30	-1163137,20	measured	414,10	measured	15,0
325	510774	JB72	P059532	-752906,30	-1163056,70	measured	414,30	measured	9,0
326		V1	P064215	-757738,10	-1157761,40	map	376,34	measured	7,5
327		V2	P064215	-757754,60	-1157749,10	map	376,54	measured	8,5
328		PV3	P064215	-757793,40	-1157749,30	map	376,66	measured	8,6
329		V4	P064215	-757756,00	-1157834,00	map	375,87	measured	7,5
330		V5	P064215	-757795,60	-1157940,10	map	375,71	measured	8,5
331		V6	P064215	-757823,90	-1158031,60	map	375,97	measured	7,6
332		PV7	P064215	-757829,80	-1158194,00	map	375,64	measured	8,0
333		V8	P064215	-757802,40	-1158105,80	map	375,49	measured	8,0
334		V9	P064215	-757783,10	-1158057,90	map	375,06	measured	7,5
335		PV10	P064215	-757754,40	-1158068,40	map	374,62	measured	7,6
336		V11	P064215	-757757,20	-1158017,90	map	374,64	measured	7,5
337		V12	P064215	-757719,20	-1157959,80	map	374,16	measured	8,0
338		V13	P064215	-757741,70	-1157930,50	map	374,66	measured	8,0
339		V14	P064215	-757723,90	-1157886,60	map	375,25	measured	8,0
340		V15	P064215	-757697,00	-1157795,90	map	374,69	measured	7,0
341		V16	P064215	-757707,20	-1157838,00	map	374,84	measured	7,0
342		PV17	P064215	-757672,20	-1157853,50	map	373,59	measured	7,0
343		J1	P065311	-759524,44	-1156005,91	measured	386,12	measured	5,0
344		J2	P065311	-759495,62	-1156010,76	measured	385,47	measured	4,0
345		J3	P065311	-759473,79	-1156015,60	measured	384,90	measured	4,0
346		J4	P065311	-759526,77	-1156023,51	measured	386,19	measured	5,0
347		J5	P065311	-759497,25	-1156029,02	measured	385,45	measured	6,0
348		J6	P065311	-759470,37	-1156033,44	measured	384,97	measured	4,0
349		PJ-7	P065311	-759473,89	-1156024,08	measured	385,47	measured	4,0
350		J8	P065311	-759446,36	-1156035,44	measured	384,57	measured	4,0
351	385986	V1	P069183	-759439,00	-1155952,00	map	384,20	map	17,0
352	555339	J-1(HV10)	P078195	-759198,00	-1155720,00	measured	387,71	measured	6,0
353	555332	PJ-2	P078195	-759201,00	-1155716,00	measured	386,84	measured	4,0
354	555333	J-3	P078195	-759198,00	-1155743,00	measured	390,38	measured	6,0
355	555334	J-4	P078195	-759198,00	-1155752,00	measured	390,58	measured	5,3
356	555335	PJ-5	P078195	-759190,00	-1155760,00	measured	392,80	measured	2,8
357	555336	PJ-6	P078195	-759189,00	-1155764,00	measured	393,00	measured	4,2
358	555337	J-7	P078195	-759200,00	-1155758,00	measured	390,85	measured	1,7
359	555338	J-8	P078195	-759198,00	-1155763,00	measured	391,30	measured	3,4
360	555340	HV-11	P078195	-759184,00	-1155739,00	measured	389,71	measured	4,5

361	687081	4H-088b	P119937	-759437,31	-1155449,86	measured	390,23	measured	65,0
362	687080	4H-087c	P119936	-759448,71	-1155434,01	measured	390,26	measured	168,0
363	386673	J1	P070441	-752510,00	-1160326,00	measured	440,22	measured	8,0
364	386674	J2	P070441	-752612,00	-1160623,00	measured	430,69	measured	15,0
365	386675	J4	P070441	-752640,00	-1160645,00	measured	432,41	measured	15,0
366	386676	J5	P070441	-752668,00	-1160640,00	measured	433,31	measured	15,0
367	386677	J6	P070441	-752724,00	-1160752,00	measured	429,23	measured	7,0
368	386678	J7	P070441	-752774,00	-1160910,00	measured	424,79	measured	6,0
369	386679	J8	P070441	-752824,00	-1161026,00	measured	423,71	measured	5,0
370	511102	J9	P070441	-753000,00	-1161402,00	measured	409,40	measured	6,0
371	511103	J10	P070441	-753052,00	-1161545,00	measured	407,60	measured	6,0
372	511104	J11	P070441	-753090,00	-1161670,00	measured	405,75	measured	6,0
373	511105	J12	P070441	-753124,00	-1161816,00	measured	402,50	measured	6,0
374	511106	J13	P070441	-753148,00	-1161946,00	measured	400,90	measured	6,0
375	511107	J14	P070441	-753138,00	-1162066,00	measured	398,45	measured	11,5
376	511108	J15	P070441	-753212,00	-1162064,00	measured	399,45	measured	15,0
377	511109	J16	P070441	-753156,00	-1162118,00	measured	398,41	measured	12,0
378	511110	J17	P070441	-753194,00	-1162118,00	measured	398,43	measured	13,5
379	511111	J18	P070441	-753165,00	-1162174,00	measured	398,33	measured	15,0
380	511112	J19	P070441	-753189,00	-1162157,00	measured	397,43	measured	12,0
381	511113	J20	P070441	-753181,00	-1162265,00	measured	398,23	measured	8,0
382	511114	J21	P070441	-753171,00	-1162380,00	measured	399,03	measured	15,0
383	511115	J22	P070441	-753195,00	-1162395,00	measured	398,73	measured	15,0
384	511116	J23	P070441	-753180,00	-1162543,00	measured	400,63	measured	8,0
385	511117	J24	P070441	-753168,00	-1162632,00	measured	400,50	measured	6,0
386	511118	J25	P070441	-753060,00	-1163000,00	measured	417,83	measured	7,0
387	386680	J26	P070441	-752904,00	-1160974,00	measured	422,99	measured	8,0
388	511119	J27	P070441	-753168,00	-1162344,00	measured	399,18	measured	15,0
389	511120	J28	P070441	-753144,00	-1162745,00	measured	404,93	measured	4,0
390	511121	J29	P070441	-753234,00	-1162094,00	measured	397,13	measured	10,0
391	511122	J30	P070441	-753215,00	-1162095,00	measured	396,88	measured	15,0
392	511123	J31	P070441	-753145,00	-1163095,00	measured	405,64	measured	2,0
393	511124	J32	P070441	-752782,00	-1162992,00	measured	415,20	measured	2,0
394	511125	J33	P070441	-752800,00	-1163116,00	measured	413,33	measured	2,0
395	511126	J34	P070441	-752835,00	-1163196,00	measured	412,28	measured	2,0
396	511127	J35	P070441	-752919,00	-1163217,00	measured	414,83	measured	2,0
397	386681	V-51	P070441	-734586,00	-1160494,00	measured	430,79	measured	4,0
398	386682	V-52	P070441	-734610,00	-1160546,00	measured	430,05	measured	5,0
399	511128	V-57	P070441	-735156,00	-1162026,00	measured	399,95	measured	4,0
400	511129	V-58	P070441	-735116,00	-1162191,00	measured	398,38	measured	6,0
401	511130	V-59	P070441	-735120,00	-1162161,00	measured	398,28	measured	6,0
402	511131	V-60	P070441	-735044,00	-1162921,00	measured	414,73	measured	2,0
403		US 1	V070452	-753975,50	-1162310,50	map	391,70	map	345,0
404	511144	JB-115	P072607	-753015,90	-1163120,10	measured	414,00	measured	7,0
405	511134	JB101	P072607	-753327,60	-1163361,20	measured	400,30	measured	7,0
406	386016	V1B	P073775	-757370,37	-1157467,70	map	375,85	measured	8,0
407	386017	V2	P073775	-757384,93	-1157494,19	map	374,57	measured	8,0
408	386018	V3	P073775	-757396,30	-1157471,39	map	375,47	measured	8,0
409	386020	V5	P073792	-757399,21	-1157488,01	map	374,41	measured	13,0
410	386052	V1	P073835	-757464,17	-1157552,03	map	373,22	measured	8,0
411	386053	V2	P073835	-757458,13	-1157536,91	map	373,21	measured	8,0
412	386054	V3	P073835	-757444,11	-1157540,56	map	372,88	measured	8,0
413	386055	V4	P073835	-757451,76	-1157557,13	map	373,01	measured	8,0
414	386021	V1	P073862	-757644,75	-1157149,57	map	392,33	measured	5,1
415	386022	V2	P073862	-757667,62	-1157138,81	map	391,88	measured	7,0
416	386023	V3	P073862	-757681,07	-1157115,05	map	392,01	measured	5,0
417	386024	V4	P073862	-757583,26	-1157314,63	map	384,40	measured	7,5
418	386025	V5	P073862	-757602,30	-1157330,77	map	383,48	measured	7,5
419	386026	V6	P073862	-757595,47	-1157209,61	map	389,70	measured	6,0
420	385967	J1	P067984	-757254,40	-1157328,70	measured	429,48	measured	5,5

421	385968	J2	P067984	-757259,80	-1157310,20	measured	434,43	measured	6,0
422	385969	J3	P067984	-757291,30	-1157293,10	measured	434,89	measured	6,0
423	385970	J4	P067984	-757160,20	-1157371,20	measured	438,32	measured	10,0
424	385971	J5	P067984	-757169,20	-1157347,80	measured	438,75	measured	6,0
425	385972	J6	P067984	-757276,10	-1157288,50	measured	437,26	measured	5,0
426	385973	J7	P067984	-757247,00	-1157304,40	measured	434,62	measured	4,0
427	386067	HV-10	P083860	-755321,25	-1159701,06	measured	426,01	measured	22,0
428	386068	HV-11	P083860	-755388,04	-1159719,27	measured	421,55	measured	36,0
429	386069	HV-12	P083860	-755362,81	-1159786,71	measured	411,74	measured	17,0
430	607262	V1	P085791	-756829,00	-1157549,00	map	372,00	map 1:10	7,3
431	607263	V2	P085791	-756830,00	-1157573,00	map	372,00	map 1:10	8,0
432	607264	V3	P085791	-756830,00	-1157588,00	map	372,00	map 1:10	7,5
433	600265	V3	P092310	-757557,00	-1157652,00	map	373,62	measured	6,0
434	600266	V4	P092310	-757583,00	-1157683,00	map	373,33	measured	4,5
435	600267	V5	P092310	-757565,00	-1157719,00	map	373,23	measured	4,5
436	616437	V1	P095549	-756837,00	-1157865,00	map	372,50	map 1:10	7,5
437	616438	V2	P095549	-756854,00	-1157886,00	map	372,50	map 1:10	7,5
438		V3	P095549	-756867,00	-1157867,00	map	372,50	map 1:10	7,5
439	637365	V11	P099221	-753440,00	-1163450,00	map	400,87	measured	8,0
440	637362	V-3	P099221	-753740,00	-1163749,00	map	400,64	measured	7,0
441	637363	V-6	P099221	-753527,00	-1163733,00	map	403,02	measured	8,0
442	637364	V-7	P099221	-753574,00	-1163577,00	map	400,68	measured	4,5
443		V3	P099307	-757661,00	-1157131,00	map	391,01	measured	3,0
444	646680	US-2a	P101250	-753303,30	-1162390,00	map	397,50	map 1:10	97,5
445	511286	US-2	P101250	-753296,00	-1162382,00	map	397,50	map 1:10	127,7
446	645063	V101	P101572	-756825,00	-1157765,00	map	374,22	measured	9,2
447		4672/42	P101572	-756682,00	-1157787,00	map	372,50	measured	52,1
448	645025	V1	P101580	-758120,00	-1156708,00	map	379,00	map 1:10	7,5
449	653228	VS1	P103865	-753255,00	-1162377,00	map	377,80	map 1:10	60,0
450	662969	V-2	P109457	-757878,80	-1157234,00	measured	378,77	measured	6,0
451	663365	BP4	P110137	-756720,71	-1158682,20	measured	373,14	measured	309,0
452	663962	HV-1	P110180	-754347,00	-1160438,00	map	436,00	map	25,0
453	672457	V101	P113401	-757960,00	-1156834,00	map	388,11	measured	4,5
454	672410	V101	P113423	-753175,30	-1163898,70	measured	407,89	measured	8,0
455	672412	V106	P113423	-753109,80	-1163886,90	measured	408,45	measured	7,5
456	676361	J-1	P115398	-755326,26	-1159885,96	measured	423,08	measured	17,5
457	676362	J-2	P115398	-754944,19	-1159730,98	measured	463,78	measured	53,0
458	676364	J-3	P115398	-754099,80	-1158808,35	measured	488,00	measured	65,0
459	676363	J-4	P115398	-753975,85	-1158560,75	measured	455,12	measured	30,0
460	676365	J-5	P115398	-753850,84	-1158311,29	measured	446,06	measured	18,0
461	679565	J3	P116281	-756777,61	-1157126,55	measured	370,41	measured	15,0
462		HV-10	P118401	-754774,00	-1160490,00	map	404,00	map	45,0
463	511096	S-25	V038424	-753085,00	-1163620,00	map	406,40	map	10,0
464	511095	S-24	V038424	-753275,00	-1163595,00	map	403,30	map	5,0
465	511094	S-23	V038424	-753440,00	-1163574,00	map	401,70	map	10,0
466	511089	S-15	V038424	-753125,00	-1163916,00	map	406,70	map	10,0
467		1/153	V046625/046665	-752860,00	-1149400,00	map	429,00	map	15,0
468	509742	1/40	V046625/046665	-753700,00	-1163450,00	map	398,00	map	25,0
469		SONDA1	V054304	-757910,38	-1156920,14	map	386,60	map	7,5
470		SONDA2	V054304	-757897,76	-1156937,26	map	385,70	map	2,5
471		SONDA3	V054304	-757887,40	-1156955,50	map	385,30	map	2,5
472		SONDA5	V054304	-757921,86	-1156963,83	map	383,70	map	3,5
473		SONDA6	V054304	-757908,80	-1156983,87	map	383,50	map	9,5
474		SONDA7	V054304	-757818,26	-1156966,53	map	387,50	map	3,5
475		SONDA8	V054304	-757832,45	-1156981,39	map	386,55	map	3,5
476		W1	V068630	-757924,14	-1157378,83	measured	376,46	measured	5,1
477		W2	V068630	-757908,04	-1157380,31	measured	376,22	measured	5,0
478	510264	V-9	V075942	-753508,30	-1162514,00	measured	395,70	measured	10,0
479		JV101	P120279	-756721,32	-1157884,45	map	374,35	measured	12,0
480		HV102	P120279	-756719,78	-1157806,20	map	374,39	measured	20,0

481		HV103	P120279	-756724,29	-1157761,85	map	374,45	measured	13,0
482		HV104	P120279	-756721,52	-1157713,27	map	374,37	measured	20,0
483		HV105	P120279	-756719,99	-1157664,39	map	374,47	measured	13,0
484		HV106	P120279	-756717,49	-1157613,49	map	373,91	measured	20,0
485		JV107	P120279	-756716,15	-1157543,19	map	373,72	measured	11,0
486		V3	FZ001728	-760771,28	-1154434,94	measured	396,05	measured	93,0
487		V1	V045594	-753386,00	-1166056,00	map	400,38	map	45,0
488	509630	VS1	V061665	-754040,00	-1167090,00	map	402,00	map	52,0
489		HV 1	V069324	-752417,30	-1165158,40	?	415,70	?	203,0
490		B1	P025438	-759866,00	-1178513,00	map	523,80	map 1:10	4,0
491		B3	P025438	-759643,00	-1178945,00	map	534,00	map 1:10	6,0
492		A1	P025438	-761387,00	-1182605,00	map	559,80	map 1:10	5,0
493		A3	P025438	-761706,00	-1182675,00	map	559,20	map 1:10	5,2
494		PV1	V071250	-755017,90	-1163561,50	measured	390,58	measured	8,0
495		V2	V071250	-755048,10	-1163555,40	measured	390,43	measured	8,0
496		V3	V071250	-755054,20	-1163528,90	measured	390,81	measured	8,0
497		PV4	V071250	-755058,70	-1163482,80	measured	391,05	measured	8,0
498		V5	V071250	-755019,60	-1163483,40	measured	391,61	measured	8,0
499		V6	V071250	-754987,40	-1163492,20	measured	391,81	measured	8,0
500		V7	V071250	-755006,20	-1163504,30	measured	391,31	measured	8,0
501		V1	P073252	-756390,20	-1161909,30	measured	379,79	measured	10,0
502		PV3	P073252	-756131,40	-1162502,80	measured	380,19	measured	10,0
503		V5	P073252	-755699,10	-1163254,60	measured	380,61	measured	5,0
504		PV6	P073252	-756018,10	-1163848,30	measured	381,62	measured	8,0
505		V7	P073252	-756006,40	-1163877,40	measured	381,39	measured	8,0
506		V8	P073252	-755735,30	-1164353,00	measured	381,98	measured	8,0
507		V9	P073252	-755755,00	-1164429,70	measured	382,18	measured	8,0
508		V11	P073252	-755499,80	-1164684,30	measured	383,67	measured	8,0
509		PV12	P073252	-755314,00	-1164832,40	measured	384,03	measured	10,0
510		V13	P073252	-755292,00	-1164856,10	measured	385,41	measured	10,0
511		V14	P073252	-755221,10	-1164764,10	measured	383,48	measured	10,0
512		V15	P073252	-755101,90	-1164721,30	measured	383,14	measured	10,0
513		V16	P073252	-755015,70	-1164712,20	measured	384,26	measured	8,0
514		PV17	P073252	-755163,20	-1164713,90	measured	383,32	measured	8,0
515		J101	P103526	-755391,96	-1164088,75	measured	383,35	measured	12,0
516		J102	P103526	-755412,14	-1164088,81	measured	383,00	measured	12,0
517		J103	P103526	-755387,61	-1164110,78	measured	383,10	measured	12,0
518		J2A	P103526	-755358,90	-1164124,80	measured	383,20	measured	10,5
519	507141	V1	V051090	-754986,00	-1163190,00	map	389,50	map 1:10	16,0
520	507142	V2	V051090	-755012,00	-1163264,00	map	390,50	map 1:10	25,0
521	507132	SONDA1	V050284	-755175,00	-1162875,00	map	388,10	map 1:10	8,2
522	507134	SONDA2A	V050284	-755147,00	-1162870,00	map	388,20	map 1:10	8,2
523	507135	SONDA3	V050284	-755150,00	-1162825,00	map	388,00	map 1:10	8,2
524	507136	SONDA4	V050284	-755125,00	-1162851,00	map	388,40	map 1:10	8,2
525	507137	SONDA5	V050284	-755127,00	-1162821,00	map	388,20	map 1:10	8,1
526	507138	SONDA6	V050284	-755113,00	-1162845,00	map	388,50	map 1:10	9,0
527	507139	SONDA7	V050284	-755213,00	-1163078,00	map	388,00	map 1:10	8,2
528	507140	SONDA7A	V050284	-755125,00	-1162876,00	map	388,50	map 1:10	8,2
529		J1	P110036	-755199,99	-1164678,67	measured	384,05	measured	15,0
530		J3	P110036	-755053,60	-1164559,46	measured	384,54	measured	15,0
531		J6	P110036	-754890,00	-1164464,58	measured	390,68	measured	6,0
532		PJ7	P110036	-754821,28	-1164365,87	measured	396,26	measured	9,0
533		J8	P110036	-754785,36	-1164296,98	measured	396,24	measured	8,0
534		J9	P110036	-754788,00	-1164337,08	measured	396,77	measured	8,0
535		J10	P110036	-754764,18	-1164318,49	measured	397,21	measured	15,0
536		J11	P110036	-754737,37	-1164286,35	measured	396,95	measured	8,0
537		J12	P110036	-754695,55	-1164309,99	measured	397,29	measured	5,0
538		J13	P110036	-754702,86	-1164247,62	measured	395,88	measured	6,0
539		J14	P110036	-754644,18	-1164182,31	measured	392,63	measured	15,0
540		J15	P110036	-754620,30	-1164159,41	measured	393,18	measured	15,0

541		APJ21	P110036	-755042,95	-1164631,17	measured	384,53	measured	8,0
542		APJ2	P110036	-754751,14	-1164347,42	measured	397,62	measured	10,0
543	507257	HV101	P057423	-755306,00	-1162763,00	map	380,07	measured	6,0
544	507258	PV101/1	P057423	-755307,00	-1162768,00	map	380,10	measured	5,0
545	507259	PV101/2	P057423	-755310,00	-1162784,00	map	380,17	measured	5,0
546	507260	PV101/3	P057423	-755312,00	-1162761,00	map	379,99	measured	5,0
547	507261	PV101/4	P057423	-755328,00	-1162758,00	map	379,82	measured	5,0
548	509285	V4	P081862	-755247,00	-1164657,00	map	383,70	measured	6,0
549	506249	V5	P081862	-755275,00	-1164768,00	map	383,90	measured	8,0
550	506251	PV7	P081862	-755282,00	-1164776,00	map	383,69	measured	8,0
551	578563	HK1	P090926	-755114,00	-1163115,00	map	390,00	measured	15,0
552		V1	P40655/12	-755561,20	-1164528,00	measured	383,01	measured	8,0
553		PV2	P40655/12	-755545,40	-1164539,40	measured	383,13	measured	8,0
554		V3	P40655/12	-755560,80	-1164554,60	measured	382,58	measured	8,0
555		V4	P40655/12	-755541,60	-1164561,50	measured	382,86	measured	8,0
556		V5	P40655/12	-755275,00	-1164768,80	measured	383,90	measured	8,0
557		V6	P40655/12	-755264,30	-1164777,90	measured	383,92	measured	8,0
558		PV7	P40655/12	-755282,20	-1164776,20	measured	383,69	measured	8,0
559		V8	P40655/12	-755271,00	-1164786,30	measured	383,77	measured	8,0
560		V9	P40655/12	-755181,20	-1164739,00	measured	382,74	measured	6,0
561		V10	P40655/12	-755048,10	-1164923,90	measured	384,33	measured	8,0
562		PV11	P40655/12	-755040,20	-1164931,80	measured	384,52	measured	8,0
563		PV14	P40655/12	-754861,90	-1166421,80	measured	389,86	measured	10,0
564		J1	P70442/9	-755108,00	-1164625,00	measured	383,97	measured	15,0
565		J2	P70442/9	-755079,00	-1164635,00	measured	384,04	measured	15,0
566		J3	P70442/9	-755050,00	-1164592,00	measured	384,54	measured	15,0
567		J4	P70442/9	-755048,00	-1164615,00	measured	384,44	measured	15,0
568		J5	P70442/9	-754863,00	-1164493,00	measured	390,79	measured	6,0
569		J6	P70442/9	-754788,00	-1164472,00	measured	395,33	measured	9,0
570		J7	P70442/9	-754795,00	-1164435,00	measured	396,66	measured	8,0
571		J8	P70442/9	-754712,00	-1164385,00	measured	397,92	measured	10,0
572		J9	P70442/9	-754688,00	-1164408,00	measured	398,12	measured	10,0
573		J10	P70442/9	-754618,00	-1164345,00	measured	397,65	measured	7,5
574		J11	P70442/9	-754873,00	-1164393,00	measured	395,34	measured	8,0
575		K2	P70442/9	-754856,00	-1164563,00	measured	390,59	measured	3,3
576		K5	P70442/9	-754575,00	-1164300,00	measured	395,25	measured	3,0
577		HV1	V077389	-755072,70	-1162348,90	measured	387,42	measured	41,0
578	511459	V1	V75806	-755445,00	-1171830,00	map	396,26	measured	15,0
579	511460	V2	V75806	-755400,00	-1171790,00	map	396,00	measured	10,0
580	506907	P1	V75806	-757340,00	-1169080,00	map	387,87	measured	13,3
581	506908	P2	V75806	-757300,00	-1169040,00	map	387,37	measured	16,5
582	385267	B1	V75806	-757320,00	-1160695,00	map	375,93	measured	17,5
583	385268	B2	V75806	-757280,00	-1160700,00	map	376,02	measured	16,7
584	511458	R1	V75806	-755980,00	-1171520,00	map	402,53	measured	20,1
585	385269	H1	V75806	-754950,00	-1161060,00	map	387,56	measured	36,0
586		V1	P67983	-754906,10	-1162264,10	measured	389,29	map	8,0
587		V2	P67983	-754900,70	-1162264,10	measured	389,31	map	8,0
588		V3	P67983	-754912,10	-1162276,40	measured	389,43	map	7,0
589		PV4	P67983	-754905,80	-1162278,10	measured	389,31	map	7,5
590		V5	P67983	-754919,40	-1162293,70	measured	389,50	map	8,0
591		V6	P67983	-754913,50	-1162293,10	measured	389,62	map	8,0
592		HV3	P110155	-754544,00	-1162749,00	map	395,00	measured	18,5
593		V1	P122278	-754781,00	-1161774,00	map	386,99	measured	6,0
594		V2	P122278	-754770,00	-1161808,00	map	387,46	measured	6,0
595		V4	P122278	-754735,00	-1161817,00	map	387,58	measured	6,0
596		J3	P70758	-751770,10	-1164433,30	measured	429,30	measured	4,0
597		J6	P70758	-752030,00	-1164260,30	measured	423,93	measured	5,0
598		J9	P70758	-754054,20	-1162388,60	measured	392,11	measured	3,5
599		V1	P81842	-755097,00	-1161124,00	map	384,70	map 1:10	7,5
600		V2	P099288	-756202,00	-1160977,00	map	379,00	map 1:10	6,0

601		V6	P099288	-756169,00	-1160955,00	map	379,00	map 1:10	6,0
602		V1	P089489	-752717,00	-1162281,00	map	406,10	map 1:10	6,0
603		V2	P089489	-752714,00	-1162296,00	map	405,90	map 1:10	7,0
604		V2	P122257	-755839,00	-1156791,00	map	373,45	measured	8,0
605	684530	HV5	P118496	-756025,00	-1156882,00	map	385,00	map	24,0
606		V2	P116485	-756436,90	-1157048,20	map	381,83	measured	6,0
607		K1	V052186	-755593,97	-1157005,52	measured	386,07	measured	2,5
608		K2	V052186	-755603,25	-1157011,02	measured	384,05	measured	3,0
609		K3	V052186	-755633,25	-1157019,61	measured	380,27	measured	4,1
610		K4	V052186	-755630,28	-1156990,60	measured	382,85	measured	2,7
611		K5	V052186	-755638,06	-1156996,47	measured	381,75	measured	5,2
612		K6	V052186	-755651,71	-1156948,56	measured	383,66	measured	10,1
613		K7	V052186	-755664,23	-1156952,88	measured	379,51	measured	6,2
614		W8	V052186	-755665,54	-1156925,46	measured	383,64	measured	9,9
615		K9	V052186	-755676,96	-1156935,62	measured	379,31	measured	4,1
616		W10	V052186	-755674,76	-1156901,01	measured	382,30	measured	9,0
617		K11	V052186	-755684,83	-1156912,99	measured	380,20	measured	8,1
618		V12	V052186	-755591,41	-1156962,89	measured	387,40	measured	2,9
619		V13	V052186	-755563,00	-1156950,22	measured	389,43	measured	2,9
620		W14	V052186	-755578,81	-1156919,36	measured	387,93	measured	4,9
621		K15	V052186	-755607,39	-1156929,50	measured	386,27	measured	6,1
622		W16	V052186	-755645,06	-1156960,50	measured	383,32	measured	6,0
623		W18	V052186	-755638,37	-1156977,20	measured	385,99	measured	2,0
624		W19	V052186	-755642,25	-1156967,88	measured	383,18	measured	7,3
625		K20	V052186	-755619,10	-1156948,80	measured	384,39	measured	3,1
626		HV1	V057043	-755474,43	-1157173,01	measured	384,09	measured	21,0
627		HVJ16	V052715	-755595,98	-1156945,18	measured	386,90	measured	38,5
628		K1	P103866	-756151,00	-1156899,00	map	386,00	map 1:10	45,0
629		U1	V021011	-754106,00	-1162295,00	map	390,50	map 1:10	71,5
630		HPVIII	V025997	-756938,00	-1159356,00	map	374,00	map 1:10	80,0
631		HPVIII	V025997	-756935,00	-1159385,00	map	374,00	map 1:10	200,0
632		HPVI	V025977	-756967,00	-1159374,00	map	374,00	map 1:10	314,1
633		BP1	P029119	-756949,75	-1159357,98	map	374,18	map 1:10	294,0
634		BP2	P029119	-756985,23	-1161855,41	map	377,66	map 1:10	272,0
635	506866	V-2	P049013	-754183,30	-1165625,10	measured	400,80	measured	8,0
636	506873	PV-9	P049013	-754183,10	-1165584,00	measured	401,10	measured	8,0
637	508653	SONDA 6	P027109	-754065,00	-1163887,00	map	401,80	measured	8,0
638	509489	S-6	P035298	-753680,00	-1164770,00	map	400,30	measured	8,0
639	509534	V-2	P048340	-753633,70	-1165148,80	measured	402,90	measured	15,0
640	509547	PV-17	P048340	-753546,40	-1165196,60	measured	404,00	measured	20,0
641	509569	NT-16	P046597	-753925,00	-1164687,00	map	400,30	measured	8,0
642	509572	NT-19	P046597	-753776,00	-1164585,00	map	400,00	measured	10,0
643	509574	NT-21	P046597	-753841,00	-1164667,00	map	400,30	measured	8,0
644	510372	319	V045310	-753056,00	-1164247,00	map	407,70	measured	10,0
645	510383	340	V045310	-753202,00	-1164517,00	map	405,30	measured	17,0
646	510413	W-32	V068451	-753617,30	-1164538,40	measured	401,80	measured	5,0
647	510414	W-33	V068451	-753607,20	-1164598,80	measured	402,50	measured	5,0
648	510416	W-35	V068451	-753618,70	-1164729,60	measured	402,30	measured	8,0
649	510425	W-53	V068451	-753531,10	-1164607,90	measured	402,90	measured	7,0
650	510575	S-4	V070860	-753851,00	-1165080,00	map	401,40	measured	6,2
651	510582	S-11	V070860	-753948,00	-1165113,00	map	400,70	measured	7,5
652	510584	S-13	V070860	-753993,00	-1165116,00	map	400,50	measured	7,5
653	510596	S-25	V070860	-753923,00	-1165159,00	map	400,80	measured	6,0
654	641315	J-26	P100716	-753337,70	-1164665,30	measured	406,43	measured	10,0
655	680370	V-101	P116474	-753424,00	-1164318,00	map	404,80	measured	7,5
656	696054	V-1	P122256	-753968,00	-1165328,00	map	401,07	measured	6,0
657	506197	V-16	P030322	-754425,70	-1164950,60	measured	400,80	measured	9,0
658	508648	SONDA 1	P027109	-754070,00	-1163885,00	map	400,80	measured	8,0
659	508650	SONDA 3	P027109	-754085,00	-1163887,00	map	400,50	measured	8,0
660	509562	NT-9	P046597	-753741,00	-1164673,00	map	400,80	measured	10,0

661	510364	307	V045310	-753156,00	-1164169,00	map	407,70	measured	10,0
662	510428	PW-56	V068451	-753507,70	-1164736,20	measured	403,60	measured	7,5
663	510574	S-3	V070860	-753896,00	-1165043,00	map	401,40	measured	6,0
664	510579	S-8	V070860	-753842,00	-1165140,00	map	401,10	measured	6,0
665	510755	V-432	V078323	-753266,00	-1164753,00	map	406,40	measured	9,7
666	510757	V-434	V078323	-753295,00	-1164760,00	map	406,70	measured	10,0
667	511085	S-5	V038424	-753505,00	-1164055,00	map	404,30	measured	10,0
668	511086	S-6	V038424	-753340,00	-1164077,00	map	406,00	measured	4,0
669	558554	J-24	P078190	-754249,50	-1165540,10	measured	400,98	measured	4,5
670	602772	424	V045592	-753438,00	-1164570,00	map	404,00	measured	6,0
671	602774	405	V045593	-752976,00	-1164197,00	map	409,00	measured	6,0
672	602779	522	V045593	-753762,00	-1164427,00	map	401,20	measured	7,4
673	602780	526	V045593	-753671,00	-1164334,00	map	402,50	measured	11,0
674	637209	V-2	P099326	-753945,00	-1165032,00	map	401,00	map	6,0
675	641313	J-24	P100716	-753297,60	-1164688,20	measured	406,52	measured	10,0
676	641314	J-25	P100716	-753343,80	-1164637,00	measured	406,20	measured	10,0
677	641316	J-27	P100716	-753370,30	-1164641,60	measured	406,06	measured	3,0
678	673965	J-2	P114387	-754087,86	-1165566,26	measured	397,63	measured	15,0
679	697122	V-2	P122279	-753279,00	-1164434,00	map	407,12	measured	6,0
680	506195	V-14	P030322	-754429,50	-1164900,20	measured	400,70	measured	9,0
681	506867	PV-3	P049013	-754204,10	-1165617,90	measured	400,80	measured	8,0
682	509095	JB-85	P072607	-753976,20	-1163767,30	measured	399,10	measured	10,0
683	509536	V-5	P048340	-753603,90	-1165164,00	measured	403,00	measured	20,0
684	509565	NT-12	P046597	-753757,00	-1164631,00	map	400,30	measured	10,0
685	509582	V-1	P046834	-752725,60	-1164336,70	measured	412,10	measured	3,0
686	509663	W-1	V079237	-753447,70	-1165143,20	measured	405,30	measured	7,7
687	510108	S-5	P034150	-753639,00	-1165148,00	map	403,00	map	10,0
688	510367	311	V045310	-753195,00	-1164220,00	map	406,90	measured	7,0
689	510409	W-26	V068451	-753666,80	-1164616,30	measured	401,50	measured	5,5
690	510415	W-34	V068451	-753552,80	-1164648,20	measured	403,10	measured	5,0
691	510417	W-36	V068451	-753620,20	-1164772,30	measured	402,90	measured	6,5
692	510422	W-47	V068451	-753604,50	-1164464,80	measured	402,90	measured	5,0
693	510423	W-50	V068451	-753566,20	-1164460,50	measured	403,20	measured	5,0
694	510429	W-57	V068451	-753525,90	-1164761,30	measured	403,50	measured	5,0
695	510434	W-63	V068451	-753505,30	-1164639,10	measured	403,40	measured	6,5
696	510435	W-64	V068451	-753511,40	-1164603,60	measured	403,10	measured	6,8
697	510576	S-5	V070860	-753859,00	-1165110,00	map	401,20	measured	8,0
698	510586	S-15	V070860	-753998,00	-1165222,00	map	400,90	measured	6,0
699	558549	PJ-12	P078190	-754172,00	-1165489,00	measured	401,22	measured	5,3
700	558574	PJ-10	P078190	-754016,10	-1165621,50	measured	401,62	measured	5,0
701	637227	V-1	P099299	-754242,00	-1163702,00	map	398,03	measured	6,0
702	641350	PJ-13	P100716	-753238,10	-1164596,30	measured	406,55	measured	10,0
703	657992	V-2	P106752	-753208,00	-1163997,00	map	408,29	measured	6,0
704	680371	V-102	P116474	-753446,00	-1164233,00	map	404,00	measured	7,5
705	696055	V-3	P122256	-754012,00	-1165317,00	map	401,07	measured	6,0
706	506199	V-18	P030322	-754359,40	-1164914,20	measured	400,60	measured	9,0
707	506871	PV-7	P049013	-754145,50	-1165601,80	measured	401,30	measured	8,0
708	509484	S-1	P035298	-753800,00	-1164630,00	map	400,00	measured	8,0
709	509486	S-3	P035298	-753600,00	-1164610,00	map	400,00	measured	6,5
710	509533	PV-1	P048340	-753687,80	-1165147,10	measured	402,80	measured	15,0
711	509539	V-8	P048340	-753589,50	-1165164,30	measured	403,00	measured	35,0
712	510110	S-6	P034150	-753594,00	-1165165,00	map	403,00	map	10,0
713	510112	S-8	P034150	-753646,00	-1165251,00	map	403,00	map	7,5
714	510407	W-24	V068451	-753636,70	-1164772,90	measured	402,90	measured	5,8
715	510424	W-51	V068451	-753556,80	-1164529,90	measured	402,80	measured	5,0
716	510580	S-9	V070860	-753878,00	-1165130,00	map	401,00	measured	6,0
717	510588	S-17	V070860	-753971,00	-1165198,00	map	400,80	measured	6,0
718	510590	S-19	V070860	-753878,00	-1165224,00	map	401,10	measured	6,0
719	510593	S-22	V070860	-753819,00	-1165183,00	map	401,20	measured	6,0
720	511087	S-11	V038424	-753717,00	-1163838,00	map	401,30	measured	10,0

721	637167	V-6	P099331	-754642,00	-1163346,50	map	395,93	measured	4,5
722	637206	V-1	P099326	-753965,00	-1165023,00	map	401,00	map	9,0
723	652700	J-5	P104631	-753321,22	-1164493,82	measured	406,01	measured	6,8
724	673964	J-1	P114387	-754049,90	-1165541,64	measured	398,81	measured	16,0
725	680374	V-101	P116477	-753800,00	-1165098,00	map	402,00	map	7,5
726	506201	PV-20	P030322	-754357,20	-1164976,20	measured	400,40	measured	9,0
727	506869	V-5	P049013	-754177,80	-1165608,50	measured	401,00	measured	8,0
728	508286	J-1	P065718	-754196,20	-1165350,60	measured	401,00	measured	7,0
729	508525	S-3	V047323	-754005,00	-1164105,00	map	408,20	measured	8,0
730	509011	S-9	V038424	-754015,00	-1163800,00	map	398,90	measured	10,0
731	509487	S-4	P035298	-753820,00	-1164730,00	map	400,50	measured	8,0
732	509538	V-7	P048340	-753588,30	-1165149,30	measured	403,00	measured	20,0
733	509567	NT-14	P046597	-753867,00	-1164714,00	map	400,40	measured	10,0
734	510109	S-4	P034150	-753706,00	-1165129,50	map	403,00	map	9,0
735	510111	S-7	P034150	-753728,00	-1165237,00	map	403,00	map	7,5
736	510365	308	V045310	-753112,00	-1164164,00	map	408,40	measured	7,0
737	510366	309	V045310	-753068,00	-1164158,00	map	408,90	measured	15,0
738	510399	212	V045310	-753285,00	-1164233,00	map	406,20	measured	8,0
739	510408	W-25	V068451	-753658,50	-1164670,50	measured	401,60	measured	5,0
740	510412	PW-29	V068451	-753694,80	-1164430,60	measured	401,80	measured	5,0
741	510433	W-62	V068451	-753496,00	-1164709,70	measured	403,90	measured	6,5
742	511084	S-3	V038424	-753745,00	-1164025,00	map	401,80	measured	10,0
743	602776	503	V045593	-752930,00	-1164075,00	map	409,20	measured	10,0
744	637208	V-4	P099326	-753894,00	-1164991,00	map	401,00	map	7,5
745	637228	V-2	P099299	-754248,00	-1163679,00	map	397,75	measured	6,0
746	652697	J-1	P104631	-753399,26	-1164506,94	measured	405,44	measured	7,0
747	672209	V-104	P113421	-754129,30	-1163584,80	map	398,31	measured	6,0
748	506202	V-21	P030322	-754357,50	-1164961,70	measured	400,40	measured	9,0
749	506868	V-4	P049013	-754155,50	-1165618,10	measured	401,10	measured	8,0
750	506870	V-6	P049013	-754194,30	-1165600,40	measured	401,10	measured	8,0
751	508524	S-2	V047323	-754149,00	-1164025,00	map	407,70	measured	8,0
752	508652	SONDA 5	P027109	-754075,00	-1163890,00	map	400,80	measured	8,0
753	509100	JB-90	P072607	-754114,90	-1163874,10	measured	399,40	measured	9,0
754	509485	S-2	P035298	-753750,00	-1164620,00	map	399,90	measured	6,5
755	509554	NT-1	P046597	-753660,00	-1164660,00	map	401,20	measured	10,0
756	509560	NT-7	P046597	-753852,00	-1164763,00	map	400,60	measured	10,0
757	509573	NT-20	P046597	-753720,00	-1164547,00	map	400,30	measured	10,0
758	510363	305	V045310	-753245,00	-1164181,00	map	406,30	measured	10,0
759	510368	313	V045310	-753106,00	-1164208,00	map	408,20	measured	7,0
760	510403	W-13	V068451	-753565,60	-1165215,80	measured	403,80	measured	5,1
761	510411	W-28	V068451	-753687,80	-1164476,20	measured	401,20	measured	5,0
762	510427	W-55	V068451	-753510,60	-1164711,50	measured	403,70	measured	6,5
763	602773	426	V045592	-753426,00	-1164715,00	map	404,80	measured	10,0
764	637207	V-5	P099326	-753890,00	-1165016,00	map	401,00	map	6,0
765	637253	V-6	P099286	-753813,00	-1165083,00	map	401,60	map	7,5
766	641317	J-28	P100716	-753384,50	-1164677,20	measured	406,35	measured	3,0
767	657993	V-3	P106752	-753216,50	-1163959,00	map	408,06	measured	6,0
768	696056	V-4	P122256	-754048,00	-1165288,00	map	400,86	measured	7,5
769	506196	V-15	P030322	-754427,30	-1164919,50	measured	400,70	measured	9,0
770	507917	JB-57	P059532	-753987,10	-1163747,00	measured	399,00	measured	10,0
771	508523	S-1	V047323	-754025,00	-1164010,00	map	407,30	measured	8,0
772	508649	SONDA 2	P027109	-754068,00	-1163890,00	map	401,00	measured	8,0
773	508651	SONDA 4	P027109	-754080,00	-1163895,00	map	400,70	measured	8,0
774	509010	S-1	V038424	-754040,00	-1163985,00	map	399,20	measured	10,0
775	509571	NT-18	P046597	-753829,00	-1164620,00	map	400,00	measured	10,0
776	509664	PW-2	V079237	-753465,30	-1165181,00	measured	405,50	measured	8,0
777	510105	S-1	P034150	-753699,00	-1165079,00	map	403,00	map	10,0
778	510369	314	V045310	-753067,00	-1164203,00	map	408,50	measured	10,0
779	510405	W-15	V068451	-753583,80	-1165130,90	measured	403,30	measured	5,0
780	510410	W-27	V068451	-753676,90	-1164551,10	measured	401,40	measured	5,0

781	510421	W-42	V068451	-753579,80	-1164769,10	measured	402,90	measured	5,0
782	510426	W-54	V068451	-753523,20	-1164640,70	measured	403,40	measured	6,3
783	510432	W-61	V068451	-753493,10	-1164733,40	measured	403,80	measured	6,3
784	510591	S-20	V070860	-753831,00	-1165234,00	map	401,30	measured	6,0
785	570450	V-3	P089463	-753753,00	-1163967,00	map	402,20	map	6,0
786	637254	V-7	P099286	-753840,00	-1165055,00	map	401,50	map	7,5
787	657990	V-3	P106753	-753467,00	-1164277,00	map	403,50	map	7,5
788	695686	J-2	P122083	-754193,77	-1165569,02	measured	400,95	measured	10,0
789	697123	V-7	P122279	-753219,00	-1164505,00	map	407,16	measured	6,0
790	506200	V-19	P030322	-754358,30	-1164948,70	measured	400,50	measured	9,0
791	506865	PV-1	P049013	-754161,80	-1165635,70	measured	400,80	measured	8,0
792	506872	V-8	P049013	-754164,60	-1165590,90	measured	401,20	measured	8,0
793	509492	S-9	P035298	-753730,00	-1164770,00	map	401,10	measured	6,5
794	509542	V-11	P048340	-753559,80	-1165164,80	measured	403,50	measured	20,0
795	509545	V-14A	P048340	-753526,90	-1165137,30	measured	403,50	measured	20,0
796	509556	NT-3	P046597	-753781,00	-1164760,00	map	400,90	measured	10,0
797	510572	S-1	V070860	-753908,00	-1165097,00	map	401,00	measured	7,0
798	510578	S-7	V070860	-753810,00	-1165150,00	map	401,10	measured	7,5
799	510581	S-10	V070860	-753913,00	-1165120,00	map	400,80	measured	6,0
800	510583	S-12	V070860	-753978,00	-1165083,00	map	400,50	measured	6,0
801	510587	S-16	V070860	-753956,00	-1165235,00	map	401,00	measured	6,0
802	510589	S-18	V070860	-753926,00	-1165211,00	map	401,00	measured	6,0
803	510594	S-23	V070860	-753853,00	-1165176,00	map	401,10	measured	6,0
804	510595	S-24	V070860	-753888,00	-1165166,00	map	400,90	measured	6,0
805	510597	S-26	V070860	-753957,00	-1165146,00	map	400,60	measured	7,0
806	510613	S-10	V077981	-753493,00	-1165200,00	map	404,70	measured	3,0
807	576654	HJ64	P083887	-754160,70	-1165441,20	map	401,00	map	46,0
808	641309	J-16	P100716	-753226,10	-1164677,60	measured	406,86	measured	10,0
809	641310	J-17	P100716	-753274,60	-1164598,40	measured	406,43	measured	11,7
810	641311	J-20	P100716	-753261,50	-1164682,70	measured	406,77	measured	15,1
811	641312	J-21	P100716	-753308,50	-1164600,10	measured	406,30	measured	10,0
812	651068	PJ-10	P103578	-754711,95	-1163411,79	measured	395,47	measured	4,0
813	651071	PJ-40	P103578	-754583,15	-1163560,21	measured	395,79	measured	4,0
814	652698	J-2	P104631	-753402,09	-1164478,64	measured	405,70	measured	6,8
815	652699	J-4	P104631	-753326,11	-1164470,45	measured	406,03	measured	6,0
816	680377	V-1	P116481	-754263,50	-1163751,50	map	398,15	measured	6,0
817		JV3	P057829	-754927,00	-1163383,00	map	392,60	map 1:10	10,0
818		JV7	P057829	-754957,00	-1163361,00	map	392,40	map 1:10	10,0
819		JB78	P059532	-752586,00	-1162897,00	map	419,00	map 1:10	5,0
820		JB79	P059532	-752450,00	-1162862,00	map	419,60	map 1:10	5,0
821		JB55	P059532	-753941,00	-1163711,00	map	399,50	map 1:10	14,0
822		JB56	P059532	-753923,00	-1163691,00	map	399,50	map 1:10	14,0
823		JB57	P059532	-753988,00	-1163749,00	map	400,00	map 1:10	10,0
824		JB58	P059532	-753900,00	-1163710,00	map	399,50	map 1:10	14,0
825		JB59	P059532	-753917,00	-1163731,00	map	399,50	map 1:10	14,0
826		JB60	P059532	-753862,00	-1163778,00	map	399,80	map 1:10	8,0
827		JB61	P059532	-753806,00	-1163647,00	map	399,50	map 1:10	10,0
828		JB63	P059532	-753696,00	-1163579,00	map	399,50	map 1:10	8,0
829		JB64	P059532	-753584,00	-1163501,00	map	399,70	map 1:10	6,0
830		JB65	P059532	-753466,00	-1163431,00	map	400,10	map 1:10	6,0
831		JB66	P059532	-753362,00	-1163361,00	map	400,10	map 1:10	6,0
832		JB67	P059532	-753236,00	-1163280,00	map	400,30	map 1:10	6,0
833		JB68	P059532	-753110,00	-1163201,00	map	403,50	map 1:10	7,0
834		JBV69	P059532	-752984,00	-1163138,00	map	414,00	map 1:10	15,0
835		JB72	P059532	-752906,00	-1163057,00	map	415,00	map 1:10	9,0
836		JB73	P059532	-752790,00	-1163021,00	map	417,20	map 1:10	9,0
837		JBV76	P059532	-752695,00	-1162944,00	map	420,00	map 1:10	12,0
838		PV1	P065696	-755171,70	-1162726,10	map	382,48	measured	10,0
839		V2	P065696	-755166,30	-1162702,20	map	382,32	measured	10,0
840		V3	P065696	-755143,80	-1162726,40	map	382,84	measured	10,0

841		PV4	P065696	-755143,70	-1162708,60	map	382,93	measured	10,0
842		K1	P097725	-756252,50	-1156902,10	measured	386,28	measured	3,5
843		K2	P097725	-756186,90	-1156829,30	measured	384,98	measured	3,5
844		K3	P097725	-756175,70	-1156750,80	measured	380,84	measured	3,5
845		K4	P097725	-756253,90	-1156773,10	measured	377,81	measured	3,8
846		K5	P097725	-756255,30	-1156814,00	measured	381,35	measured	2,3
847		K6	P097725	-756323,30	-1156869,10	measured	379,04	measured	4,0
848		V2	P099266	-756166,00	-1156730,00	map	379,00	map 1:10	4,5
849		V2	P102905	-754989,00	-1163028,00	map	389,30	measured	6,5
850		V2	P102912	-755122,00	-1163384,00	map	390,89	measured	6,0
851		H1	P103864	-756220,00	-1156840,00	map	383,00	map 1:10	44,0
852	654220	HV2	P104031	-756227,00	-1156860,00	map	384,00	map 1:10	28,0
853	654238	HV3	P104056	-756193,00	-1156818,00	map	383,00	map 1:10	44,0
854	654239	HV4	P104057	-756204,00	-1156785,00	map	380,20	map 1:10	39,0
855		HV8	P124468	-755937,00	-1156821,00	map	382,00	map 1:10	24,0
856		J1	P124655	-755186,26	-1164068,82	measured	388,21	measured	6,0
857		J2	P124655	-755196,96	-1164081,91	measured	388,05	measured	6,0
858		S1	V075106	-755167,00	-1162725,00	map	388,56	measured	11,5
859		S2	V075106	-755165,00	-1162712,00	map	388,29	measured	12,0
860		HYDRO S1	V075106	-755142,00	-1162720,00	map	388,54	measured	20,0
861	510256	PV1	V075942	-753675,00	-1162517,00	map	395,05	measured	9,0
862	510257	V2	V075942	-753661,00	-1162480,00	map	394,48	measured	8,0
863	510258	V3	V075942	-753723,00	-1162469,00	map	393,82	measured	8,0
864	510259	V4	V075942	-753636,00	-1162519,00	map	394,83	measured	8,0
865	510260	V5	V075942	-753626,00	-1162489,00	map	394,74	measured	8,0
866	510261	V6	V075942	-753604,00	-1162494,00	map	394,97	measured	8,0
867	510262	V7	V075942	-753612,00	-1162549,00	map	394,97	measured	8,0
868	510263	V8	V075942	-753538,00	-1162573,00	map	395,57	measured	8,0
869	510264	V9	V075942	-753508,00	-1162514,00	map	395,71	measured	10,0
870	510265	V10	V075942	-753581,00	-1162555,00	map	394,96	measured	8,0
871	510266	PV11	V075942	-753571,00	-1162529,00	map	395,08	measured	8,0
872	510267	V12	V075942	-753561,00	-1162503,00	map	395,30	measured	8,0
873	507210	S1	V076594	-755280,00	-1163350,00	map	389,00	map 1:10	9,0
874	507211	S2	V076594	-755282,00	-1163374,00	map	389,00	map 1:10	8,0
875	511088	S13	V038424	-753465,00	-1163850,00	map	403,68	measured	10,0
876	511090	S17	V038424	-753692,00	-1163692,00	map	400,43	measured	5,0
877	511092	S19	V038424	-753292,00	-1163742,00	map	404,60	measured	5,0
878	511093	S22	V038424	-753679,00	-1163542,00	map	400,85	measured	10,0
879		HL3	P018881	-763681,76	-1156191,21	measured	388,23	measured	131,5
880		65/18	P018881	-753520,00	-1157122,00	map	425,00	map	50,0
881	607265	V-4	#GF P085793	-755060,00	-1166080,00	map	387,60	map	9,0
882	657842	HR-10	#GF P106606	-756347,00	-1171275,00	map	404,00	map	20,0
883	510517	PV-47	#GF V061447	-754358,87	-1167791,44	measured	405,17	measured	8,0
884	565839	V-3	#GF P081860	-757888,00	-1169236,00	map	399,30	map	9,0
885	508577	V-1	#GF P060994	-754779,00	-1165925,00	map	389,60	map	9,5
886	506317	V-1	#GF P043448	-756213,00	-1167243,00	map	391,90	map	6,5
887	506376	HV-1	#GF P033725	-756808,30	-1168598,60	measured	393,67	measured	10,5
888	677533	J-604	#GF P114836	-757016,69	-1163109,63	measured	382,24	measured	7,6
889	698825	JV-3	GF P124301	-754469,68	-1167069,86	measured	393,30	measured	10,0
890	508541	HV-1	#GF V062112	-758605,00	-1169615,00	map	402,00	map	20,0
891	507844	V-1	#GF V064861	-755608,90	-1164962,30	measured	384,40	measured	15,0
892	509514	V-5	#GF P047146	-754220,00	-1169280,00	map	409,10	map	4,7
893	506006	V-110	#GF V073317	-756662,20	-1167688,20	measured	389,60	measured	7,0
894	506702	V-4	#GF P038344	-755670,00	-1166220,00	map	386,50	map	8,0
895	506774	8/112	#GF V046625	-754640,00	-1168920,00	map	396,00	map	15,1
896	653033	Va-1	#GF P103862 - GF P128127	-753063,00	-1167459,00	map	420,00	map	20,0
897	673534	T+-1	#GF P114580	-756122,00	-1170222,00	map	399,00	map	60,0
898	507409	HV-2	#GF V077438 - GF P106644	-757214,70	-1162244,60	measured	379,45	measured	49,0
899	507464	S-8	#GF V045587	-756153,00	-1167615,00	map	392,20	map	10,0
900	508544	HV-1	#GF V062715	-755995,00	-1169716,00	map	395,00	map	12,0

901	509634	W 211	#GF V075194	-753890,00	-1168280,00	map	418,40	map	7,0
902	509662	PV-316	#GF V078339	-753307,00	-1168363,00	measured	429,12	measured	20,0
903	511519	V-152	#GF P023388	-755335,20	-1172375,60	measured	397,10	measured	5,3
904	509180	V-4	#GF P073839	-756376,00	-1167803,00	map	393,30	map	8,0
905	507041	VJ-5	#GF P053982	-755416,00	-1165019,60	measured	384,70	measured	15,0
906	507095	B-1	#GF P012368	-756998,00	-1163435,00	measured	385,50	measured	5,0
907	507384	PV-110	#GF V061447	-754512,85	-1168320,73	measured	404,78	measured	12,0
908	506066	V-9	#GF P039978	-756468,00	-1167464,00	map	391,10	map	8,0
909	506760	PV-1	#GF P051339	-755937,40	-1165642,00	measured	385,50	measured	12,0
910	506601	W 324	#GF V076292	-756897,20	-1164110,80	measured	383,70	measured	6,0
911	511958	V-4	#GF V069720	-755701,20	-1170986,20	measured	395,40	measured	10,0
912	508605	V-1	#GF P063020	-755900,00	-1167250,00	map	389,60	map	6,5
913	506427	K 101	#GF P045949	-755460,00	-1166380,00	map	387,00	map	9,0
914	696065	V-1	#GF P122255	-755175,00	-1166136,00	map	387,16	map	9,0
915	509006	V-2	#GF P069173	-755358,00	-1165200,00	map	385,20	map	8,0
916	621764	PV-371	#GF P096898	-757929,95	-1168414,38	measured	396,32	measured	9,0
917	508283	V-1	#GF P065687	-754506,30	-1168071,40	measured	405,30	measured	5,0
918	506778	8/128	#GF V046625	-757320,00	-1163340,00	map	385,00	map	9,8
919	506911	HP-IV	#GF P025997 - GF P069398	-759871,37	-1169750,19	measured	422,57	measured	189,0
920	649492	V-1	#GF P102919	-756002,00	-1165467,00	map	384,50	map	6,0
921	510507	PV-35	#GF V061447	-754243,59	-1167573,08	measured	405,35	measured	6,0
922	686392	J-6	GF P119185	-757262,73	-1162442,96	measured	380,63	measured	5,4
923	695893	PJ-3	GF P124125	-757312,92	-1162797,51	measured	382,59	measured	5,0
924	696172	V-1018	GF P122300	-757264,19	-1164612,00	measured	388,46	measured	10,0
925	696606	V-2	GF P122316	-757467,00	-1165835,00	map	389,11	map	10,5
926	697339	HV-11	GF P124544	-756103,00	-1172192,00	map	402,50	map	12,0
927	509002	V-2	#GF P069182	-755167,00	-1165480,00	map	386,50	map	8,0
928	509648	V-301	#GF V078339	-753497,00	-1168494,00	measured	421,60	measured	8,5
929	637105	V-2	#GF P099305	-757947,00	-1169567,00	map	400,98	map	6,0
930	644880	V-1001	#GF P101611	-755842,00	-1165233,00	map	385,25	map	6,0
931	508361	J-8	#GF P028396	-759517,40	-1166435,20	measured	436,22	measured	8,2
932	509202	V-1	#GF P044309	-755291,00	-1166303,00	map	387,40	map	11,0
933	509263	V-15	#GF P078232	-757500,00	-1163500,00	map	386,10	map	8,0
934	507176	V-1	#GF P057414	-756058,70	-1167162,80	measured	387,50	measured	12,0
935	507459	S-3	#GF V045587	-756034,00	-1167688,00	map	391,70	map	10,0
936	506418	S-8	#GF P035299	-755984,00	-1167393,00	map	392,20	map	11,0
937	686389	PJ-3	GF P119185	-757353,31	-1162512,74	measured	380,61	measured	5,5
938	696058	V-106	GF P122263	-758979,00	-1171343,00	map	412,38	map	10,5
939	508428	V-1001	#GF V068627	-757618,80	-1164761,90	measured	389,00	measured	9,0
940	509264	V-16	#GF P078232	-757750,00	-1163150,00	map	384,30	map	8,0
941	507108	B-14	#GF P012368	-758187,00	-1160867,00	measured	378,00	measured	7,0
942	507380	PV-30	#GF V061447	-754388,18	-1167444,74	measured	402,28	measured	12,0
943	600931	S-93	#GF V045586	-757925,00	-1167666,00	map	389,60	map	7,5
944	506496	V-1	#GF P045955	-757807,00	-1165440,00	map	388,70	map	9,0
945	654926	PJ-503	#GF P105590	-757335,40	-1162699,82	measured	381,84	measured	5,0
946	654927	PJ-504	#GF P105590	-757114,30	-1162637,30	measured	381,03	measured	5,5
947	683540	HV-7	#GF P118432	-757743,00	-1167927,00	map	392,80	map	11,0
948	684404	HV-6	#GF P118513	-754882,00	-1168403,00	map	392,70	map	15,0
949	509638	W 216	#GF V075194	-753760,00	-1168350,00	map	421,20	map	5,6
950	509644	V-207	#GF V075260	-753600,00	-1168120,00	map	423,80	map	7,0
951	643450	V-1	#GF P101575	-756336,00	-1168723,00	map	395,17	map	7,5
952	508493	S-7	#GF P034239	-756968,00	-1165171,00	map	382,80	map	7,5
953	509210	V-1	#GF P076399	-755480,00	-1165240,00	map	385,40	map	8,0
954	509253	V-5	#GF P078232	-757850,00	-1164400,00	map	389,00	map	8,0
955	509280	V-1	#GF P081852	-755890,00	-1165500,00	map	384,80	map	12,0
956	509286	J-1	#GF P080073	-755491,30	-1166179,10	measured	387,30	measured	15,0
957	506031	V-816/V-4MO70a	#GF P020833 - GF P112373	-755420,00	-1170500,00	map	392,85	map	7,8
958	506663	W-60	#GF V079237	-754808,20	-1168091,80	measured	395,80	measured	6,0
959	506664	W-63	#GF V079237	-754938,30	-1167857,30	measured	390,20	measured	8,8
960	662750	HSV-6	#GF P110170	-753325,00	-1167380,00	map	411,00	map	14,5

961	677530	J-601	#GF P114836	-757186,57	-1163118,45	measured	383,97	measured	10,0
962	686387	J-1	GF P119185	-757347,78	-1162329,91	measured	380,34	measured	5,3
963	508985	V-1	#GF V069938	-756293,70	-1168375,20	measured	394,20	measured	10,0
964	509102	V-1	#GF P069695	-755010,00	-1165480,00	map	386,70	map	8,0
965	509692	W-53	#GF V079237	-754287,70	-1168553,90	measured	405,70	measured	5,3
966	637244	V-1	#GF P099275	-755988,00	-1167012,00	map	387,50	map	6,2
967	511478	V-106	#GF P023388	-755598,50	-1173405,90	measured	403,00	measured	10,2
968	507096	B-2	#GF P012368	-757082,00	-1162840,00	measured	381,20	measured	5,0
969	671752	V-101	#GF P113433	-755337,00	-1166131,00	map	387,12	map	7,5
970	510492	PV-13	#GF V061447	-754044,92	-1167573,03	measured	408,82	measured	7,0
971	696872	HV-1	GF P124459	-755212,00	-1165849,00	map	388,00	map	10,0
972	508936	J-1	#GF P061876	-756056,40	-1168039,70	measured	394,10	measured	9,5
973	509646	V-209	#GF V075260	-753770,00	-1168050,00	map	420,00	map	7,0
974	508379	V-704	#GF V061664	-756047,60	-1165059,70	measured	385,00	measured	10,0
975	508382	V-707	#GF V061664	-756062,50	-1165190,80	measured	385,20	measured	10,0
976	507888	PV-1	#GF V077455	-756609,00	-1167900,50	measured	390,10	measured	8,0
977	511503	K 132	#GF P023388	-755213,70	-1173239,30	measured	422,60	measured	10,0
978	511876	CB-4	#GF P018879	-755647,90	-1170951,70	measured	394,50	measured	258,8
979	508542	HV-1	#GF V062586 - GF P027827	-755987,00	-1167481,00	measured	387,75	measured	270,0
980	511479	PV 107	#GF P023388	-755494,70	-1173424,00	measured	407,00	measured	12,0
981	511485	K 113	#GF P023388	-755437,10	-1173299,50	measured	414,60	measured	3,1
982	511497	V-126	#GF P023388	-755498,10	-1173189,30	measured	405,00	measured	13,3
983	511689	W 8072	#GF V074277	-755457,60	-1173282,80	measured	410,30	measured	7,5
984	511487	PV 115	#GF P023388	-755337,20	-1173316,10	measured	418,80	measured	9,5
985	511515	V-146	#GF P023388	-755245,00	-1173237,30	measured	419,80	measured	8,7
986	511438	8/132	#GF V046625	-759780,00	-1172700,00	map	446,00	map	10,0
987	511484	V-112	#GF P023388	-755471,80	-1173294,20	measured	409,20	measured	15,0
988	511875	CB-3	#GF P018879	-757390,20	-1170461,40	measured	403,20	measured	239,0
989	621828	S-3	#GF P096958	-756552,00	-1167825,00	map	390,20	map	235,0
990	511491	V-120	#GF P023388	-755458,20	-1173246,30	measured	409,10	measured	11,7
991	511483	PV 111	#GF P023388	-755524,30	-1173286,70	measured	404,70	measured	11,2
992	511486	K 114	#GF P023388	-755386,80	-1173306,80	measured	417,70	measured	7,7
993	511490	V-118	#GF P023388	-755510,50	-1173240,30	measured	405,10	measured	12,4
994	511493	PV 122	#GF P023388	-755375,10	-1173260,00	measured	416,20	measured	5,6

Curriculum

Clemens Porpaczy

Wittgensteinstraße 50

1130 Wien

Tel.: 0699 121 92 406

E-Mail: clemens.porpaczy@europe.com

clemens.porpaczy@gmx.at

Persönliche Daten

Geburtsdatum:	18.08.1984
Geburtsort:	Wien
Familienstand:	ledig
Staatsbürgerschaft:	Österreich

Schul- und Hochschulbildung

1991-2003	Rudolf-Steiner Schule Wien Mauer
2003-2004	BORG Anton-Krieger Gasse Liesing Matura mit ausgezeichnetem Erfolg
2004-2005	Ableistung des Wehrdienstes von 8 Monaten beim Bundesheer (Garde)
2005-2009	Studium der Erdwissenschaften in Wien, Abschluß mit Bakk. rer. Nat. Bakkalaureatsarbeit: „Sandstein- und Konglomeratpetrographie der Nierental-Formation im Profil Groisbach (NÖ)“
2009-2011	Masterstudium Erdwissenschaften Masterarbeit: „Tectonic Evolution of the Budejovice Basin (Czech Republic), with special focus on the Hluboka-Fault“

Weitere Ausbildungen und Kenntnisse:

Führerschein B
Ausbildung zum Sprengbefugten gem. § 6 der Verordnung BGBI Nr. 441/1975
Vertiefende PC-Kenntnisse: MS-Office, ESRI ArcGIS, Corel Draw, GoCAD, Tectonics FP
Grundkenntnisse: Petrel,

Berufserfahrung:

2007	Bengt Karlsson
2008-2009	Ferialjob Jugend am Werk
2009-2011	EGU General Assembly – Student Assistant
1.8. 2010-2011	Anstellung als Projektmitarbeiter beim Projekt „AIP [Austrian Interfacing Project]: Paleoseismology of Temelin's Near-Regional Faults" im Zuge der Masterarbeit

Tutorentätigkeit:

SS 2010	Tutor im Rahmen der Lehrveranstaltung „Strukturgeologie und Tektonik"
SS 2011	Tutor im Rahmen der Lehrveranstaltung „Kartierung im Gelände"

Konferenzbeiträge:

2011	EGU General Assembly 2011 Clemens Porpaczy, Dana Homolova & Kurt Decker: **A 3D basin model of the Budějovice Basin (southern Bohemia) with a special focus on the Hluboká-Fault Zone** (Poster)
2011	CETEG 2011 – 9th Meeting of the Central European Tectonic Groups Clemens Porpaczy, Dana Homolova & Kurt Decker: **Slip-History of the Hluboká Fault derived from structural data and 3D modelling of the Budejovice Basin** (Vortrag)